NUMERICAL SIMULATION STUDY TO INVESTIGATE EXPECTED PRODUCTIVITY IMPROVEMENT USING THE "SLOT-DRILL" COMPLETION

A Thesis

by

TIOLUWANIMI OLUWAGBEMIGA ODUNOWO

Submitted to the Office of Graduate Studies of
Texas A&M University
in partial fulfillment of the requirements for the degree of

MASTER OF SCIENCE

May 2012

Major Subject: Petroleum Engineering

Numerical Simulation Study to Investigate Expected Productivity Improvement Using the “Slot-Drill”

NUMERICAL SIMULATION STUDY TO INVESTIGATE EXPECTED PRODUCTIVITY IMPROVEMENT USING THE "SLOT-DRILL" COMPLETION

A Thesis

by

TIOLUWANIMI OLUWAGBEMIGA ODUNOWO

Submitted to the Office of Graduate Studies of
Texas A&M University
in partial fulfillment of the requirements for the degree of

MASTER OF SCIENCE

Approved by:

Co-Chairs of Committee,	Thomas A. Blasingame
	George J. Moridis
Committee Members,	Peter P. Valko
	Yalchin R. Efendiev
Head of Department,	A. Dan Hill

May 2012

Major Subject: Petroleum Engineering

ABSTRACT

Numerical Simulation Study to Investigate Expected Productivity Improvement Using the "Slot-Drill" Completion. (May 2012)

Tioluwanimi Oluwagbemiga Odunowo, B.S., University of Ibadan

Co-Chairs of Advisory Committee: Dr. Thomas A. Blasingame
Dr. George J. Moridis

The "slot-drill" completion method, which utilizes a mechanically cut high-conductivity "slot" in the target formation created using a tensioned abrasive cable, has been proposed as an alternative stimulation technique for shale-gas and other low/ultra-low permeability formations.

This thesis provides a comprehensive numerical simulation study on the "slot drill" completion technique. Using a Voronoi gridding scheme, I created representative grid systems for the slot-drill completion, as well as for the case of a vertical well with a single fracture, the case of a horizontal well with multiple hydraulic fractures, and various combinations of these completions. I also created a rectangular slot configuration, which is a simplified approximation of the actual "slot-drill" geometry, and investigated the ability of this rectangular approximation to model flow from the more complicated (actual) slot-drill configuration(s).

To obtain the maximum possible diagnostic and analytical value, I simulated up to 3,000 years of production, allowing the assessment of production up to the point of depletion (or boundary-dominated flow). These scenarios provided insights into all the various flow regimes, as well as provided a quantitative evaluation of all completion schemes considered in the study.

The results of my study illustrated that the "slot-drill" completion technique was not, in general, competitive in terms of reservoir performance and recovery compared to the more traditional completion techniques presently in use. Based on my modeling, it appears that the larger surface area to flow that multistage hydraulic fracturing provides is much more significant than the higher conductivity achieved using the slot-drill technique.

This work provides quantitative results and diagnostic interpretations of productivity and flow behavior for low and ultra-low permeability formations completed using the slot-drill method. The results of this study can be used to (a) help evaluate the possible application of the "slot-drill" technique from the perspective of performance and recovery, and (b) to establish aggregated economic factors for comparing the slot-drill technique to more conventional completion and stimulation techniques applied to low and ultra-low permeability reservoirs.

DEDICATION

This thesis is dedicated to my family and friends.

ACKNOWLEDGEMENTS

I want to express thanks to the following people:

Dr. Tom Blasingame: for his supervision and high standard of perfection.

Dr. George Moridis: for his insightful advice and reviews during the course of this research.

Dr. Peter Valko and Dr. Yalchin Efendiev: for serving as members of my advisory committee.

TABLE OF CONTENTS

CHAPTER Page

LIST OF FIGURES

FIGURE Page

FIGURE Page

FIGURE Page

FIGURE Page

FIGURE Page

FIGURE Page

FIGURE Page

FIGURE Page

FIGURE Page

FIGURE Page

LIST OF TABLES

CHAPTER I

INTRODUCTION

1.1 Statement of the Problem

As conventional oil and gas reservoirs continue to be depleted, and the world's energy demand continues to increase, increasing emphasis is being placed on unconventional resources to fill the created gap. Currently, more than 25 percent of the natural gas daily production in the United States is derived from unconventional reservoirs (Naik, 2005). Although such reservoirs contain hydrocarbons, shale-gas, tight-gas, and tight/shale-oil reservoirs are considered unconventional because of their associated extremely low permeabilities compared to those in conventional reservoirs.

Unconventional reservoirs were overlooked in the past because of the low reservoir quality (as defined by low porosity and permeability) of the associated rocks. To produce from these formations, we need to stimulate the reservoir rock to overcome the low permeability challenge. The proposed Slot-Drill (hereafter referred to as "*SD"*) completion method that I investigated in this work is such a stimulation technique.

1.2 Objectives

The objectives of the proposed research were:

- To create unstructured grids using an adaptation of TAMMESH (Olorode, 2011), that would adequately discretize the reservoir in order to model the irregular and complex geometry of the "slot-drill" completion.
- To compare by means of numerical simulation the productivity improvement of the "slot-drill" method to that of hydraulically fractured reservoirs.
- To compare the performance of the detailed "slot-drill" model to that using a simplified approximation in order to determine if the latter approach can be used for future studies.

1.3 Importance

The potential advantages of the "slot-drill" completion strategy over multistage hydraulic fracturing (the industry's current preferred method of stimulation for these formations) include:

- The elimination of the massive volumes of water required for hydraulic fracturing.
- The control over the resulting fracture (slot) geometry and penetration.

This thesis follows the style and format of the *SPE Journal*.

- The reduced environmental impact (since it is a mechanical process and does not involve the introduction of the chemicals contained in hydraulic fracturing treatments to the subsurface).
- The creation of slots of about 1-1/2 inches with higher conductivities ($k_f w_f$) than typical hydraulic-fracture conductivities.
- The lower cost of implementing this method (about half the cost of a hydraulic fracturing job).

With such potential benefits, a rigorous study of the performance of this completion method was in order. In this study, I considered the performance of this completion method in three low-permeability reservoir systems. These are the Cotton Valley (tight-gas), Marcellus (shale-gas) and Bakken (tight/shale-oil) formations.

1.4 Reference Reservoir and Completion Parameters

The average reservoir and completion properties and parameters for the three formations used in this work are shown in Tables 1.1, 1.2 and 1.3.

Table 1.1—Representative Cotton Valley tight-gas parameters

Parameters	SI Units	Field Units
Fracture half-length, x_f	100 m	328.08 ft
Fracture width, w_f	3 mm	0.118 in
Slot width, w_{slot}	12.7 mm	0.5 in
Fracture spacing, d_f	108.86 m	357.14 ft
Well length, L_w	762 m	2500 ft
Number of fractures	7	7
Reservoir thickness, h	45.72 m	150 ft
Reservoir width, w	304.8 m	1000 ft
Permeability, k_{sand}	$5.92\text{x}10^{-18}$ m^2	$6.0\ \text{x}10^{-3}$ md
Fracture permeability, k_{frac}	$5.0\text{x}10^{-11}$ m^2	$5.07\ \text{x}10^{4}$ md
Slot permeability, k_{slot}	$1.0\text{x}10^{-10}$ m^2	$1.01\ \text{x}10^{5}$ md
Matrix porosity, ϕ	0.08	0.08
Fracture porosity, ϕ_{frac}	0.33	0.33
Temperature, T	119.44 ^{0}C	247 ^{0}F
Well radius, r_w	0.1 m	0.32 ft
Reservoir pressure, p_i	$2.864\text{x}10^{7}$ Pa	4154 psia
Well pressure, p_{wf}	$3.45\text{x}10^{6}$ Pa	500 psia

Table 1.2—Representative Marcellus shale-gas parameters

Parameters	SI Units	Field Units
Fracture half-length, x_f	100 m	328.08 ft
Fracture width, w_f	3 mm	0.118 in
Slot width, w_{slot}	12.7 mm	0.5 in
Fracture spacing, d_f	108.86 m	357.14 ft
Well length, L_w	762 m	2500 ft
Number of fractures	7	7
Reservoir thickness, h	45.72 m	150 ft
Reservoir width, w	304.8 m	1000 ft
Permeability, k_{sand}	7.402×10^{-20} m^2	7.5×10^{-5} md
Fracture permeability, k_{frac}	5.0×10^{-11} m^2	5.07×10^{4} md
Slot permeability, k_{slot}	1.0×10^{-10} m^2	1.01×10^{5} md
Matrix porosity, ϕ	0.09	0.09
Fracture porosity, ϕ_{frac}	0.33	0.33
Temperature, T	51.667 ^{0}C	125 ^{0}F
Well radius, r_w	0.1 m	0.32 ft
Reservoir pressure, p_i	2.413×10^{7} Pa	3500 psia
Well pressure, p_{wf}	3.45×10^{6} Pa	500 psia

Table 1.3—Representative Bakken tight-oil parameters

Parameters	SI Unit	Field Unit
Fracture half-length, x_f	100 m	328.08 ft
Fracture width, w_f	3 mm	0.118 in
Slot width, w_{slot}	12.7 mm	0.5 in
Fracture spacing, d_f	108.86 m	357.14 ft
Well length, L_w	762 m	2500 ft
Number of fractures	7	7
Reservoir thickness, h	12.50 m	41 ft
Permeability, k_{sand}	1.974×10^{-17} m^2	2.0×10^{-2} md
Reservoir width, w	1219.2 m	4000 ft
Fracture permeability, k_{frac}	5.0×10^{-11} m^2	5.07×10^{4} md
Slot permeability, k_{slot}	1.0×10^{-10} m^2	1.01×10^{5} md
Matrix porosity, ϕ	0.07	0.07
Fracture porosity, ϕ_{frac}	0.33	0.33
Temperature, T	76.667 ^{0}C	170 ^{0}F
Well radius, r_w	0.1 m	0.32 ft
Reservoir pressure, p_i	3.208×10^{7} Pa	4653 psia
Well pressure, p_{wf}	3.45×10^{6} Pa	500 psia

1.5 Validation

My research was conducted using TAMSIM (Freeman, 2010b), a fully-implicit, non-isothermal, multi-dimensional numerical simulator - based on the TOUGH+ family of codes (Moridis et al., 2010) - for the analysis of flow and transport in unconventional gas reservoirs. Freeman (2010b) presented a validation of TAMSIM using analytical solutions, the results from a commercial software package (ECLIPSE) and field data from the Haynesville shale formation. Additionally, Olorode (2011) provided another validation of TAMSIM using comparisons to forecasts made using the numerical model in KAPPA (Ecrin® product suite 2009), i.e., a commercial software package for shale/tight gas analysis. Select plots from these validation studies are shown in Fig. 1.1 and 1.2.

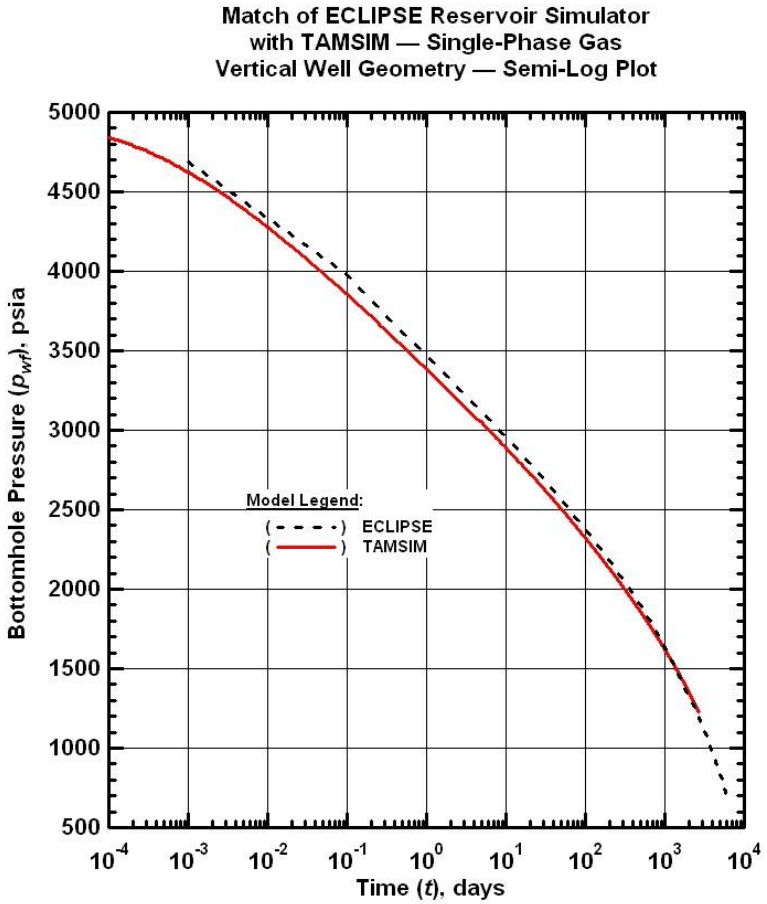

Fig. 1.1—A comparison of simulation results from TAMSIM and ECLIPSE (from Freeman 2010b)

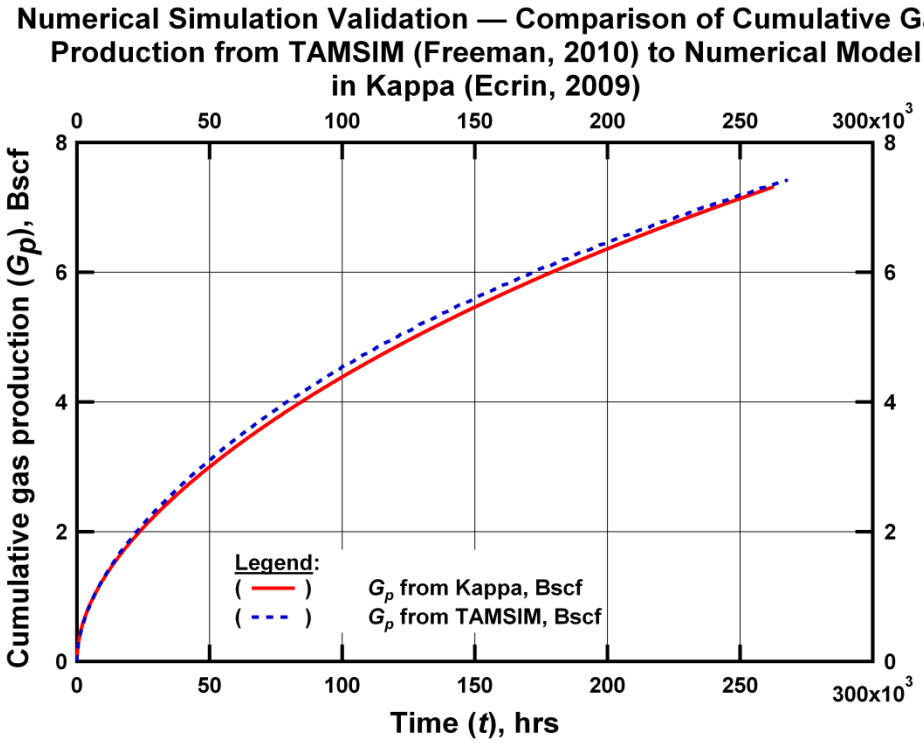

Fig. 1.2— Comparison of simulation results from TAMSIM and Ecrin® (2009); from Olorode (2011)

1.6 Research Overview

In this research, I studied the production performance of the "slot-drill" completion method in three low-permeability (tight-gas, shale-gas and tight/shale-oil) formations. Additionally, I investigated (a) the ability of an approximate SD representation to adequately model production from the "slot-drill" completion (as compared to that from a full representation), and (b) the production performance of a scenario where the SD method is combined with hydraulic fracturing to further boost production.

To accomplish the stated goals, I used a modified version of TAMMESH (Olorode, 2011), which is a 3D Voronoi mesh-maker that uses the voro++ library (Rycroft, 2007) to generate unstructured grid meshes, while conducting the fluid-flow simulations using TAMSIM, an unconventional-gas reservoir simulator developed at Texas A&M University (Freeman et al., 2010b). I developed algorithms for generating the unstructured grid centers needed to accurately represent the SD system in patterns that result in representative meshes for all the scenarios.

In the ensuing chapters, I discuss the model set-up, simulation results and my inferences and conclusions.

CHAPTER II

LITERATURE REVIEW

In this chapter I present a review of the current state of knowledge in the various subject areas upon which this research was based. I investigated the SD technique in its entirety, discussing in detail its concepts and processes. Additionally, I provide a brief overview of the geology of the selected formations, of modeling and production performance analysis in tight-gas, shale-gas and tight-oil reservoirs, and a review of the application of Voronoi Grids in petroleum (reservoir) engineering studies.

2.1 The “slot-drill” completion method

The proposed SD technique is an advanced cable-saw method that works like a "downhole hacksaw." It is suitable for application at depths ranging from 1,000 to 10,000 ft (Carter, 2009). It involves the use of a tensioned abrasive cable, which is attached to the drill-pipe, to create a slot perpendicular to the wellbore up to a hundred feet deep into the target formation (see Fig. 2.1). The SD is purported to provide a large surface area and a high-conductivity conduit in the low-permeability formation, thus enhancing hydrocarbon flow and production.

The process description is as follows. First, the well is drilled (to a predetermined kick-off depth in the target formation) and cased. This kick-off depth is usually a few feet into the target formation to ensure that the slot is formed within it. Next, the horizontal section of the well is drilled, but with the tip pointing upward in a mirrored J-like manner (as illustrated in Fig. 2.1). The drill string is then retrieved and the cutting abrasive cable is attached to its tip with a special downhole shoe-joint tool. The cable is a 1.5 in. diameter steel wire rope (Fig. 2.1). Note that Carter (2009) proposed a cable system with embedded diamond beads for more effecting cutting into the hydrocarbon-bearing tight formation.

On the rig, an automatic tension-regulating winch maintains a specific tension on the cable as the drill string assembly is lowered back into the hole. This tension prevents the pipe from turning and wrapping up the cable on its way back down. It also makes the abrasive cable "cling" to the inner radius of the curved wellbore, while the compressive forces (on the drill pipe) push the drill pipe against the outer radius.

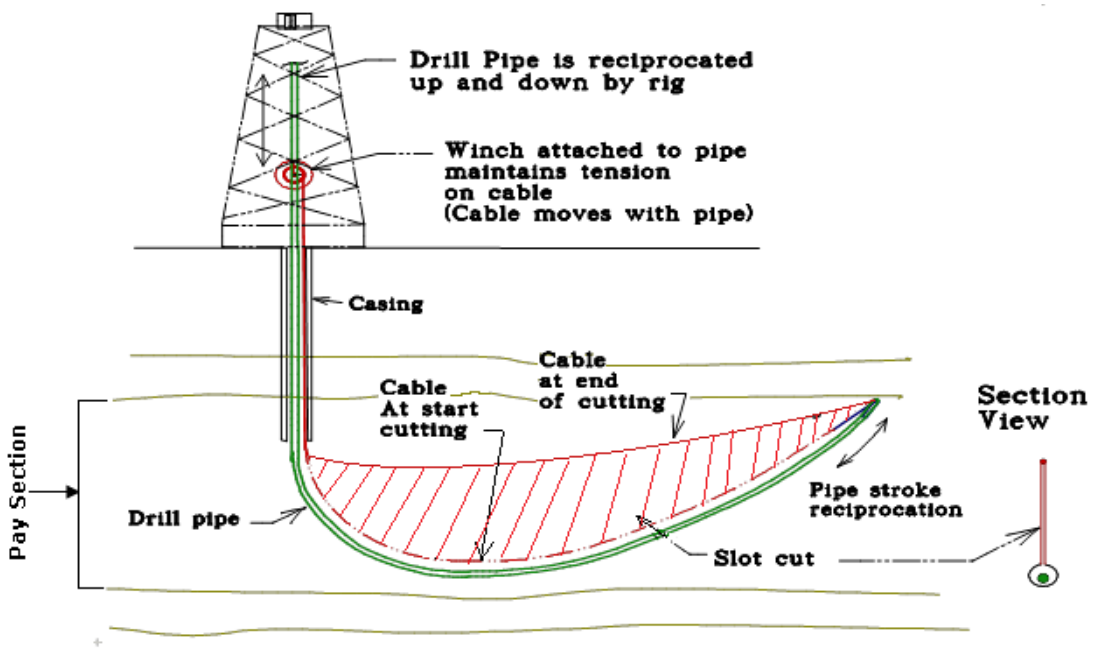

Fig. 2.1— Schematic of SD process with section view (Carter, 2009).

Fig. 2.2— Steel abrasive cable can cut through target formation (Carter, 2009).

The reciprocating "up and down" motion of this assemblage is the driving force on the "saw" to create the slot in the formation. The resulting cutting force at any point is a function of the local cable tension and the radius of curvature. This process is expected to yield a crescent-shaped slot, the thickness of which is controlled by the diameter of the cutting cable (1-1/2 in, as initially proposed by carter (2009)).

There are no prior numerical studies that quantitatively assess the effectiveness of the SD by fully describing the complexity of the system, so this study is the first such attempt. This said, Carter (2009) provided an initial estimate of productivity improvement stemming from the application of the SD

method. This was based on an approximation using the analytical method of distributed volumetric sources (DVS) (Valko and Amini, 2007), which assumes a production source of rectilinear geometry inside a surrounding rectilinear reservoir. Thus, in trying to estimate the improved productivity, the SD was represented by 10 boxes to try and capture the curved geometry. The study considered hypothetical isotropic and anisotropic reservoirs of large (4000 ft.) and moderate (400 ft.) thicknesses. The results of the study showed only moderate benefits of the SD in the reservoirs with large thicknesses, but significant improvements (up to 3 times increase in the productivity index) in those with moderate thicknesses (when compared to vertical and horizontal well production). The perceived shortcomings of this study are: (a) the failure to compare the performance of the SD completion with that of multistage hydraulic fracturing (which, as stated earlier, is the preferred completion method in unconventional reservoirs), (b) the use of disjointed boxes to represent the SD's complex geometry (see Fig. 2.3) (this representation is significantly different from the actual geometry of the SD completion), and (c) the use of a value of the transient flow productivity index as a measure for the comparison of the production performance of the SD against the vertical and horizontal well cases considered, which is inadequate since its value keeps changing with time.

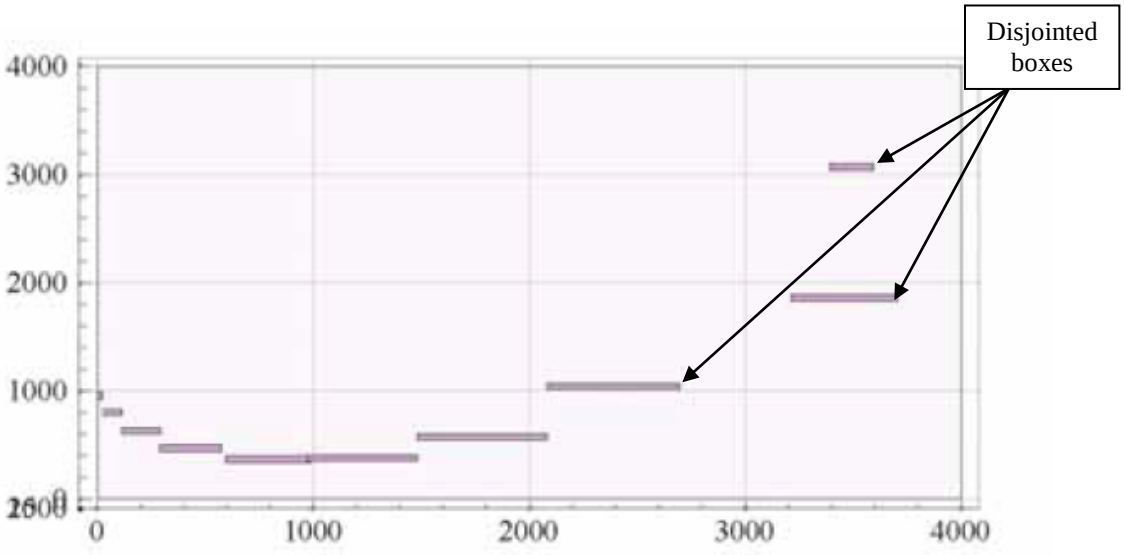

Fig. 2.3— Representation of the SD using Valko's model is different from the actual (length dimensions in feet); (from Carter 2009).

My study involved two computational components: (a) the use of a numerical simulator, developed by Freeman (2010b), that accounts for the various physical phenomena of importance in these type of reservoir systems, and (b) the use of unstructured (Voronoi) gridding for efficient spatial discretization. This approach was used so as to accurately estimate production performance, and facilitate diagnostic interpretations of flow behavior for low and ultra-low permeability formations completed using the SD.

2.2 Geology of the selected formations

As I already indicated in the previous chapter, the three formations I selected for the SD evaluation are (a) the Cotton Valley (a tight-gas formation), (b) the Marcellus (a shale-gas formation), and (c) the Bakken (a tight/shale-oil formation).

The Upper Jurassic and Lower Cretaceous Cotton Valley Group is an extensive, coastal strand-plain sandstone deposition in east Texas and in northwest Louisiana that overlies the Haynesville/Bossier shale. Although it comprises laminated shale, sandstone, and limestone deposits (Dyman and Condon, 2006), this study focused only on the productive sandstone formation.

The Marcellus shale is one of the main shale gas plays of North America in terms of total gas resource, extent, production rates, and economic potential. In the US, it covers regions in New York, northern and western Pennsylvania, eastern Ohio, western Maryland, and most of West Virginia. The organic-rich shale of the Marcellus was deposited in a foreland basin setting that was sediment-starved and allowed for accumulation and preservation of the organic material (Zagorski et al., 2011). The Marcellus Shale Formation occurs in the lower part of the Hamilton Group, which is bounded above by the Middle Devonian Tully Limestone and below by the Lower Devonian Onondaga Limestone. The Upper and Lower Marcellus Shale are separated by the Cherry Valley/Purcell Limestone.

The Bakken formation is a rock unit from the Late Devonian to Early Mississippian age that occupies about 200,000 square miles (520,000 km^2) of the subsurface of the Williston Basin. It covers parts of Montana, North Dakota, and Saskatchewan. It is divided into three rock units or members, comprising the 18-ft thick upper member, the 41-ft thick middle member and the 19-ft thick lower member (Boleneus, 2010). Both the upper and lower members contain a high percentage of organic carbon and are classified by some investigators as oil shales. The middle member is an argillaceous dolomite and has proven to be the most productive of the three so far, hence it being where recent industry activity has focused (Flannery and Kraus, 2006). Oil was first discovered within the Bakken in 1951, but early efforts to produce it were met with difficulties (Heck et al., 1994). However, recent advances in hydraulic-fracturing technology have caused a boom in oil production from the Bakken formation. By the end of 2010 oil production rates had reached 458,000 BOPD, outstripping the capacity to transport the produced oil from the region (FoxNews, 2011).

2.3 Modeling and production performance analysis in tight-gas, shale-gas and tight-oil reservoirs

Because of their associated very low permeabilities, analysis of production from these formations is more challenging than similar analysis in conventional reservoirs. Although there is a consensus that

there is still a lot we do not understand about the flow and storage mechanisms in these unconventional reservoirs, there is no dearth of published work that tries to bridge this gap. I in no way attempt to provide an extensive review of these attempts; however I highlight a few studies of interest.

Clarkson et al. (2011) classified the existing rate-transient and production analysis methods into: (a) straight-line (flow-regime) methods; (b) type-curve methods; (c) analytical and numerical simulation and (d) empirical methods. He argued that no single method could be relied solely upon, but a combination of several of these methods, in addition to sound reservoir engineering judgment, should be employed to analyze production data from such reservoirs.

Production from fractured tight-gas wells usually exhibit linear flow trends for most of the life of the well (Stright Jr. and Gordon, 1983). Wattenbarger et al. (1998) presented decline curve analysis techniques that are useful for such wells for both constant-rate and constant-bottomhole-pressure production cases. Their solutions were developed for vertical wells with fully penetrating hydraulic fractures in rectangular reservoirs. They illustrated how the use of log-log plots of dimensionless rate (or pseudo-pressure difference in the constant-rate production case) versus dimensionless time and square-root of time plots could be used to analyze tight-gas production data.

Of the three target formations being considered, most of the recent work seems to have concentrated on shale-gas formations. To investigate the impact of the various flow and transport phenomena believed to be prevalent in such reservoirs, Freeman et al. (2009) used a representative well/fracture/matrix repetitive element ("stencil") for their simulations, and they evaluated the influence of various reservoir and completion parameters on the performance of multiply-fractured horizontal wells in such ultra-low permeability gas reservoir systems. These parameters included fracture spacing, fracture conductivity, desorption, matrix permeability, and the presence or absence of complex fractures, natural fractures and high-conductivity layers.

Freeman (2010a) also investigated the effect of microscale flow phenomena on the production performance of gas from shale and tight gas-systems, and concluded that that the concentration of the produced was affected by the Knudsen diffusion (Civan, 2010) in nano-pores. Freeman (2010a) highlighted the potential of applying this phenomenon as a diagnostic tool, i.e., using the measured gas composition over time to determine the formation intrinsic permeability and to identify the flow boundaries. For details of the underlying concepts, assumptions, equations and findings, the interested reader is referred to his thesis dissertation (Freeman, 2010b). Insights and conclusions from these studies had a large influence on how we structured and set up our simulation runs. Studies by Moridis et al. (2010) also yielded similar conclusions to those of Freeman.

Cipolla, Lolon and Erdle et al. (2009), and Cipolla, Lolon and Mayerhofer (2009) investigated the mechanism of fluid-flow in shale-gas systems. By performing numerical simulations on reservoir models representative of the Barnett and Marcellus shale formations, the authors evaluated the relative importance of desorption and stress-dependent fracture conductivity on overall gas production in shale-gas systems. They did not employ the conventional planar representation of fractures, but simulated an effective stimulated reservoir volume (SRV) — an approach buttressed by microseismic data trends in shale-gas formations. The results of the simulations showed that the effect of desorption only becomes significant during the latter part of the life of a reservoir when pressures are significantly low.

Tight-oil/shale-oil production analysis has also benefitted from the extensive work done on their gas counterparts. Clarkson and Pedersen (2010) presented an analysis method that adapted the then existing rate-transient analysis techniques to tight-oil production analysis. Their workflow, which was made up of three stages (flow-regime/straight-line analysis, type-curve analysis, and reservoir simulation) was shown to perform well for a wide range of reservoir and fracture properties. Their study was conducted under single-phase liquid assumptions and is thus only accurately applicable to undersaturated (above bubble point) reservoirs.

2.4 Use of Voronoi grids in Petroleum (Reservoir) Engineering studies

A Voronoi block, also referred to as a perpendicular bisector (PEBI) or unstructured gridblock, is defined as a region of space that is closer to its gridpoint than any other gridpoint, and a Voronoi grid is made up of such blocks (Palagi and Aziz, 1994). By a gridpoint, I mean the center of a gridblock at which solutions are evaluated. The Voronoi grid has the property that individual gridpoints can be placed anywhere inside the domain, regardless of the position of any other grid point. This flexibility enables the accurate description and capturing details of complex geometries and heterogeneities in reservoirs to be simulated.

Vestergaard et al. (2007) presented a case study in which this gridding scheme was used in the simulation and history-matching of a large, complex, low permeability, carbonate reservoir in Qatar, the development of which had been completed with many long horizontal wells. The lateral magnitude of the field (Al Shaheen) and the multiple radial layouts of the very long horizontal wells posed a challenge in the effort to model the individual well performance using a manageable grid size, and within an acceptable run time when history-matching. The use of PEBI grids around each individual wellbore addressed this challenge by allowing for sufficient resolution between wells and alignment of the grid with the well paths to prevent non-orthogonality issues.

In this research, I employed the flexibility this gridding scheme affords to generate meshes that were accurately representative of the complex geometries of the SD schemes investigated.

CHAPTER III

SETUP OF SIMULATION MODELS

This chapter describes how I developed the numerical simulation models for my study, with emphasis on the gridding algorithms used to generate the representative meshes. My study involved two major components: (a) construction of the simulation grids to accurately represent the cases under study, and (b) conducting simulation runs with TAMSIM (Freeman, 2010b) for comparative analysis.

As part of this study, I developed a set of codes to generate gridblock centers in patterns that yield meshes that capture accurately the desired geometries. These centers were then imported into the "voro++" (Rycroft, 2007) Voronoi library to provide the Voronoi tessellations that yield the Voronoi or "perpendicular bisector" (PEBI) grids; an adaptation of TAMMESH (Olorode, 2011) was then used to convert the output from "voro++" to a format that is compatible with the TAMSIM reservoir simulator. The different geometries that I described by Voronoi grids are:

a) A horizontal well only
b) A curved well only (just the well, without the slot). This geometry is studied to assess whether the extra well length resulting from the curved well-geometry of the SD method provides a production advantage.
c) The SD completion method (the curved well with the slot above it)
d) An approximate way of representing the SD ("equivalent SD representation")
e) A horizontal well with multistage hydraulic fracturing
f) A combination of the SD completion method with multistage hydraulic fracturing

In creating the various meshes representative of these geometries, arrays of gridblock centers were generated to spatially discretize the reservoir domain. To carry out this discretization in the most representative fashion, these gridblock centers were arranged in such a way that they formed different geometric patterns in different parts (regions) of the reservoir domain. This was possible because Voronoi gridding schemes allow for such flexibility. The gridblock centers were described by their Cartesian (XYZ) coordinates. In ensuing discussions, these gridblock centers are simply referred to as "centers" or "points". The subsequent discussion is divided into sections to discuss the algorithms implemented for each of the aforementioned geometries. These sections are further subdivided into subsections that focus on the different regions within the reservoir domain (for the particular geometry being considered). I have also inserted relevant code segments (written in FORTRAN 95/2003) that show how the algorithms were implemented in the code. Where referenced in the discussion, the code variables are written in italics.

3.1 Discretizing the horizontal well system (Geometry A)

In generating the points for the horizontal well geometry, I created a grid system with a circular/cylindrical pattern around the wellbore to emphasize radial flow in that region and a rectangular pattern (regular Cartesian grid) farther away from the well. The well was placed right at the center of the reservoir domain. Details of this implementation are discussed in the following sections.

3.1.1 Geometry A: Generating the coordinates for the well centers (Region A1)

Computing the coordinates of the well centers in this case was quite straight forward. The Y and Z coordinates were simply just half of the reservoir dimensions in those respective directions, while the X coordinates were obtained by dividing the reservoir X dimension by the desired number of X segments or subdivisions (as specified in the code inputs). The FORTRAN (95/2003) code listing shown in Fig. 3.1 illustrates how this is accomplished in the code.

```
!
      centers_distance = ( Length_X/REAL(num_x_div) )
!
!**********************************************************************
!*                                                                    *
!*                      COMPUTING THE WELL POINTS                     *
!*                                                                    *
!**********************************************************************
!
      Well_Centers_DO: DO i=1,num_well_centers
!
! -------
! ... Compute the x-coordinate
! -------
!
         well_centers(i,1) = ( REAL(i) - 0.5d0 ) * centers_distance
!
! -------
! ... Compute the y-coordinate
! -------
!
          well_centers(i,2) = (0.5d0 * Length_Y)
!
! -------
! ... Compute the z-coordinate
! -------
!
          well_centers(i,3) = -( 0.5d0 * Length_Z )
!
!
      END DO Well_Centers_DO
!
```

Fig. 3.1—FORTRAN (95/2003) code for computing the coordinates of the well centers (Geometry A)

3.1.2 Geometry A: Generating the coordinates for the cylindrical points around the well (Region A2)

In this region, the code was set up to place points out radially from the earlier determined well centers in gridblocks of logarithmically increasing dimensions. This resulted in increasing gridblock sizes as the distance from the well center increased. The logarithmic spacing was computed using the geometric series given below:

$$\Delta r_{i+1} = \Delta r_i \times f \quad \text{..... 3.1}$$

Where:

Δr_i is the radial increment (subdivision) of gridblock i, the center of which is at a distance r_i from the origin of axes. When $i = 0$, this represents the initial radial increment.

Δr_{i+1} is the is the radial increment (subdivision) of gridblock i+1, i.e., the griblock next to gridblock i and whose center is at a radius $r_{i+1} > r_i$.

f is the increment factor (greater than 1) that determines the rate at which the value of Δr increases.

The initial radial increment (i=0) was set to twice the wellbore radius (r_w) so that the well cell boundary, which is the perpendicular bisector (PEBI) of the distance between the center and the first point, would be exactly r_w away from the center.

Once a Δr_{i+1} has been determined, points that fall on the circumference of a circle with radius of length Δr_{i+1} are then computed. The number of equally-spaced points (n) on the circumference (see Fig 3.2) to be used to approximate the circular geometry around the wellbore was set as a user-specified code input.

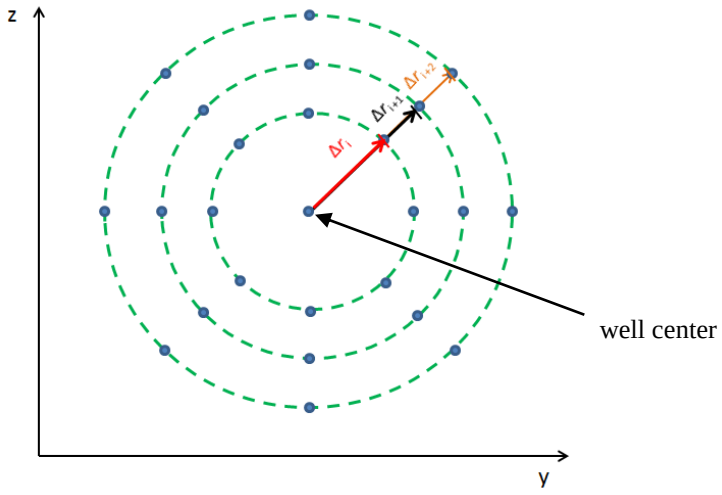

Fig. 3.2—Schematic illustrating how points in Region A2 were placed around each well center in a circular pattern (in this case, n=8).

The FORTRAN (95/2003) code segment in Fig. 3.3 illustrates how the coordinates of the points in Region A2 were computed.

```
! ... Computations
!
      DO_Center: DO m=1,num_well_centers
!
         DO_Polygon: DO n=1, poly_sides
!
            val = 0.0d0 ! Initialize the displacement from well center
!
            DO_Incr: DO p=1, chosen
!
               IF (p < chosen) THEN
                 incr = cyl_init_radius*(cyl_incr_ratio**(p-1))
                 val  = val + incr
               ELSE
                 test = (half_Z - val) / 3.0d0                  ! working with old val
                 incr = cyl_init_radius*(cyl_incr_ratio**(p-1))
                 val  = val + incr
                 test2= (half_Z - val)
                 IF (test2 < test) val = half_Z - test
                 max_val = val
               END IF
!
               y_coord = (0.5d0*Length_Y) - ( val * COS(deg_to_rad*(REAL(n)/REAL(poly_sides))*360.0d0) )
!
               z_coord = ( val * SIN(deg_to_rad*(REAL(n)/REAL(poly_sides))*360.0d0) ) - (0.5d0*Length_Z)
!
               x_coord = well_centers(m,1)
!
               IF ( p == chosen .AND. n == (poly_half+1) ) z_down = z_coord
               IF ( p == chosen .AND. n == 1 ) z_up = z_coord
!
               IF (y_coord < 0.0d0 .OR. y_coord > Length_Y .OR. z_coord > 0.0d0 .OR. z_coord < z_deep .OR.
&
 &                 x_coord < 0.0d0 .OR. x_coord > Length_X) THEN
!
                 CYCLE DO_Polygon
!
               ELSE
!
                 counter = ((m-1)*poly_sides*max_num_plus1)+((p-1)*poly_sides) + n
!
                 DOI_points(counter,1) = x_coord
                 DOI_points(counter,2) = y_coord
                 DOI_points(counter,3) = z_coord
!
               END IF
!
            END DO DO_Incr
!
         END DO DO_Polygon
!
      END DO DO_Center
```

Fig. 3.3—FORTRAN (95/2003) code for computing the coordinates of points in Region A2 (Geometry A)

3.1.3 Geometry A: Generating the coordinates of the points arranged in a rectangular pattern in the region farther from the well (Region A3)

This region encompassed the volume in the reservoir domain that was farther from the well (outside of region A2). The points were arranged in rectangular patterns in five layers across the Z axis. The X coordinates correspond with those of the well centers, while the Y coordinates become progressively

coarser (following a logarithmic pattern as the one described earlier) as the distance from the well center increases. The FORTRAN (95/2003) code listed in Fig. 3.4 shows how these points were computed.

I showed different views of the final mesh developed to represent Geometry A in Fig. 3.5 and Fig. 3.6.

```
      DO_Center_2: DO m=1,num_well_centers
!
         val = max_val ! Initialize the displacement from well center
!
         DO_Cart_Y: DO n=chosen, cart_chosen
!
            IF (n < cart_chosen) THEN
              incr = cyl_init_radius*(cyl_incr_ratio**(n-1))
              val  = val + incr
            ELSE
              test = (half_Y - val) / 3.0d0                  ! working with old val
              incr = cyl_init_radius*(cyl_incr_ratio**(p-1))
              val  = val + incr
              test2= (half_Y - val)
              IF (test2 > test) val = half_Y - test
            END IF
!
            DO_Cart_Incr: DO p=1, 5
!
               IF ( p == 1 ) THEN
                 z_coord = -half_Z
               ELSE IF ( p == 2 ) THEN
                 z_coord = z_up
               ELSE IF ( p == 3 ) THEN
                 z_coord = z_down
               ELSE IF ( p == 4 ) THEN
                 z_val = (-z_up)/3.0d0
                 z_coord = -z_val
               ELSE
                 z_val = (Length_Z + z_down)/3.0d0
                 z_coord = z_val - Length_Z
               END IF
!
               y_coord_1 = half_Y - val
               y_coord_2 = half_Y + val
               x_coord = well_centers(m,1)
!
               IF (y_coord_1 < 0.0d0 .OR. y_coord_1 > Length_Y .OR. & y_coord_2 < 0.0d0 .OR. &
&                  y_coord_2 > Length_Y .OR. z_coord > 0.0d0 .OR. z_coord < z_deep .OR. &
&                  x_coord < 0.0d0 .OR. x_coord > Length_X) THEN
!
                 CYCLE DO_Cart_Incr
               ELSE
                 counter_1 = ((m-1)*2*cart_chosen*5)+((n-1)*5) + p
                 counter_2 = (cart_chosen*5) + counter_1
!
                 cartesian_points(counter_1,1) = x_coord
                 cartesian_points(counter_1,2) = y_coord_1
                 cartesian_points(counter_1,3) = z_coord
!
                 cartesian_points(counter_2,1) = x_coord
                 cartesian_points(counter_2,2) = y_coord_2
                 cartesian_points(counter_2,3) = z_coord
!
               END IF
!
            END DO DO_Cart_Incr
!
         END DO DO_Cart_Y
!
      END DO DO_Center_2
```

Fig. 3.4—FORTRAN (95/2003) code for computing the coordinates of points in Region A3 (Geometry A)

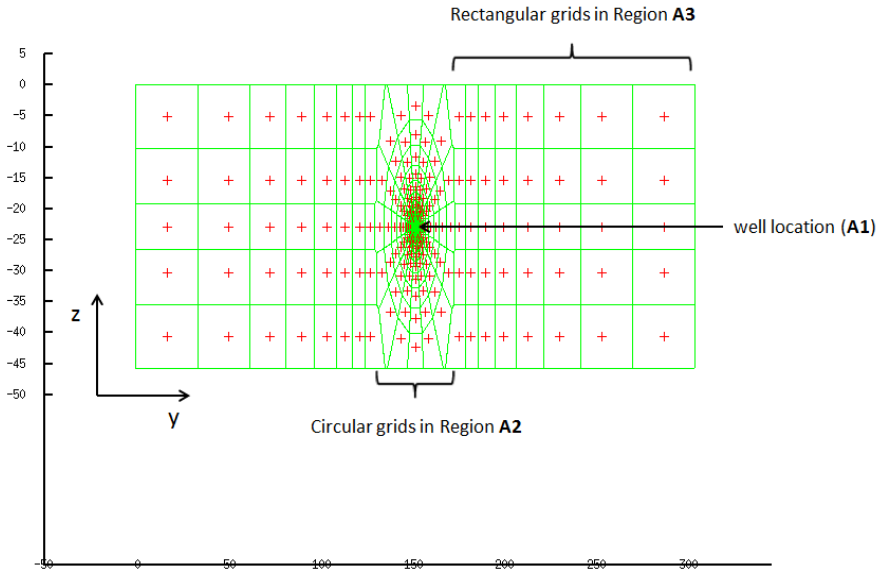

Fig. 3.5—Visualization of the mesh generated to discretize the domain in the case of Geometry A: Horizontal well only (front view/Y-Z plane)

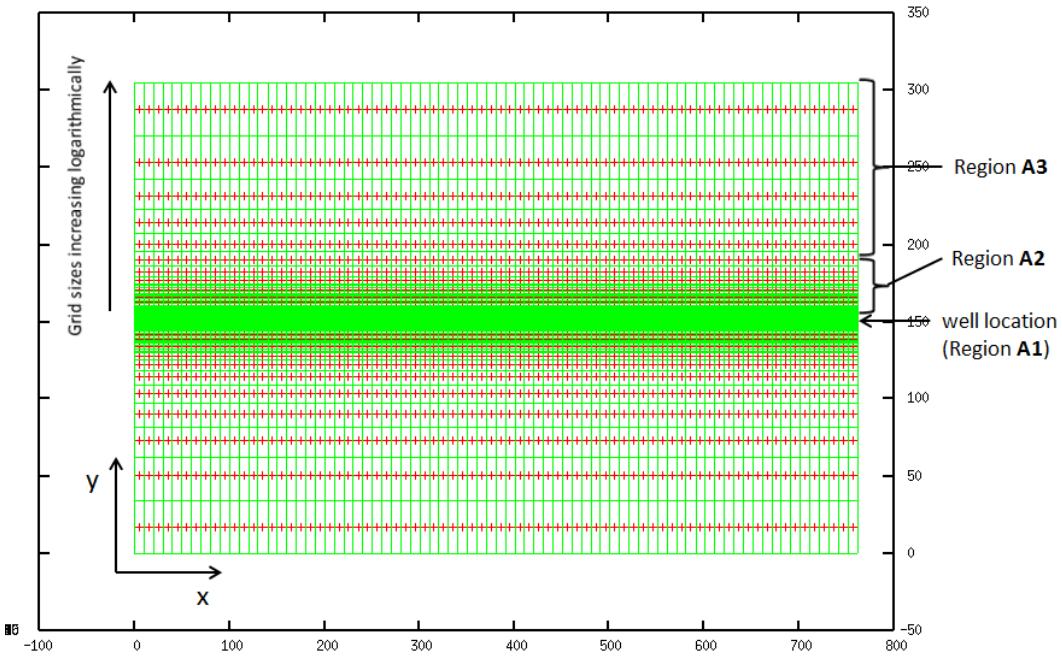

Fig. 3.6—Visualization of the mesh generated to discretize the domain in the case of Geometry A: Horizontal well only (plan view/X-Y plane)

3.2 Discretizing the curved well system (Geometry B)

Here the objective was to develop the grid describing in a representative manner the curvature of the SD completion (including the well and the slot). In this case the grid development was more complicated and demanding because not only did it include cylindrical-type grids around the well, but it also needed to describe the initial well curve along the length of the well. The approach I followed was to work in terms of inclined planes along the X-axis. Details of this implementation are discussed in the following sections.

3.2.1 Setup concept and some key code setup parameters

Since the SD completion requires a wellbore with a curved trajectory, I modeled this as an arc belonging to a circle with radius, *ROC* (Radius of Curvature) and which substends an angle, *arc_angle* at the center of the circle. The arc angle is estimated based on the constraint that the distance from the deepest point of the arc to its chord has to be equal to the slot height, *h_slot* (a user-specified input). The dotted red lines in Fig. 3.7, which divide the arc sector into smaller sectors, become planes when one considers the third dimension (the Y dimension). It is on these planes that the code is set up to place all the points in order to get the desired curved well trajectory. The planes are separated from each other by a user-specified angular difference, *omega*. The angle made by each plane (the dotted red lines) with the normal (the solid red line) was computed and stored as a property of each plane and was considered positive if the plane was to the right of the normal and negative if otherwise. This angle (*alpha*) was used to resolve the location of the points on that plane to orthogonal (XYZ) coordinates. The FORTRAN (95/2003) code listed in Fig. 3.8 illustrates the algorithm used to compute these key parameters.

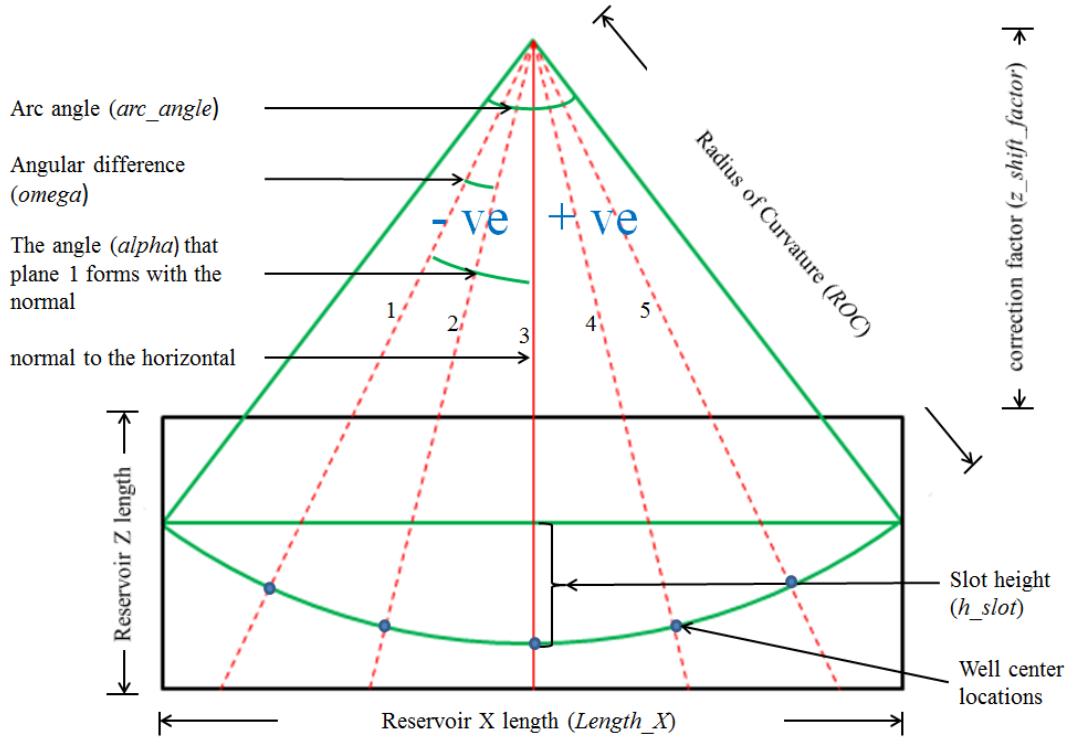

Fig. 3.7—Schematic illustrating the geometric characteristics of the curved well (Geometry B) and the corresponding grid design.

```
!
! -------
! ... Computing the arc angle
! -------
!
   angle_1    = 90.0d0 - ( rad_to_deg * ATAN(2.0d0*h_slot / Length_X) )
!
   arc_angle  = 360.0d0 - (4.0d0*angle_1)
!
   radius_of_curvature = Length_X / (2.0d0 * SIN(arc_angle*deg_to_rad/2.0d0))
!
   num_well_centers = INT(arc_angle/omega) + 1
!
   centers_angle = ( omega * REAL(num_well_centers-1) )  ! Total angle btwn d choosen centers
!
   trunc_angle = arc_angle - centers_angle   ! Angle cut off on edges
!
! -------
! ... Computing the correction factor based on the radius of curvature
! -------
!
! Assuming the configuration is placed right in the middle of the formation
!
   deepest_well_depth = h_slot + r_w + ( (Length_Z - (h_slot + r_w))/2.0d0 )
!
   z_shift_factor     = radius_of_curvature - deepest_well_depth
!
```

Fig. 3.8—FORTRAN (95/2003) code for computing the key setup parameters for the Geometry B mesh

3.2.2 Geometry B: Generating the coordinates for the well centers (Region B1)

As shown earlier in Fig. 3.7, the well centers were located where the planes intersect the arc. In the third dimension (the Y dimension), the centers were located in the middle (half of the Y length). The FORTRAN (95/2003) code listed in Fig. 3.9 shows how I implemented the algorithm to compute the well center coordinates.

```
! -------
! ... Computing the well centers
! -------
!
   Well_Centers_DO: DO i=1,num_well_centers
!
! ... Compute alpha
!
      well_centers(i,4) = (0.5d0*trunc_angle) - (0.5d0*arc_angle) + ((REAL(i-1) &
&                         /REAL(num_well_centers- 1) )*centers_angle)
!
! ... Compute the x-coordinate
!
      well_centers(i,1) = (0.5d0 * Length_X) + (radius_of_curvature * &
&                         SIN(deg_to_rad*well_centers(i,4)))
!
! ... Compute the y-coordinate
!
      well_centers(i,2) = (0.5d0 * Length_Y)
!
! ... Compute the z-coordinate
!
      well_centers(i,3) = -( (radius_of_curvature*COS(deg_to_rad*well_centers(i,4))) &
&                        - z_shift_factor )
!
!
   END DO Well_Centers_DO
```

Fig. 3.9—FORTRAN (95/2003) code for computing the coordinates of the well centers (Geometry B)

3.2.3 Geometry B: Generating the coordinates for the circular-patterned points around the well (Region B2)

The points here were computed similarly to how they were computed in the straight well case (region A2 in Geometry A). In this case however, the points in region B2 were arranged to form a curved cylindrical ("banana-like") shape around the well (following the curved well trajectory). The FORTRAN (95/2003) code listed in Fig. 3.10 shows the part of the computation of the coordinates of points in region B2 that differs from the code for its straight well counterpart (region A2).

```
!
 y_coord = (0.5d0*Length_Y) - &
&          ( val * COS(deg_to_rad*(REAL(n)/REAL(poly_sides))*360.0d0) )
!
 z_coord_plane = radius_of_curvature - &
&                ( val * SIN(deg_to_rad*(REAL(n)/REAL(poly_sides))*360.0d0) )
!
 z_coord = - ((z_coord_plane * COS(deg_to_rad*expanded_well_centers(m,4))) - &
              z_shift_factor)
!
 x_coord = (0.5d0*Length_X) + &
           (z_coord_plane * SIN(deg_to_rad*expanded_well_centers(m,4)))
!
```

Fig. 3.10—FORTRAN (95/2003) code for computing the coordinates of points in region B2 (Geometry B)

3.2.4 Geometry B: Generating the coordinates of the points arranged in a rectangular pattern in the region farther from the well (Region B3)

The points in this region were generated similar to how they were generated in region A3 (see section 3.1.3).

Fig. 3.11 shows the side view of the resulting mesh generated for Geometry B while Fig. 3.12 shows the cross-sectional view of a slice taken halfway along the X-axis.

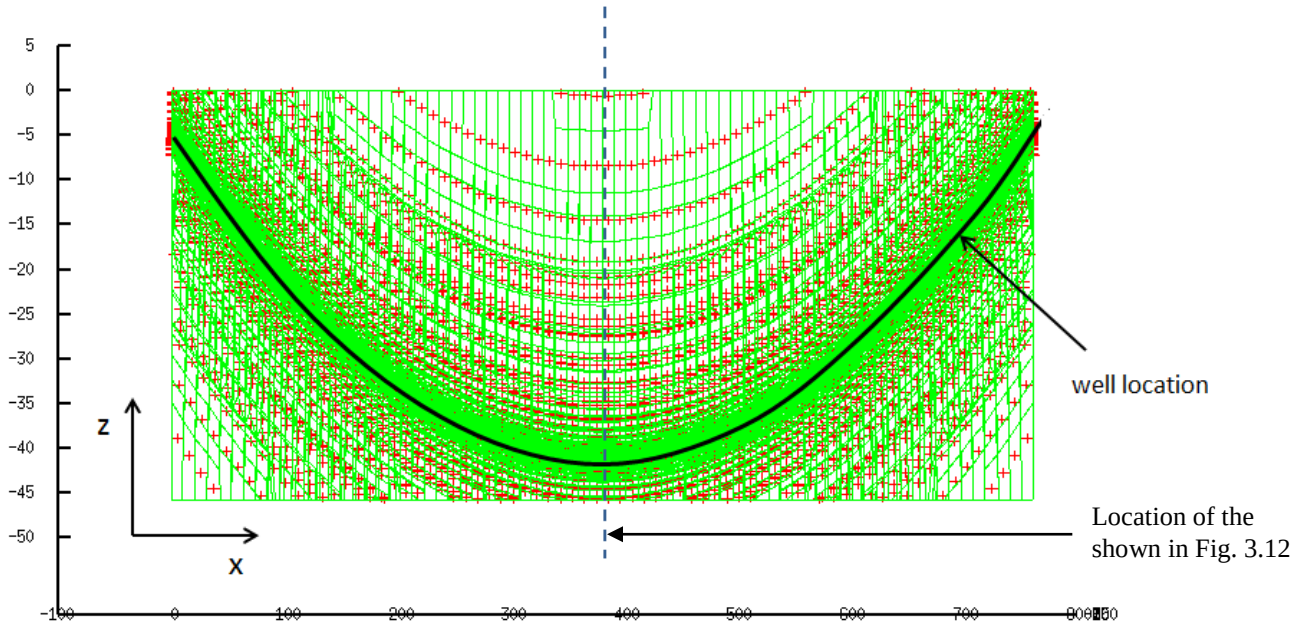

Fig. 3.11—Visualization of the mesh generated to discretize the domain in the case of Geometry B: Curved well only (side view/X-Z plane)

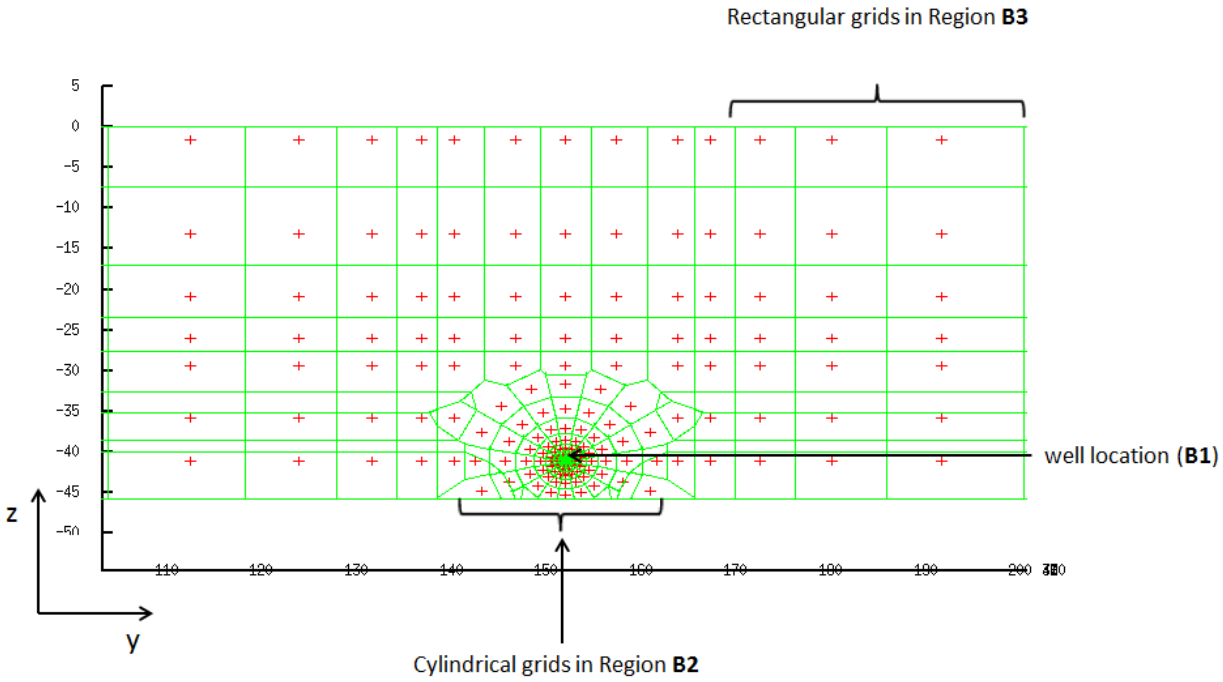

Fig. 3.12—Geometry B: Cross-sectional view of a slice taken on the plane normal to the X-axis, at X = 362m (front view/Y-Z plane)

3.3 Discretizing the SD system (Geometry C)

When implemented, the SD process is expected to create a slot that has a chord-segment shape. The spatial discretization of the simulation model in this case was by far the most challenging. It involved putting together more regions than in the previous geometries. The ensuing sections discuss how I carried out the discretization of this system.

3.3.1 Geometry C: Generating the coordinates for the well center points (Region C1)

The wells were placed along the arc trajectory, as was the case in the curved well of the Geometry B case (see Section 3.2.2). However, here the plane angles (*alpha*) were back-calculated based on predetermined X coordinates. This is because the gridblocks corresponding to the slot above the elements describing the curved well have fixed distances (*centers_distance*) between them (based on the number of desired subdivisions of the reservoir in the X direction specified by the user). The FORTRAN (95/2003) code listed in Fig. 3.13 illustrates how I generated the well center coordinates.

```
!
    Well_Centers_DO: DO i=1,num_well_centers
!
!----
! Compute alpha
!----
!
      well_centers(i,4) = rad_to_deg * ASIN( ( ((REAL(i)-0.5d0)*centers_distance + &
&                       (0.5d0*trunc_distance)) - half_X ) / ROC_buffer )
!
!----
! Compute the x-coordinate
!----
!
      well_centers(i,1) = half_X + ( radius_of_curvature * SIN(deg_to_rad*well_centers(i,4)) )
!
!----
! Compute the y-coordinate
!----
!
      well_centers(i,2) = half_Y
!
!----
! Compute the z-coordinate
!----
!
      well_centers(i,3) = -( ( radius_of_curvature * COS(deg_to_rad*well_centers(i,4)) ) &
&                       - z_shift_factor )
!
!
    END DO Well_Centers_DO
!
```

Fig. 3.13—FORTRAN (95/2003) code for computing the coordinates of the well centers (Geometry C)

3.3.2 Geometry C: Generating the coordinates for the circular-patterned points around the bottom of the well (Region C2) and top of the slot (Region C3)

The circular-patterned points above the slot were computed just as the points in the case of Region A2 (see Section 3.1.2), while those below were computed just as in the case of Region B2 (see Section 3.2.3).

3.3.3 Geometry C: Generating the coordinates for the points in the region representing the slot (Regions C4 & C5)

As stated earlier, the slot has the shape of an arc segment. The upper part of the slot (Region C4) was discretized using a rectangular arrangement of points to form a Cartesian grid. The size of the gridblocks in this region was a user specified code input. As with the earlier geometries discretized, the well and slot were placed in the middle (half of the Y length) of the Y axis of the domain. The simple FORTRAN 95/2003 instructions and DO loop used to carry out these computations are shown in Fig. 3.14.

```
      Slot_Centers_2_DO: DO j=1,num_slot_z_divisions_plus1
!
! -------
! ... Compute counter
! -------
!
          counter = ( (i-1)*max_slot_z_divisions_plus1) + j
!
! -------
! ... Compute the z-coordinate
! -------
!
          IF (j == 1) THEN
          slot_centers(counter,3) = slot_top_z_coord - init_cart_z_disp
          ELSE
          slot_centers(counter,3) = slot_top_z_coord - ( (REAL(j-1)-0.5d0) * slot_block_z ) &
&         - init_cart_z_disp
          END IF
!
! -------
! ... Compute the x-coordinate
! -------
!
          slot_centers(counter,1) = slot_top_centers(i,1)
!
! -------
! ... Compute the y-coordinate
! -------
!
          slot_centers(counter,2) = half_Y
!
!
       END DO Slot_Centers_2_DO
```

Fig. 3.14—FORTRAN (95/2003) code for computing the coordinates of points in region C4 (Geometry C)

The bottom boundary of the slot was shaped like an arc. As a result, close to the bottom boundary, I changed the discretization from Cartesian grids (in the upper part of the slot) to grids that follow the curved trend along the bottom. This was done by placing points in inclined planes like was done for Geometry B (see section 3.2.1). The thickness of this curved lower part of the slot (Region C5) was also a user specified code input. The FORTRAN (95/2003) code listed in Fig. 3.15 illustrates how I generated the points (*buffer_centers*) in this region.

```
!
  DO_buffer_centers: DO i=1, num_well_centers
!
     val = 0.0d0 ! Initialize the displacement from well center
!
     DO_buffer_centers_2: DO j=1, buffer_max_num_incr
!
        incr = init_cart_z_disp*(cyl_incr_ratio**(j-1))
        val  = val + incr
!
!
        y_coord = half_Y
!
        z_coord_plane = radius_of_curvature - val
!
        z_coord = - ( (z_coord_plane * COS(deg_to_rad*well_centers(i,4))) &
&                 - z_shift_factor )
!
        x_coord = half_X + (z_coord_plane * SIN(deg_to_rad*well_centers(i,4)))
!
        IF (y_coord < 0.0d0 .OR. y_coord > Length_Y .OR. &
 &          z_coord > slot_top_z_coord .OR. z_coord < z_deep .OR. &
 &          x_coord < 0.0d0 .OR. x_coord > Length_X) THEN
!
          CYCLE DO_buffer_centers
!
        ELSE
!
          counter = ( (i-1)*buffer_max_num_incr) + j
!
          buffer_centers(counter,1) = x_coord
          buffer_centers(counter,2) = y_coord
          buffer_centers(counter,3) = z_coord
          buffer_centers(counter,4) = well_centers(i,4)
!
        END IF
!
      END DO DO_buffer_centers_2
!
   END DO DO_buffer_centers
!
```

Fig. 3.15—FORTRAN (95/2003) code for computing the coordinates of points in region C5 (Geometry C)

3.3.4 Geometry C: Generating a Cartesian grid on both sides of the slot (Regions C6 & C7)

To discretize the volume of the domain on the sides of the slot, I set up a Cartesian grid system. The procedure I followed here was similar to how I discretized region A3 of Geometry A (see section 3.1.3). Farther away from the slot (region C7), I employed a coarser (but still Cartesian) gridding scheme. A user specified code input determined the distance from the slot at which the coarse gridding started.

Fig. 3.16 shows the side view of the resultant mesh from the discretization of Geometry C. I inserted Fig. 3.17 (a slice taken at X = 125 m) to show some of the earlier discussed regions that cannot be seen in Fig. 3.16. Finally, Fig. 3.18 shows a 3D view of the mesh.

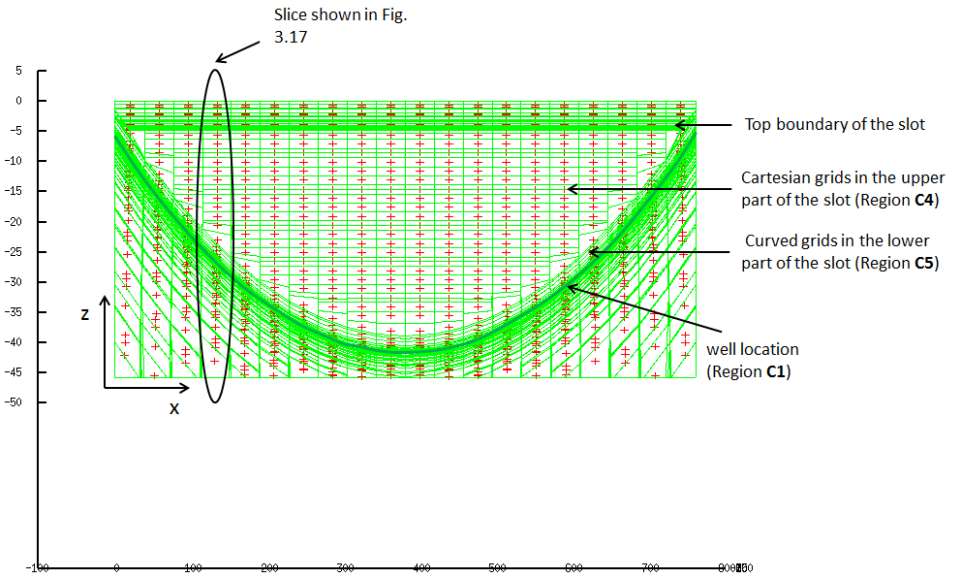

Fig. 3.16—Visualization of the mesh generated to discretize the domain in the case of Geometry C: SD completion (side view/X-Z plane)

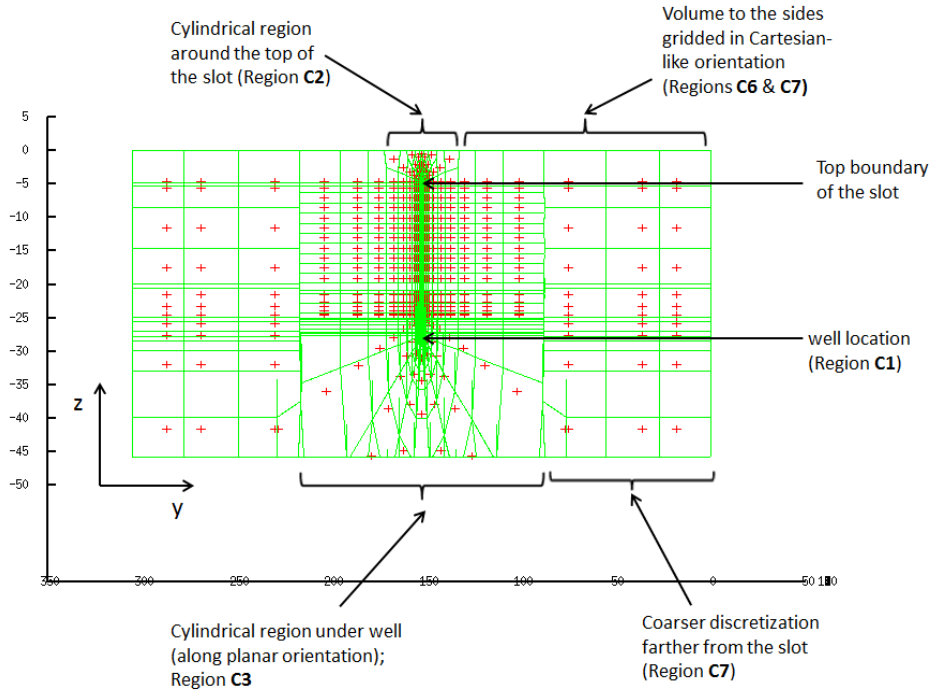

Fig. 3.17—Geometry C: Cross-sectional view of a slice taken on the plane normal to the X-axis, at X = 125 m (front view/Y-Z plane)

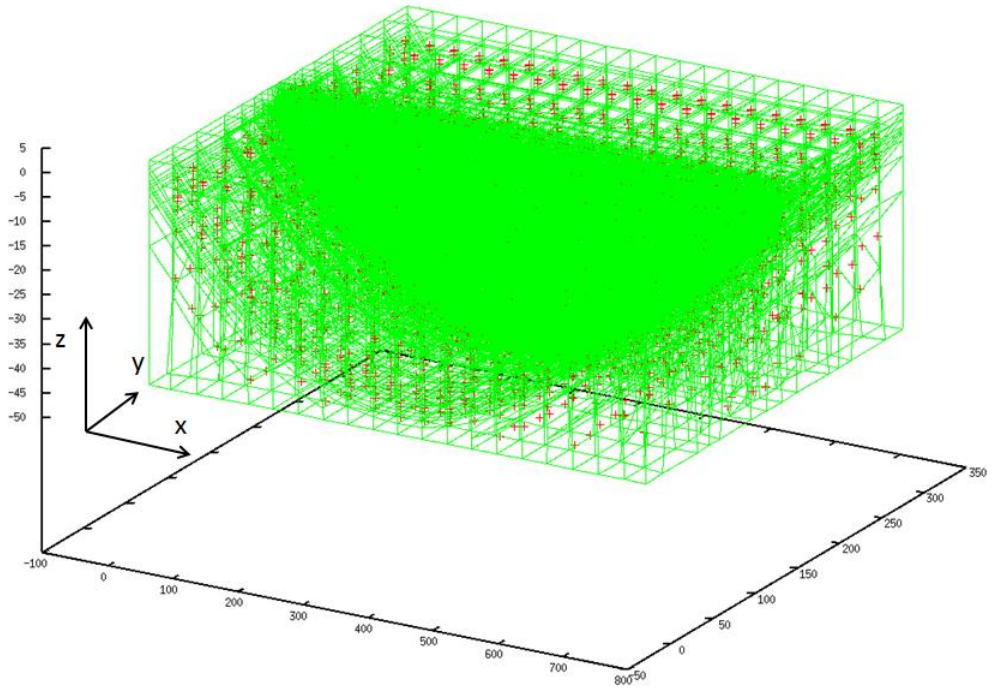

Fig. 3.18—3D-visualization of the mesh generated to discretize the domain in the case of Geometry C: SD completion

3.4 Discretizing the system with an approximate representation for the SD geometry (Geometry D)

The SD geometry is most faithfully depicted and discretized as an arc segment through the process described in Section 3.3. However, this gridding approach was complex, cumbersome and quite difficult because it involved combining regions of significantly different grid shape and orientation (inclined and non-inclined planes) to accurately describe the system geometry. Thus, I investigated the possibility of representing the SD geometry using a simpler geometry. The approach involved the representing the slot as a rectangular slab having the same surface area as the arc segment (See Fig. 3.19). With this formulation, I also kept the volume of the slot constant (since no change was made to the slot thickness). The implementation of this approximate modeling approach is discussed in details in the ensuing sections.

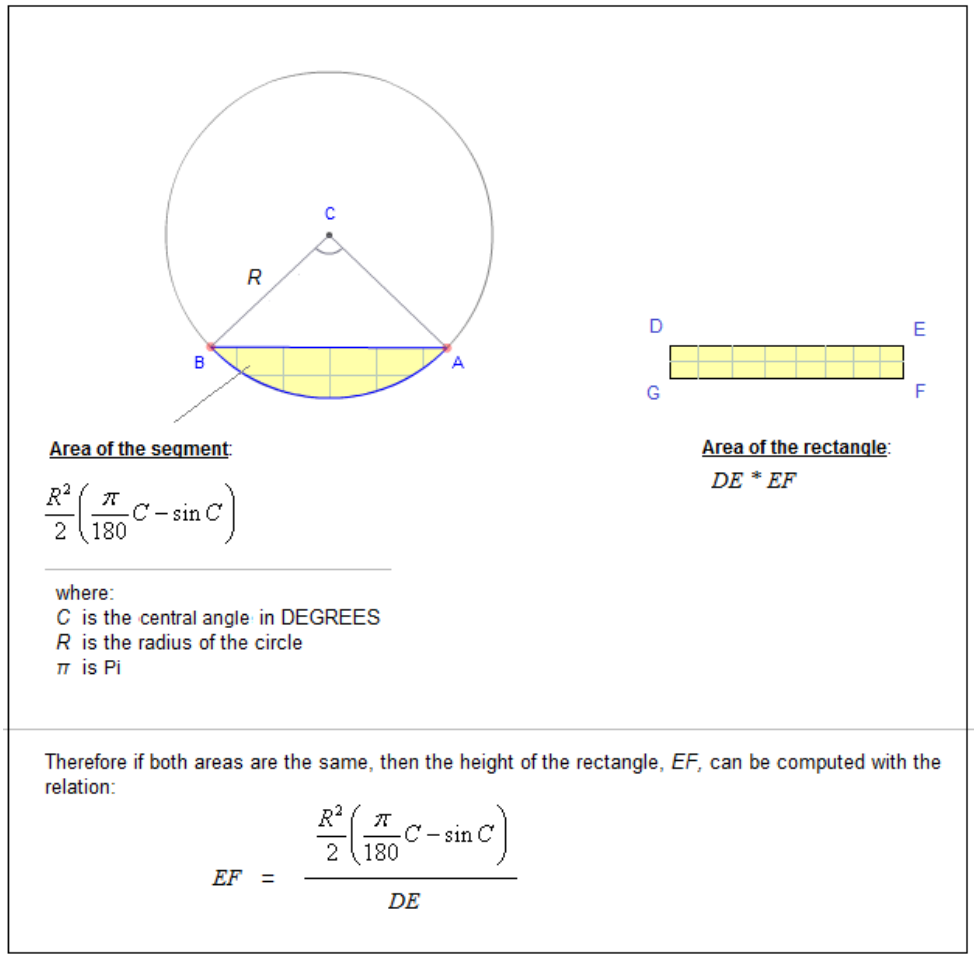

Fig. 3.19—Illustration showing how the height of the rectangular slab in Geometry D is calculated

3.4.1 Geometry D: Generating the coordinates for the well center points (Region D1)

The wells centers were placed on a grid similar to that used in the discretization of the Geometry A case (see Section 3.1.1). However, in this case the depth to the well centers was not half of the reservoir Z dimension. I calculated this depth in such a way that ensured the slab-shaped slot was placed in the middle of the formation (height-wise). The FORTRAN (95/2003) code listed in Fig. 3.20 illustrates how I implemented this in calculating the coordinates of the well centers.

```
!
! -------
! ... Computing the set-up parameters
! -------
!
      angle_1    = 90.0d0 - ( rad_to_deg * ATAN(2.0d0*h_slot / Length_X) )
!
      arc_angle  = 360.0d0 - (4.0d0*angle_1)
!
      radius_of_curvature = Length_X / (2.0d0 * SIN(arc_angle*deg_to_rad/2.0d0))
!
      surface_area = radius_of_curvature*radius_of_curvature*( (pi * arc_angle / 180.0d0) &
&                    - SIN(arc_angle*deg_to_rad) ) / 2.0d0
!
      adjusted_h_slot = surface_area / Length_X
!
      num_well_centers = num_x_div
!
      centers_distance = ( Length_X/REAL(num_x_div) )
!
      well_depth = adjusted_h_slot + init_cart_z_disp + ( (Length_Z - adjusted_h_slot + &
&                 init_cart_z_disp)/2.0d0 )   ! Assuming the configuration is centered in the formation
!
! ... Computations
!
      Well_Centers_DO: DO i=1,num_well_centers
!
! -------
! ... Compute the x-coordinate
! -------
!
         well_centers(i,1) = ( REAL(i) - 0.5d0 ) * centers_distance
!
! -------
! ... Compute the y-coordinate
! -------
!
          well_centers(i,2) = (0.5d0 * Length_Y)
!
! -------
! ... Compute the z-coordinate
! -------
!
          well_centers(i,3) = -well_depth
!
!
        END DO Well_Centers_DO
!
```

Fig. 3.20—FORTRAN (95/2003) code for computing the coordinates of the well centers (Geometry D).

3.4.2 Geometry D: Generating the coordinates for the points in the region representing the slot (Region D2)

This region was discretized in a manner similar to that of the upper part of the slot (region C4) in Geometry C (see section 3.3.3) to produce a Cartesian grid. The FORTRAN (95/2003) code listed in Fig. 3.21 describes how I set up the code to generate these points.

```
!
! -------
! ... Slot Centers
! -------
!
      num_slot_z_divisions         = INT( (adjusted_h_slot - (0.5d0*init_cart_z_disp)) &
&                                       / slot_block_size )
      total_slot_centers_distance  = REAL(num_slot_z_divisions) * slot_block_size
      slot_trunc_distance          = adjusted_h_slot - (0.5d0*init_cart_z_disp) &
&                                    - total_slot_centers_distance
      num_slot_z_divisions_plus1   = num_slot_z_divisions+1
      num_slot_z_divisions_plus2   = num_slot_z_divisions+2
      num_slot_centers             = num_slot_z_divisions_plus2 * num_well_centers
!
! -------
! ... Computing the slot centers
! -------
!
       Slot_Centers_1_DO: DO i=1,num_well_centers
!
!
          Slot_Centers_2_DO: DO j=1,num_slot_z_divisions_plus2
!
! -------
! ... Compute counter and incremented value
! -------
!
             counter = ( (i-1)*num_slot_z_divisions_plus2) + j
!
! -------
! ... Compute the x-coordinate
! -------
!
             slot_centers(counter,1) = ( REAL(i) - 0.5d0 ) * centers_distance
!
! -------
! ... Compute the y-coordinate
! -------
!
             slot_centers(counter,2) = (0.5d0 * Length_Y)
!
! -------
! ... Compute the z-coordinate
! -------
!
             IF (j == 1) THEN
             slot_centers(counter,3) = init_cart_z_disp - well_depth
             ELSE IF (j == num_slot_z_divisions_plus2) THEN
             slot_centers(counter,3) = slot_top_z_coord - init_cart_z_disp
             ELSE
             slot_centers(counter,3) = ( (REAL(j-1)-0.5d0) * slot_block_size ) + &
&                                       init_cart_z_disp - well_depth + (0.5d0*slot_trunc_distance)
             END IF
!
!
          END DO Slot_Centers_2_DO
!
!
       END DO Slot_Centers_1_DO
!
```

Fig. 3.21—FORTRAN (95/2003) code for generating the coordinates of points in region D2 (Geometry D)

3.4.3 Geometry D: Generating the coordinates for the circular-patterned points around the bottom of the well (Region D3) and top of the slot (Region D4)

Here also, as in the arc-segment case of Geometry C (see Section 3.3.2), the regions at the top of the slot (region D3) and the base of the well (region D4) were discretized using cylindrical grids. Here also, the

procedure used for computing the coordinates of the points was the same as was used for region A2 in Geometry A (see section 3.1.2).

3.4.4 Geometry D: Generating a Cartesian grid on both sides of the slot (Regions D5 & D6)

The discretization here was exactly like that of their corresponding regions in Geometry C (regions C6 & C7; see section 3.3.4) yielding Cartesian grids with coarser discretization farther from the slot (region D6).

Fig. 3.22, Fig. 3.23 and Fig. 3.24 all show the resultant mesh from the discretization of Geometry D in different views.

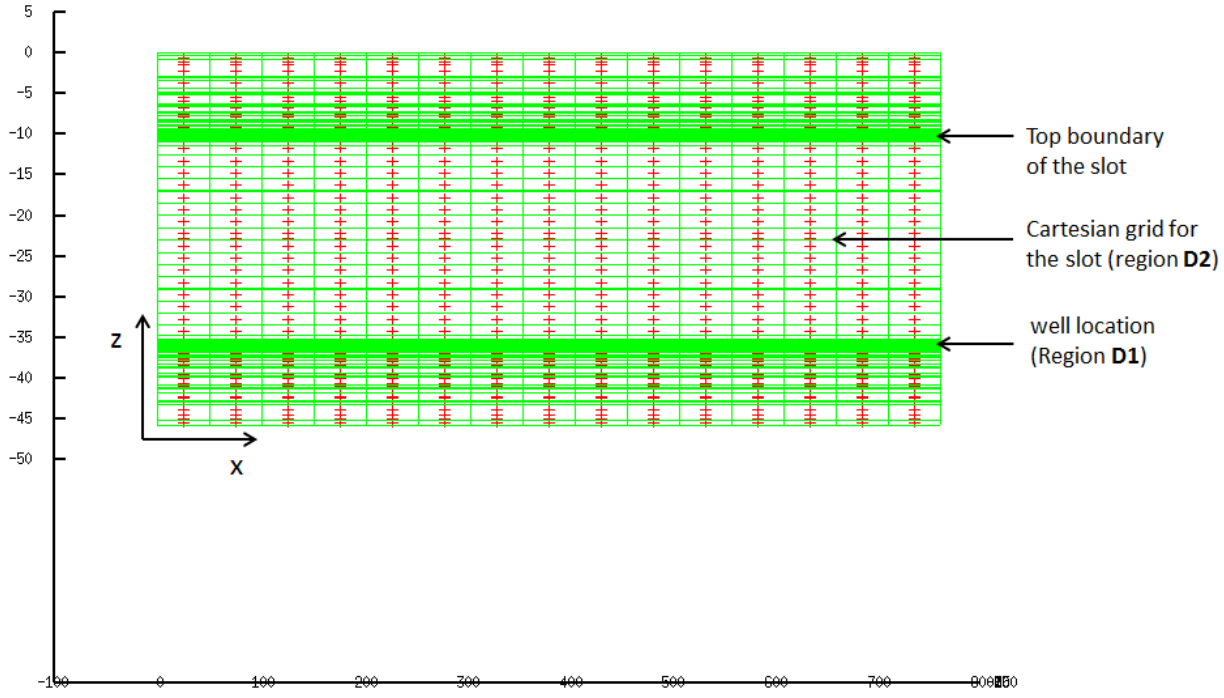

Fig. 3.22—Visualization of the mesh generated to discretize the domain in the case of Geometry D: Approximate SD representation (side view/X-Z plane)

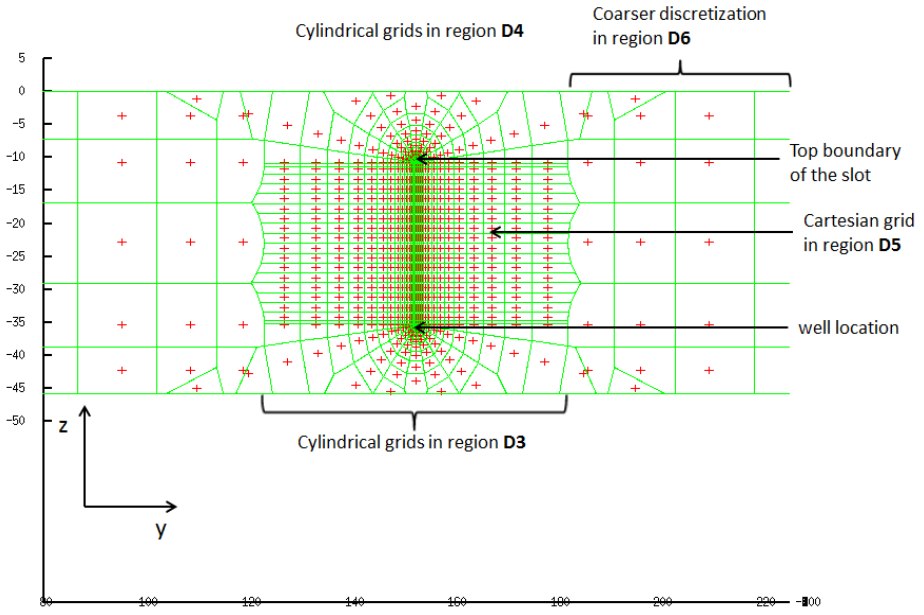

Fig. 3.23—Visualization of the mesh generated to discretize the domain in the case of Geometry D: Approximate SD representation (front view/Y-Z plane)

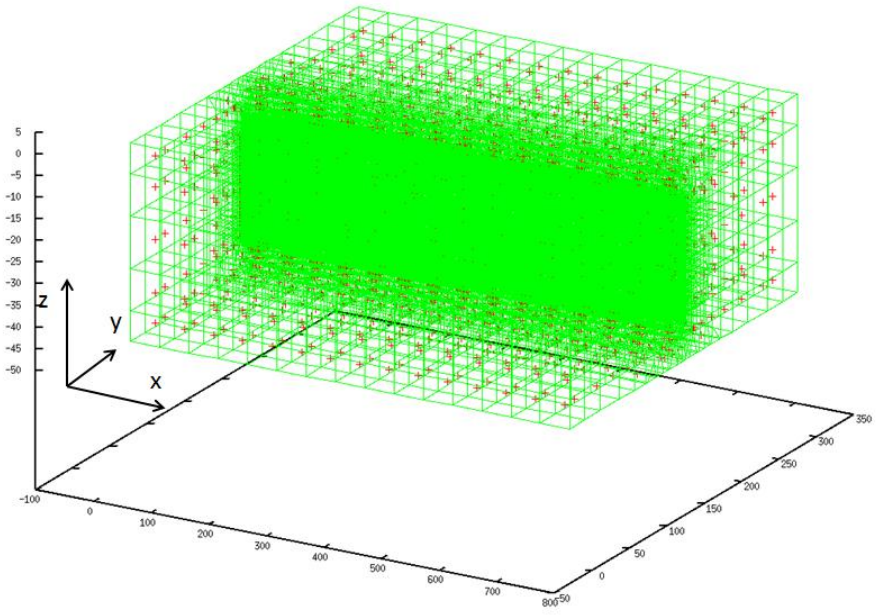

Fig. 3.24—3D visualization of the mesh generated to discretize the domain in the case of Geometry D: Approximate SD representation

3.5 Discretizing the multiple hydraulic fracturing system (Geometry E)

Here I generated representative meshes describing the domain (formation, well and stimulated region) in a system involving multistage hydraulic fracturing, and which will be used as a reference for the comparison of the performance of the SD method. The points were generated following the mesh creation approach used by Olorode (2011) in his study of planar multiply-fractured horizontal well systems. His approach involved creating a grid system with fine discretization (achieved through increased points' density) close to the wellbore, the fracture faces and with cylindrical grids around the fracture tips. Regions farther out into the formation were discretized with a regular Cartesian grid system. For a detailed description of his approach and its implementation, I refer the reader to his thesis dissertation (Olorode, 2011). The mesh corresponding to Geometry E that resulted from following his approach is shown in Fig. 3.25 and 3.26.

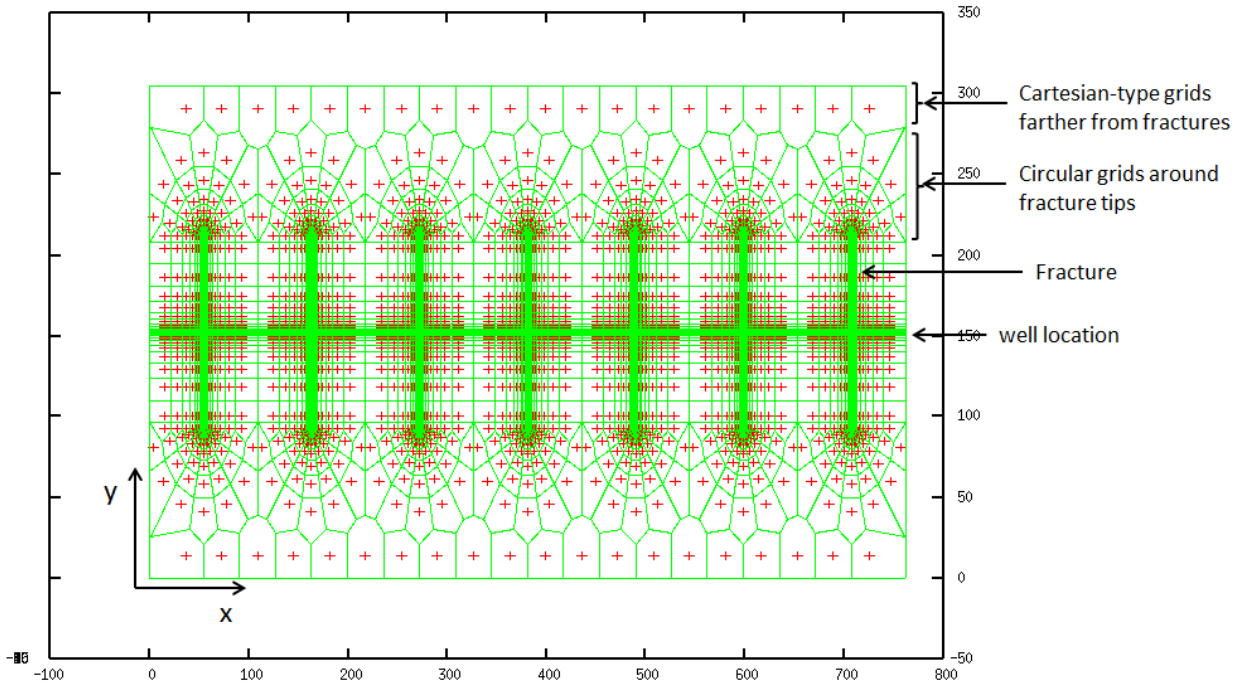

Fig. 3.25—Visualization of the mesh generated to discretize the domain in the case of Geometry E: Multiple hydraulic fracture case (plan view/X-Y plane)

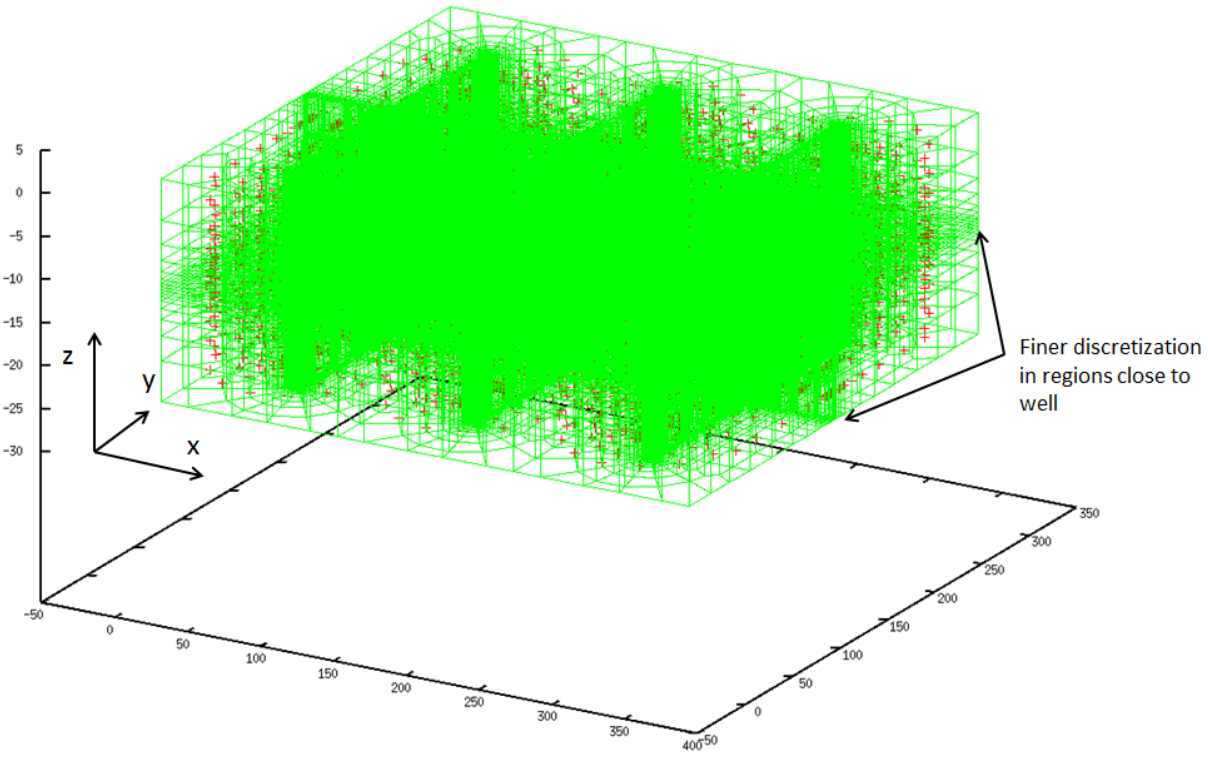

Fig. 3.26—3D visualization of the mesh generated to discretize the domain in the case of Geometry E: A 3-stage fracture example

3.6 Discretizing the domain for the case of the combination of the SD completion method with multistage hydraulic fracturing (Geometry F)

After validating the hypothesis that the approximate representation of the SD (Geometry D) could accurately model production from the full SD representation (see Section 3.3), in the combination case of Geometry F I modeled the slot as a rectangular block. Thus I did not need to change anything in the discretization of X and Y axes of the multistage fracturing case (Geometry E), but the only needed adjustment was in the discretization along the Z axis. The additional change here was to discretize the volume occupied by the slot in this case with Cartesian grids in a manner similar to how it was done in the case of Geometry D (region D2; see section 3.4.2). The resultant mesh from this implementation is shown in Fig. 3.27. Since the plan and side views of the grid in this case remains the same as in the hydraulic fracture case (Geometry E), I only show the front view.

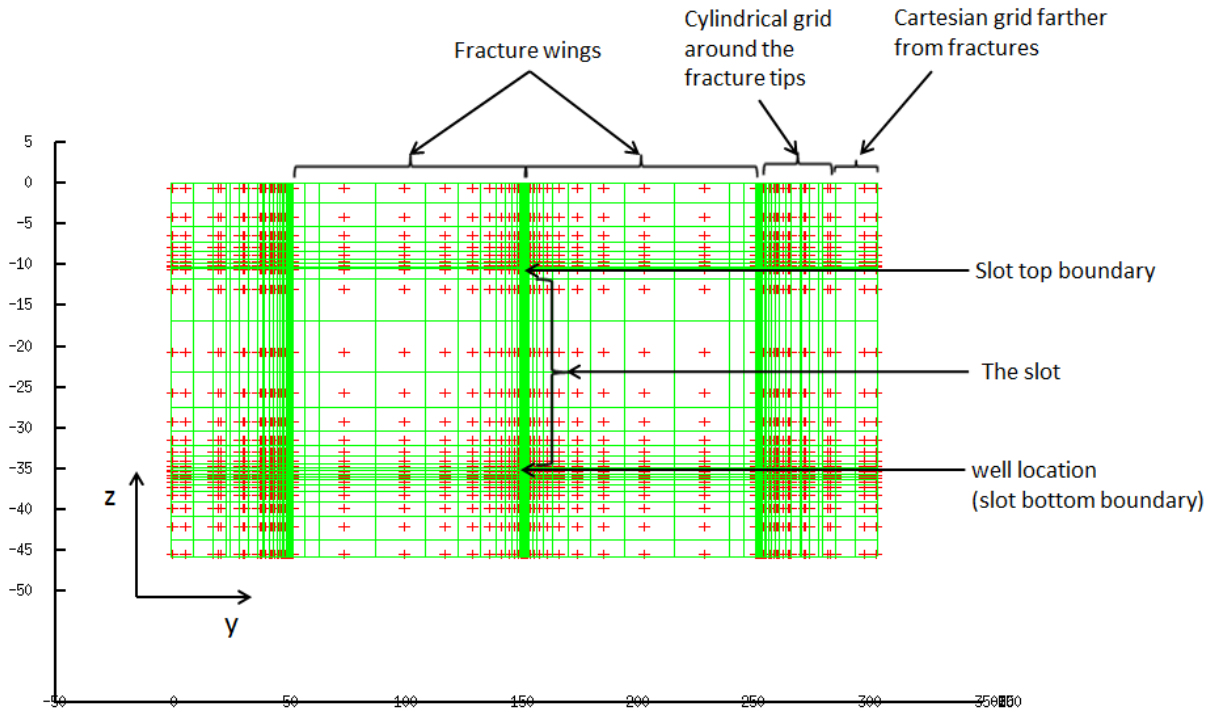

Fig. 3.27—Visualization of the mesh generated to discretize the domain in the case of Geometry F showing the combination of the slot and hydraulic fractures (front view/Y-Z plane)

3.7 The use of stencils to reduce grid size

For each of the configurations discussed, I included an option in the code to reduce the grid system from a full grid model to a stencil. By this I mean the smallest (minimum) repeatable subdomain (division or segment of the entire domain) that can provide a sufficiently representative solution to characterize the flow in the domain under study. This concept is discussed extensively by Freeman (2010b). The way I carried out this reduction in the code was to simply involve a coordinate subtraction that sets all the points that fall outside the stencil area to negative values. These negative values are then changed to zero and the code is modified to print only gridblocks with non-zero coordinates at their centers. Thus, this approach yielded only the discretized stencil. As examples, the FORTRAN (95/2003) code listed in Fig. 3.28 illustrates how this process was implemented in the fracture region of multiple hydraulic fracture case (Geometry E) and Fig. 3.29 shows the discretized stencil for the SD system (Geometry C).

```
!
! -------
! ... Stencilize the fracture points
! -------
!
      DO_frac_points_sten: DO i = 1, num_frac_points
!
         frac_points(i,1) = frac_points(i,1) - Length_X + centers_distance + 1.0d-3
         frac_points(i,2) = frac_points(i,2) - half_Y + 1.0d-3
         IF (frac_points(i,1) <= 0.0d0 .OR. frac_points(i,2) <= 0.0d0) THEN
         frac_points(i,1) = 0.0d0
         frac_points(i,2) = 0.0d0
         frac_points(i,3) = 0.0d0
         END IF
!
      END DO DO_frac_points_sten
!
!
! -------
! ... Write out the fracture points
! -------
!
      WRITE(*, 6740)
      WRITE(*, 6000)
!
      DO_print_frac_points: DO i = 1, num_frac_points
!
         IF ( frac_points(i,1) == 0.0d0 .AND. frac_points(i,2) == 0.0d0 .AND. &
&             frac_points(i,3) == 0.0d0 ) CYCLE DO_print_frac_points
!
         WRITE(*, 6001) ( frac_points(i,j), j=1,3 )
!
      END DO DO_print_frac_points
!
```

Fig. 3.28—FORTRAN (95/2003) code listing describing the stencil and the removal of all gridblocks outside it.

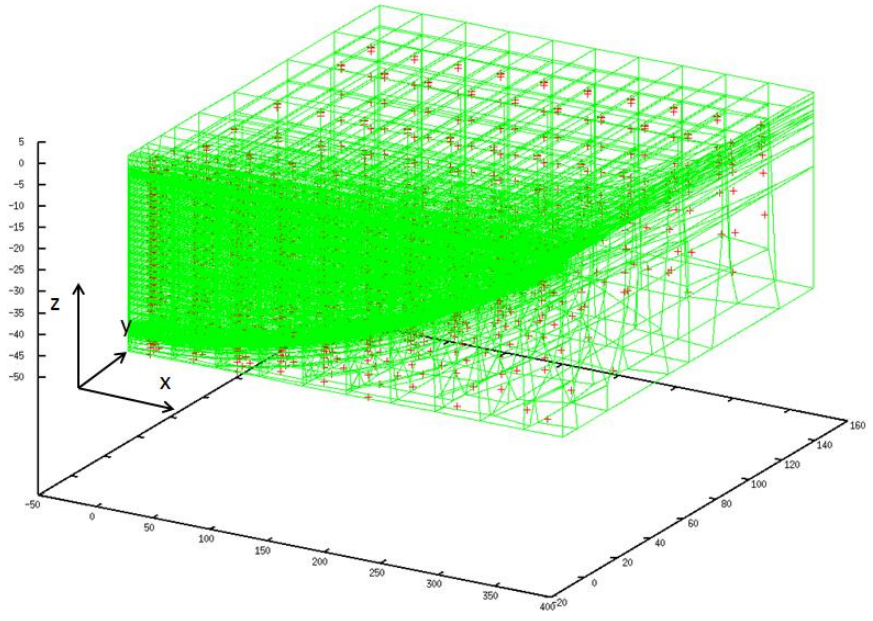

Fig. 3.29—3D visualization of the mesh generated to discretize the stencil in the case of Geometry C: SD completion

CHAPTER IV

SIMULATION RESULTS AND ANALYSES

This chapter presents the simulation results of this work and provides discussions and interpretations of my findings. For each of the three formation and fluid types I considered (tight-gas, shale-gas and tight/shale-oil), the production rates and cumulative production results were used as the basis for comparing the various completion scenarios considered (Geometry A to F). In all cases, I simulated production at a constant bottom-hole pressure of 500 psi for a period of 3000 years or until resource exhaustion/depletion. This was done to provide maximum diagnostic value and insight into the various flow regimes that occur during the depletion of the reservoir systems simulated.

4.1 The tight-gas simulation study

The simulations in this section were conducted using the properties of the Cotton-Valley formation listed in Table 1.1.

4.1.1 The tight-gas study: Stencil validations

I conducted simulations to validate the ability of the stencil (see Section 3.7) to accurately describe the flow and production in all the reservoir configurations (Geometries A to F) I assessed in this tight-gas study. Plots of the flow rates generated from simulations using these stencil models and their respective full-grid models are presented in the Fig. 4.1 through 4.6. These figures show that excellent matches of the stencil and full-grid production rates were obtained in all the reservoir configurations simulated. As a result of the validation of the stencil in all the cases, I replaced the full-grid models with their respective stencils for the rest of the tight-gas simulation study. This reduced the problem size and thus saved on the computation power and time that was required to conduct the simulations.

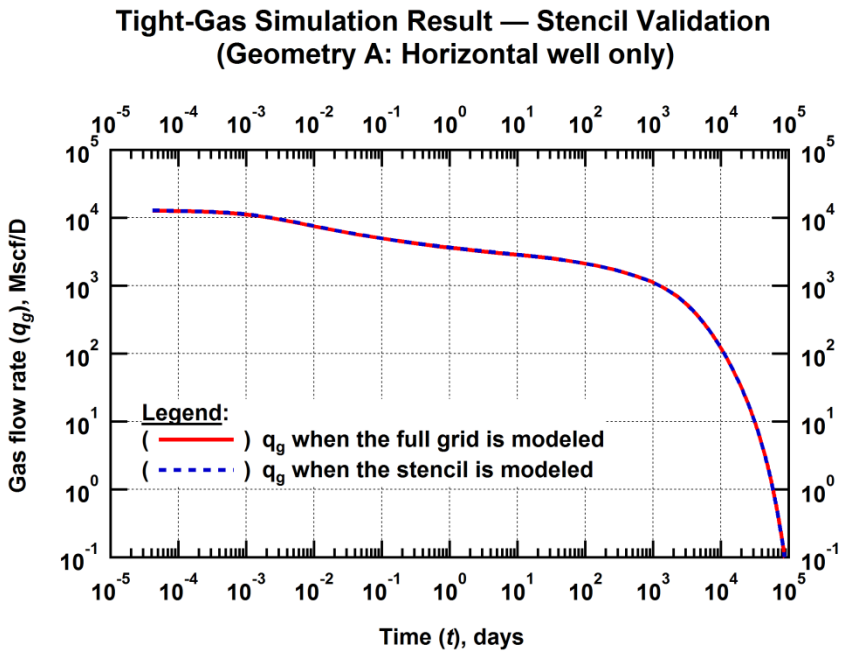

Fig. 4.1—Tight-Gas Simulation: Match between production rates show that the stencil provided an excellent approximation of the full grid model over the reservoir life in the case of Geometry A (the case of the straight horizontal well)

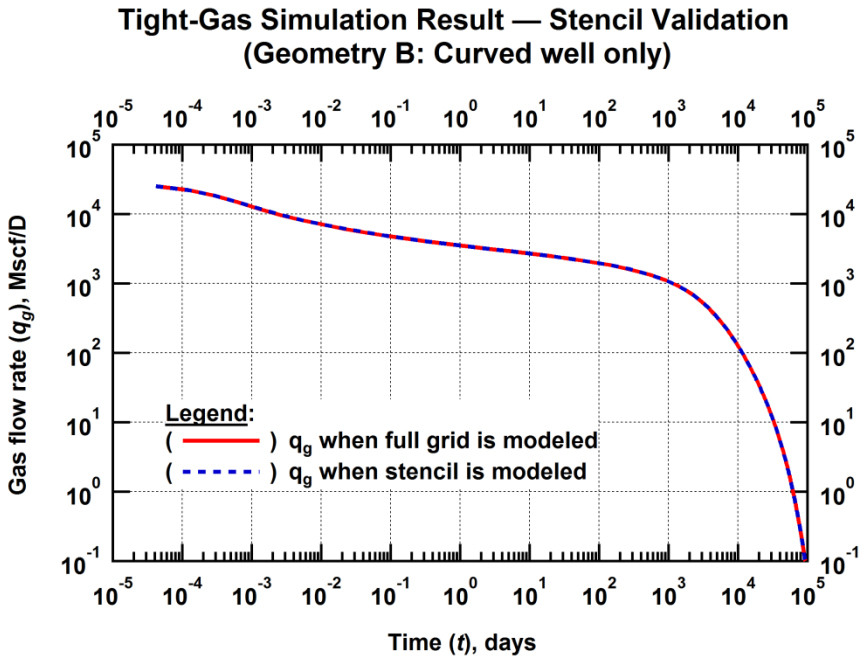

Fig. 4.2—Tight-Gas Simulation: Match between production rates show that the stencil provided an excellent approximation of the full grid model over the reservoir life in the case of Geometry B (the case of the curved well).

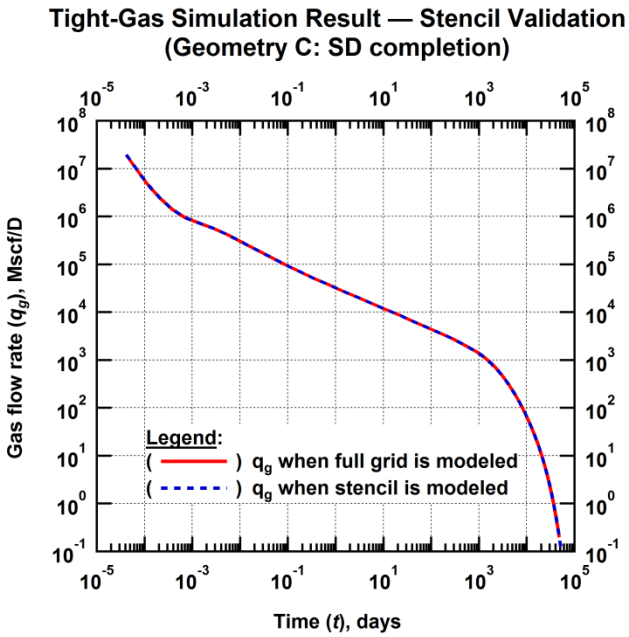

Fig. 4.3—Tight-Gas Simulation: Match between production rates show that the stencil provided an excellent approximation of the full grid model over the reservoir life in the case of Geometry C (the case of the SD Completion).

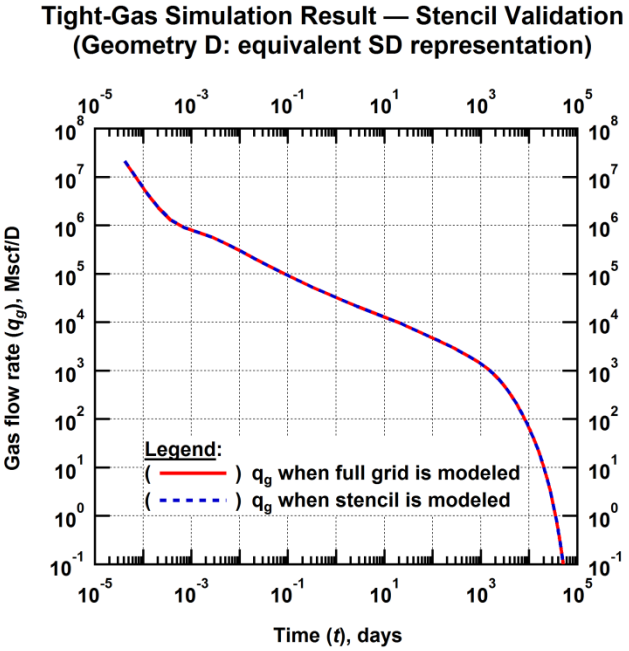

Fig. 4.4—Tight-Gas Simulation: Match between production rates show that the stencil provided an excellent approximation of the full grid model over the reservoir life in the case of Geometry D (equivalent SD representation).

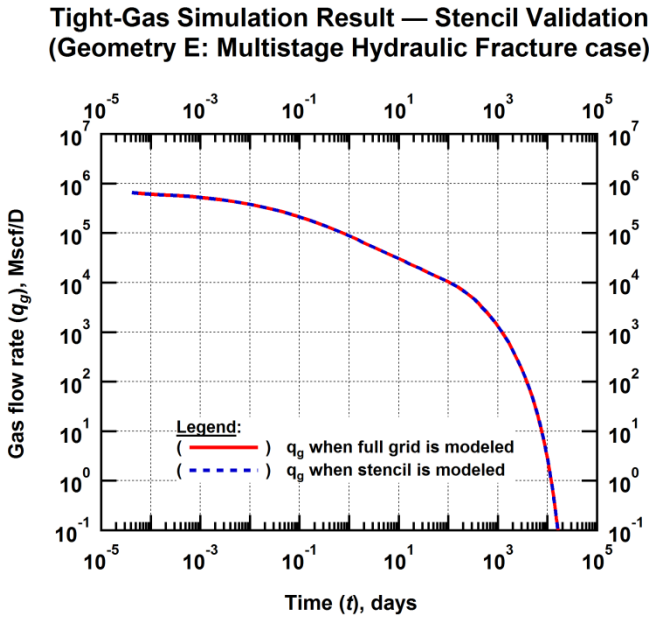

Fig. 4.5— Tight-Gas Simulation: Match between production rates show that the stencil provided an excellent approximation of the full grid model over the reservoir life in the case of Geometry E (Multistage Hydraulic Fracturing).

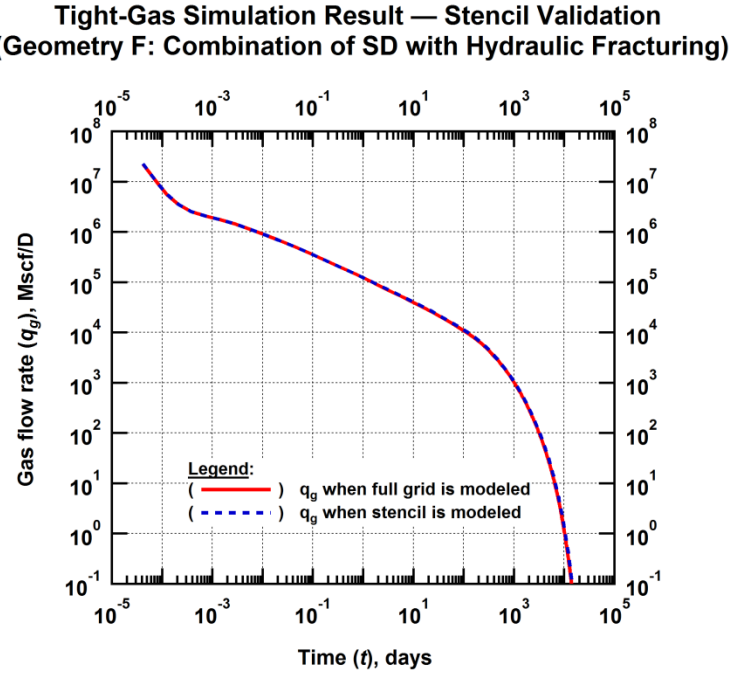

Fig. 4.6— Tight-Gas Simulation: Match between production rates show that the stencil provided an excellent approximation of the full grid model over the reservoir life in the case of Geometry F (Combination of SD and Multistage Hydraulic Fracturing).

4.1.2 The tight-gas study: Comparative studies

Four comparative studies were conducted. They are: (a) the comparison of production from the straight horizontal well (Geometry A) to that from the curved well (Geometry B), (b) the comparison of production from the more closely representative discretization of the SD method (Geometry C) to that from the equivalent SD representation (Geometry D), (c) the comparison of production from the SD method (Geometry C) to that from multiple hydraulic fracturing (Geometry E), and (d) the comparison of production from the combination of the SD method and multiple hydraulic fracturing (Geometry F) with that from multiple hydraulic fracturing only (Geometry E). The ensuing discussions elaborate on each of these studies in detail.

4.1.2.1 The tight-gas study: Straight horizontal well (Geometry A) vs. curved well (Geometry B)

The SD completion method involves drilling a well with a curved trajectory. This results in a longer well length than that of a straight well and consequently more surface area available for flow from the formation. Thus, I investigated if this extra well length would result in an advantage of the SD completion (in terms of overall gas production) over other completion methods. Fig. 4.7 shows how the production rates from the curved well and the straight horizontal well compared with each other. As can be observed, rates from both well geometries practically coincided after a very short initial period, indicating that there was no advantage of the curving (and longer) well over the straight well in the tight-gas formation used in this study. The slight deviation between the two curves at very early times (less than 0.001 days) was attributed to the different initial wellbore drainage (a plausible physical reason), but results at this time can be affected by numerical artifacts and discretization errors that are mitigated as time advances. As a result of the close match, production rates either of these wells can be used as the unstimulated reference to production from the stimulated cases (Geometries C through F). The spatial distribution of the reservoir pressure at different times for the two geometries investigated here (A and B) are shown in Fig. 4.8 and 4.9.

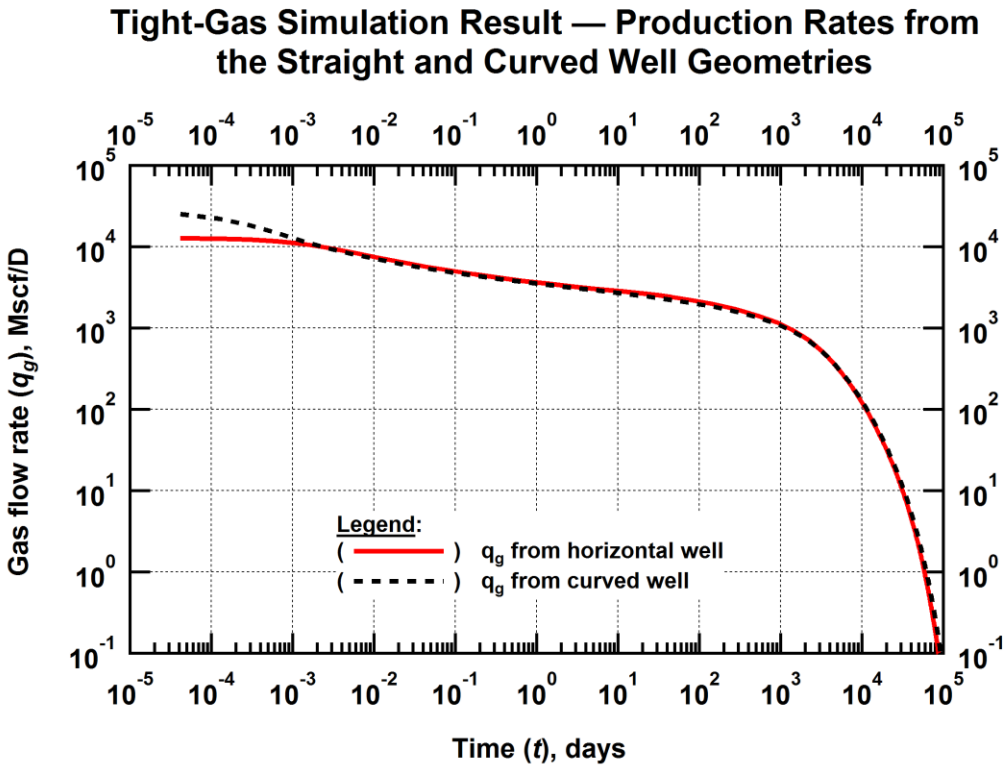

Fig. 4.7— Tight-Gas Simulation: Production rate decline for the curved well matches that of the straight horizontal well.

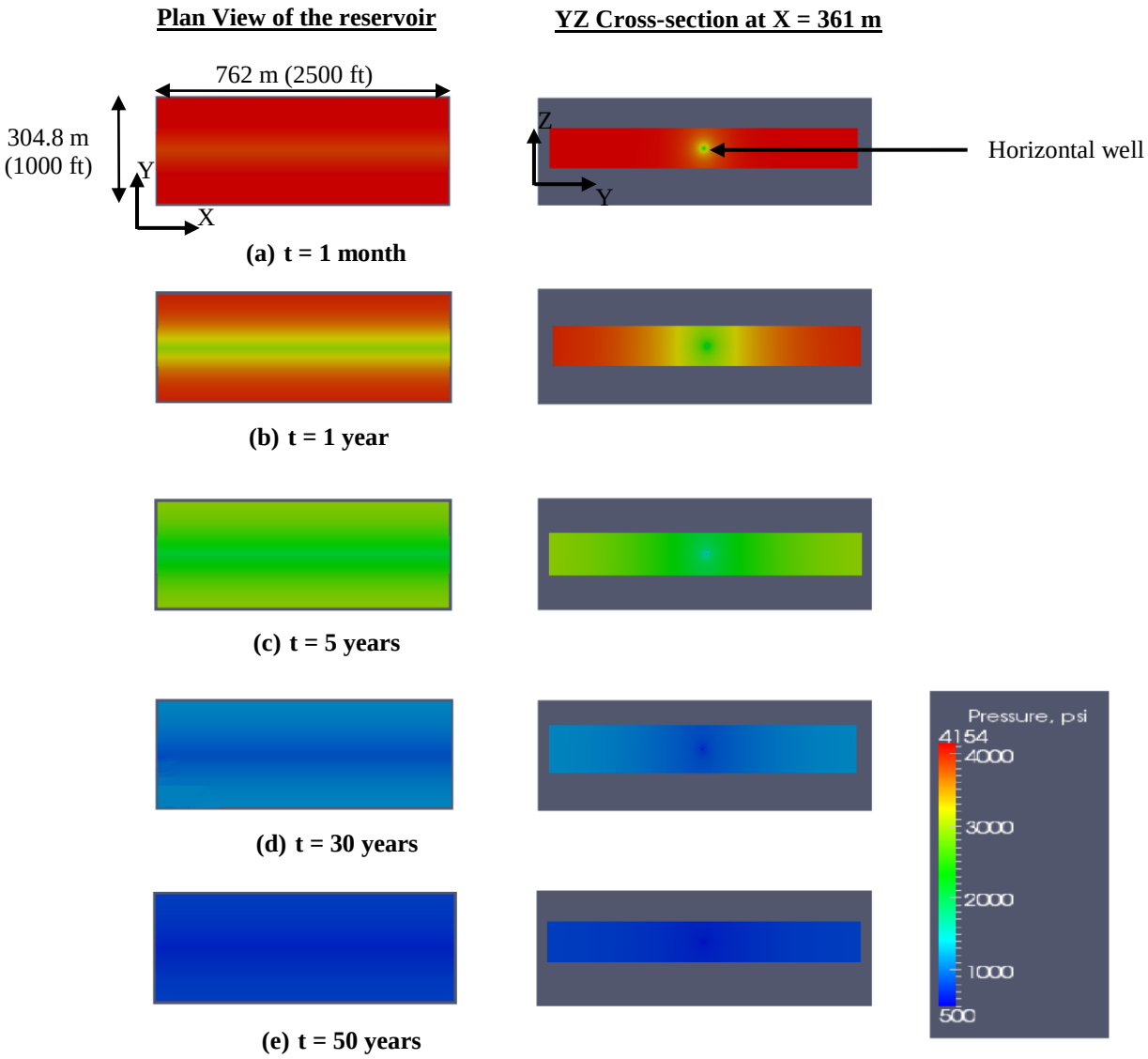

Fig. 4.8—Plan views and cross-sectional views of the spatial distribution of pressure in a tight-gas reservoir (representative of the Cotton-Valley formation) at various stages of production when using a straight horizontal well (Geometry A)

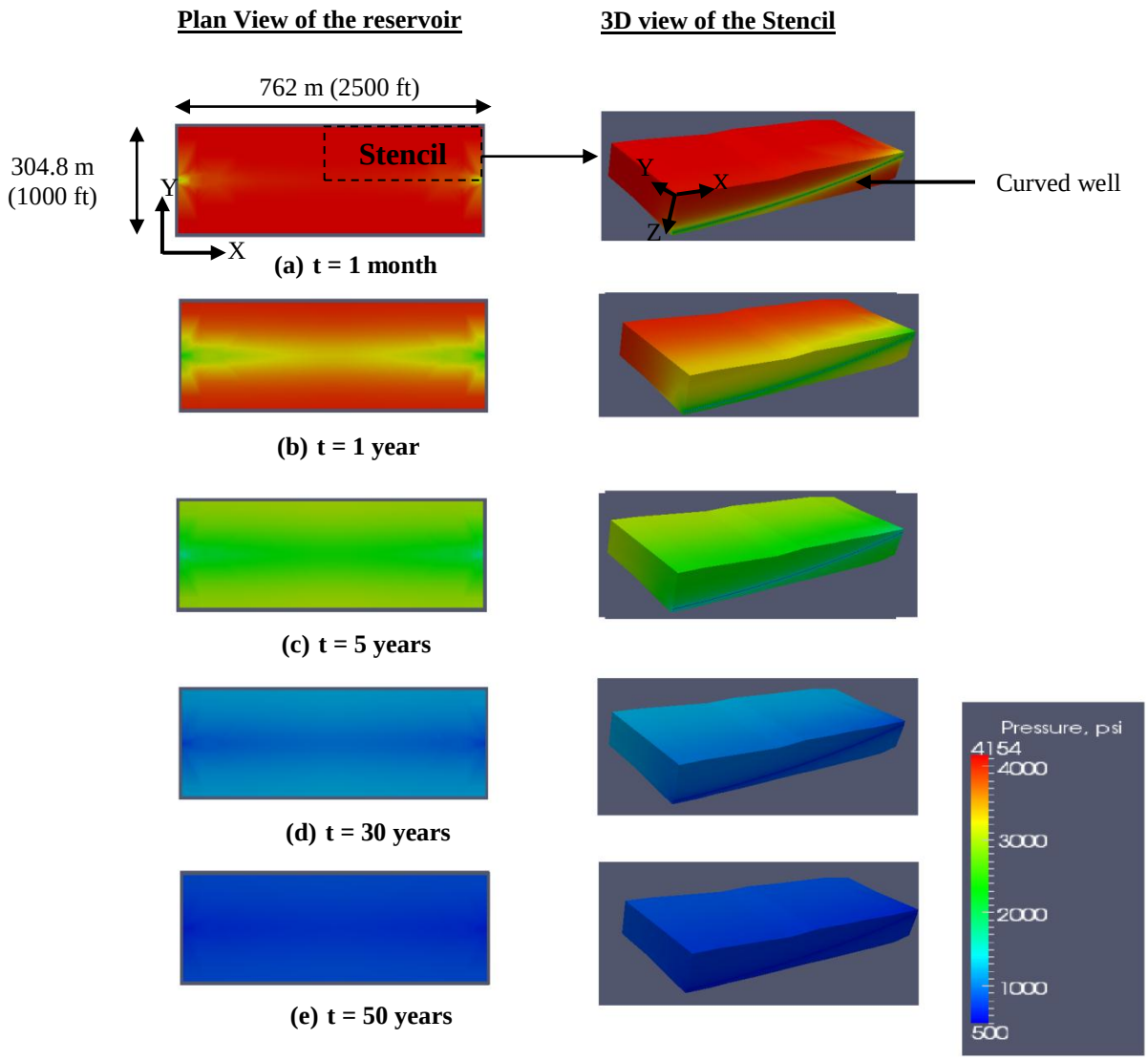

Fig. 4.9—Plan views of the full reservoir and 3D views of the stencil showing the spatial distribution of pressure in a tight-gas reservoir (representative of the Cotton-Valley formation) at various stages of production when producing from the curved well (Geometry B)

4.1.2.2 The tight-gas study: The closely representative discretization of the SD (Geometry C) vs. the approximate representation (Geometry D)

The SD geometry is rather complex and tedious to model and analyze. To avoid unnecessarily complex, demanding and time-consuming work, I investigated the possibility that a simpler grid configuration (see discussion in Section 3.4) could accurately predict production from the full SD configuration. Fig. 4.10 shows the results of this study. Production rates from both grid configurations match almost perfectly, thus validating the hypothesis that the "equivalent SD representation" was able to accurately describe the production performance of a fully-described SD completion in the tight gas reservoir I studied. In Fig. 4.11 and 4.12 we observe a similar trend in the depletion of pressure with time in the two reservoir systems (Geometry C and D).

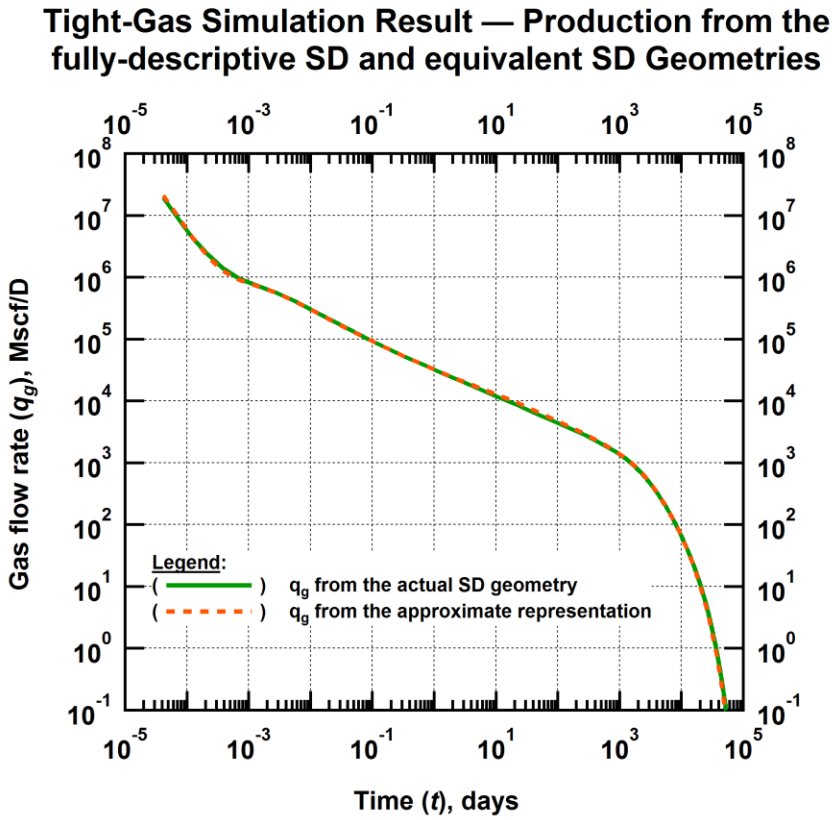

Fig. 4.10— Tight-Gas Simulation: Production rate decline for the equivalent SD representation matches that of the actual.

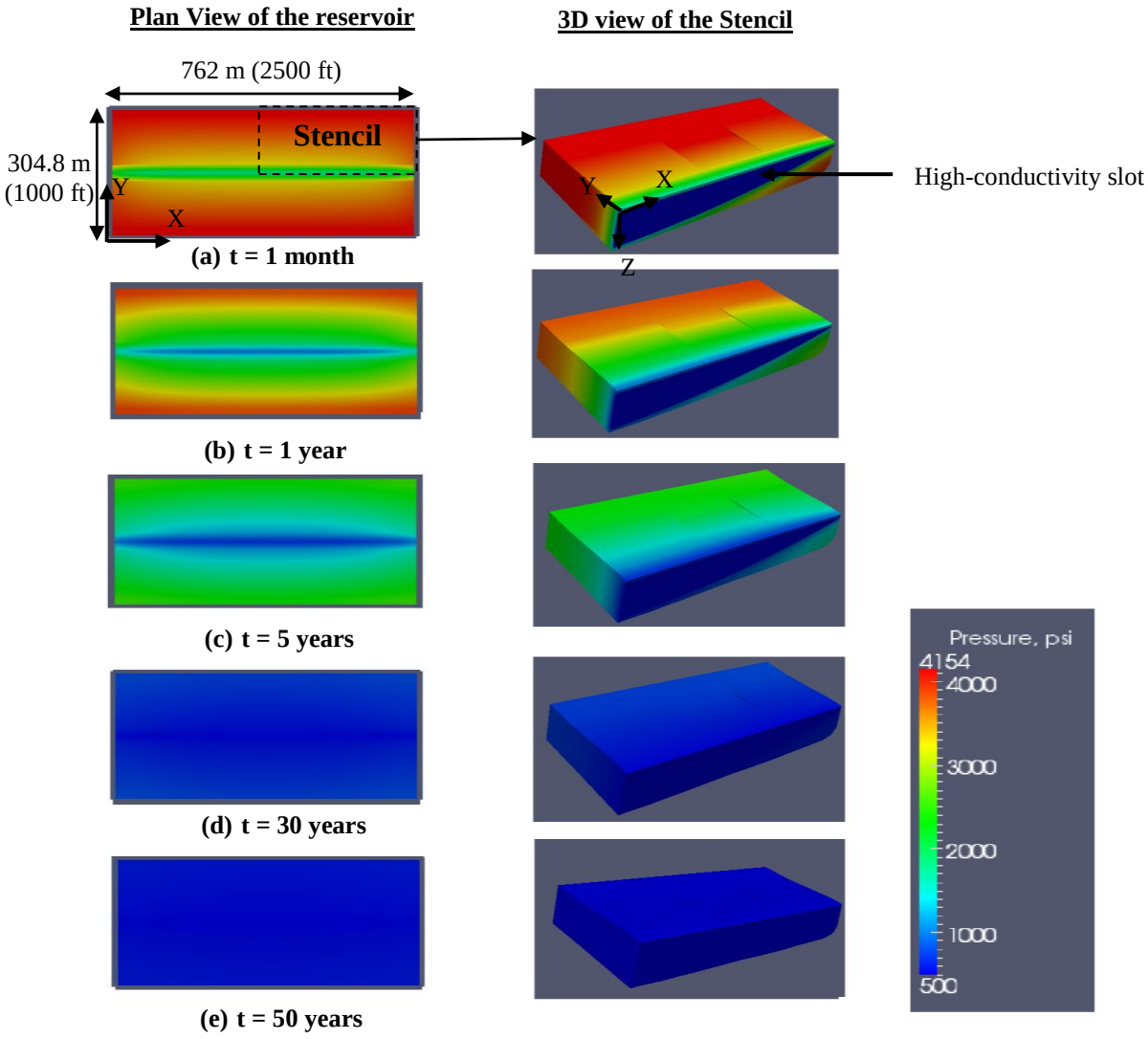

Fig. 4.11—Plan views of the full reservoir and 3D views of the stencil showing the spatial distribution of pressure in a tight-gas reservoir (representative of the Cotton-Valley formation) at various stages of production when producing from the SD completion (Geometry C)

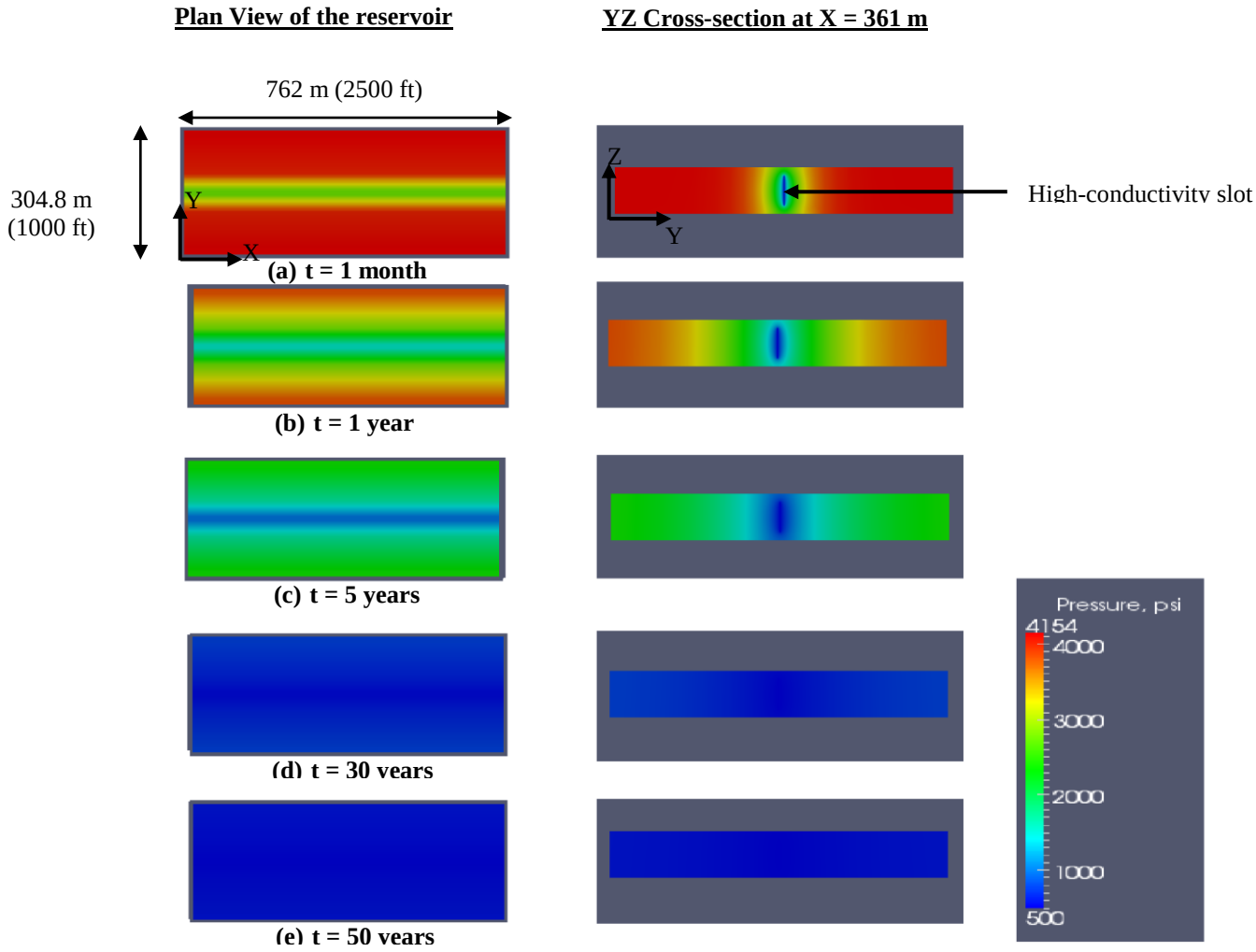

Fig. 4.12— Plan views and cross-sectionals view of the spatial distribution of pressure in a tight-gas reservoir (representative of the Cotton-Valley formation) at various stages of production when using the equivalent SD representation (Geometry D).

4.1.2.3 The tight-gas study: The SD method (Geometry C) vs. multiple hydraulic fracturing (Geometry E)

To assess the production performance of the SD completion against that of the hydraulically fractured reservoir system (the current preferred completion method in tight-gas, shale-gas and tight/shale-oil reservoirs) I employed the use of the production rates from both systems. Fig. 4.13 shows the evolution of the production rates for the two completion/stimulation methods on a log-log plot. I observed higher rates for the hydraulic fracture case over the early portion (from about 0.01 days to almost 1000 days) of the producing life of the reservoir. However, to be able to make a conclusive inference, the cumulative production from the two stimulation methods had to be included in this analysis. Fig. 4.14 shows the cumulative production from these two geometries over a period of 30 years (a reasonable approximation for the producing life). From the combination of these two plots (Fig. 4.13 and 4.14) we see that though the performance of the SD is a significant improvement over the unstimulated case (the straight horizontal well), it does not compare favorably with the performance of the multiple hydraulic fracture case. It appears that the larger surface area to flow that multistage hydraulic fracturing provides (1.378×10^6 ft.^{2} for multistage hydraulic fracturing as opposed to 0.401×10^6 ft.^{2} for the SD method) is much more significant than the higher conductivity (4208 md-ft. for the SD method as opposed to 499 md-ft. for the hydraulic fractures) achieved using the SD technique. Fig. 4.15 shows the evolution of the reservoir pressure distribution at different times in through production in the multiply hydraulically fractured reservoir.

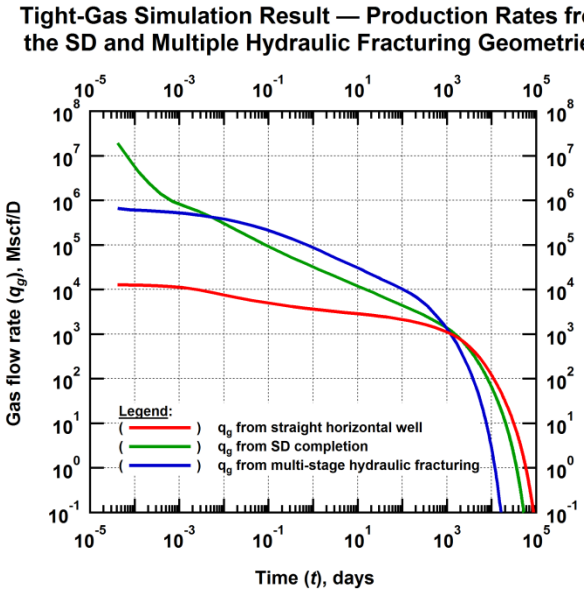

Fig. 4.13— Tight-Gas Simulation: Production rate from the SD completion was lower than that from multistage hydraulic fracturing case during the linear flow regime.

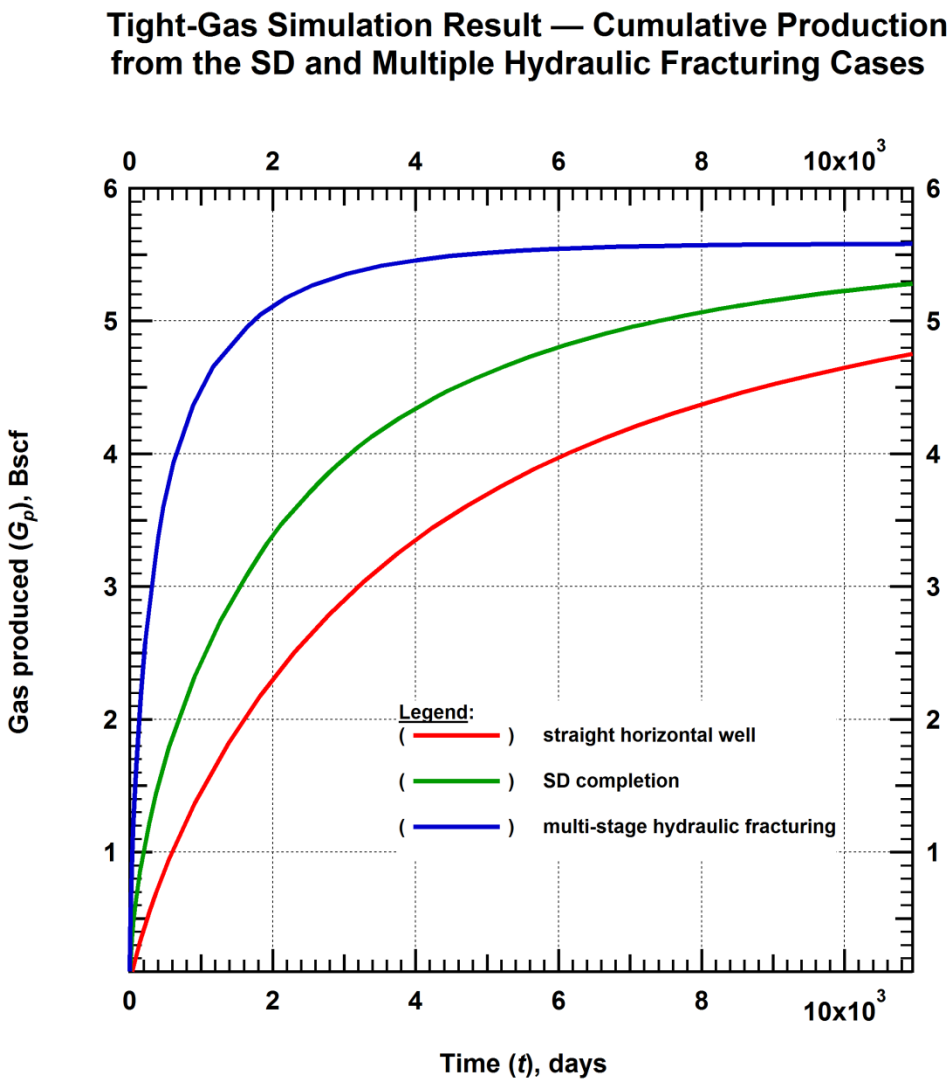

Fig. 4.14—Cumulative Production curves show that the SD completion does not compete favorably in terms of production with multistage hydraulic fracturing for the tight-gas study conducted.

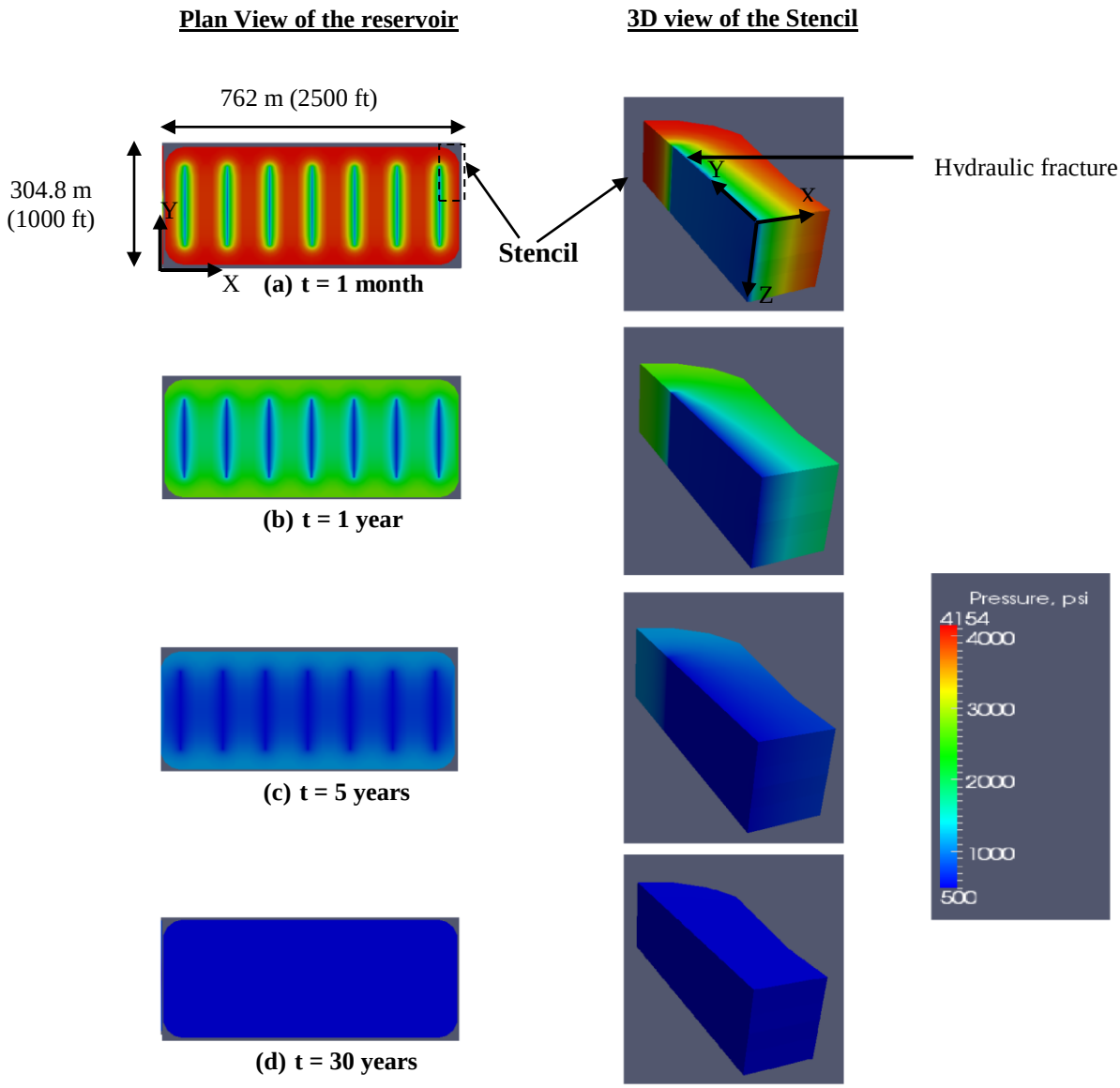

Fig. 4.15— Plan views of the full reservoir and 3D views of the stencil showing the spatial distribution of pressure in a tight-gas reservoir (representative of the Cotton-Valley formation) at various stages of production when completed with multistage hydraulic fracturing (Geometry E)

4.1.2.4 The tight-gas study: The standard multistage hydraulic fracturing method (Geometry E) vs. the combination of multiple hydraulic fracturing with the SD method (Geometry F)

The final scenario I investigated was the case of a combination of the SD technique with hydraulic fracturing to determine if such a combination could lead to a significant boost in production. Fig 4.16 shows the production rates obtained from simulating this system, as well as those from the case of the reservoir completed with the standard multistage hydraulic fracturing method. The initial production rates of the combination case is clearly higher, but the period over which this advantage is sustained is limited (less than 100 days). Similarly, in the cumulative production plot (Fig. 4.17), the period over which the production performance of the combination case dominates is short-lived. Hence, I concluded that without a full economic analysis, it cannot be known if the production boost is sufficient to justify the extra expense of creating the slot. In the pressure profile plots for this combination case shown in Fig. 4.18, we see a more rapid decline in the reservoir pressure than in the previous cases simulated.

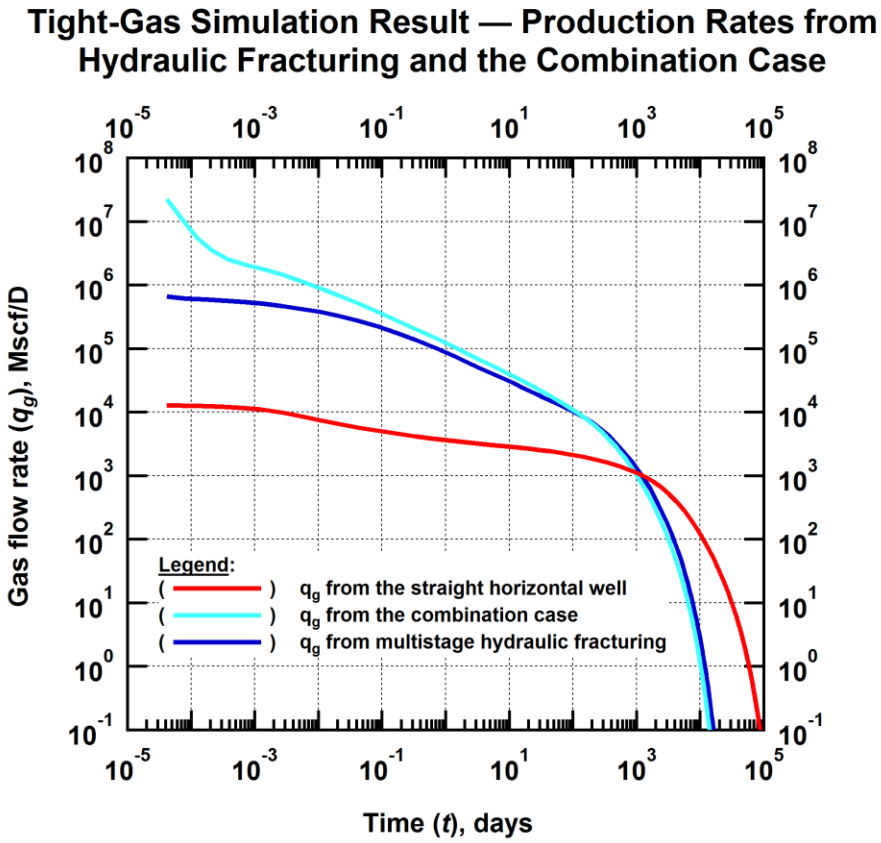

Fig. 4.16— Tight-Gas Simulation: Improvement in rates obtained from the combination case over those from the hydraulic fracturing appear to be only marginal and short-lived.

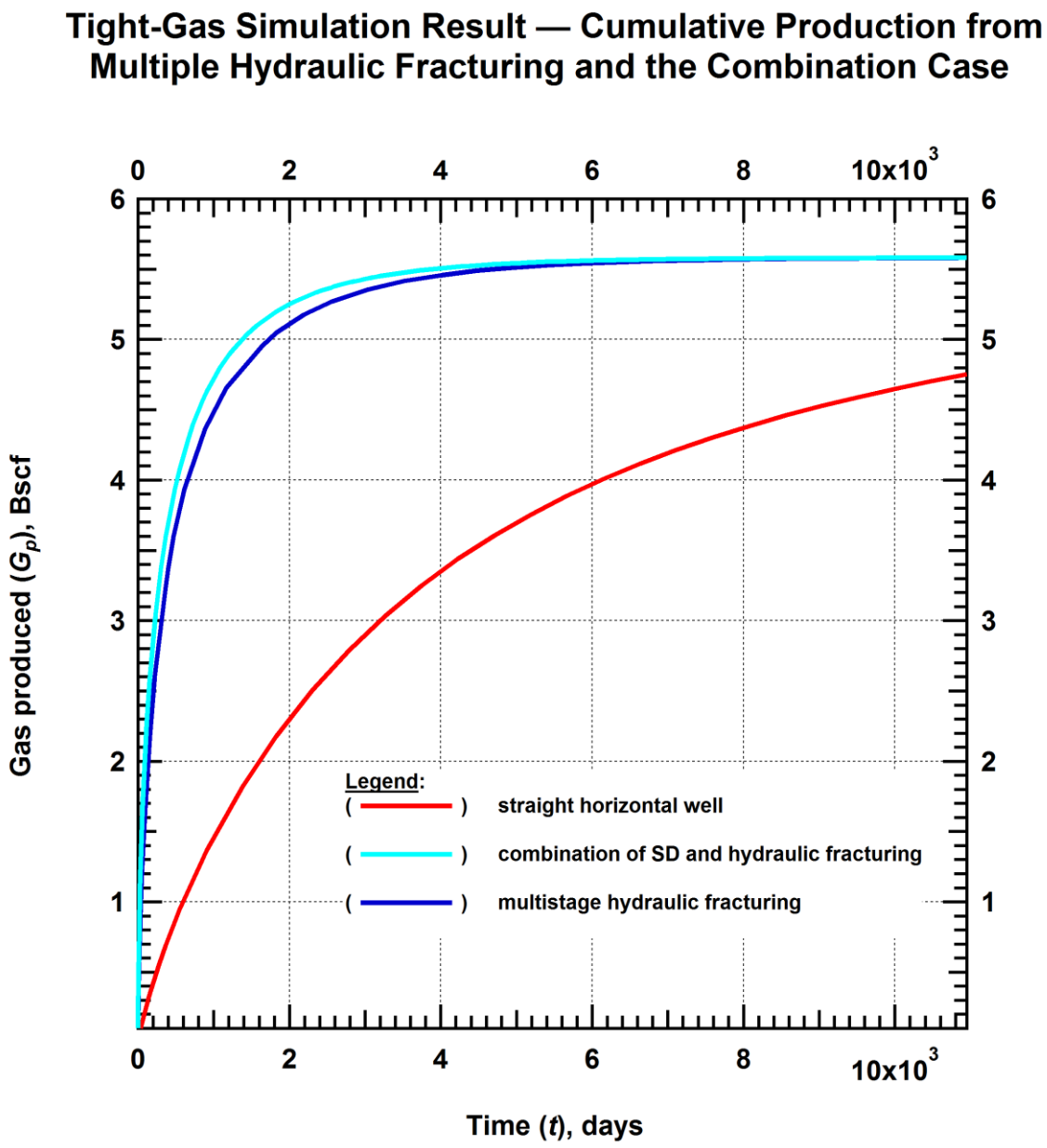

Fig. 4.17—Cumulative Production curves show marginal production advantage resulting from the combination of the SD with multistage hydraulic fracturing for the tight-gas study conducted.

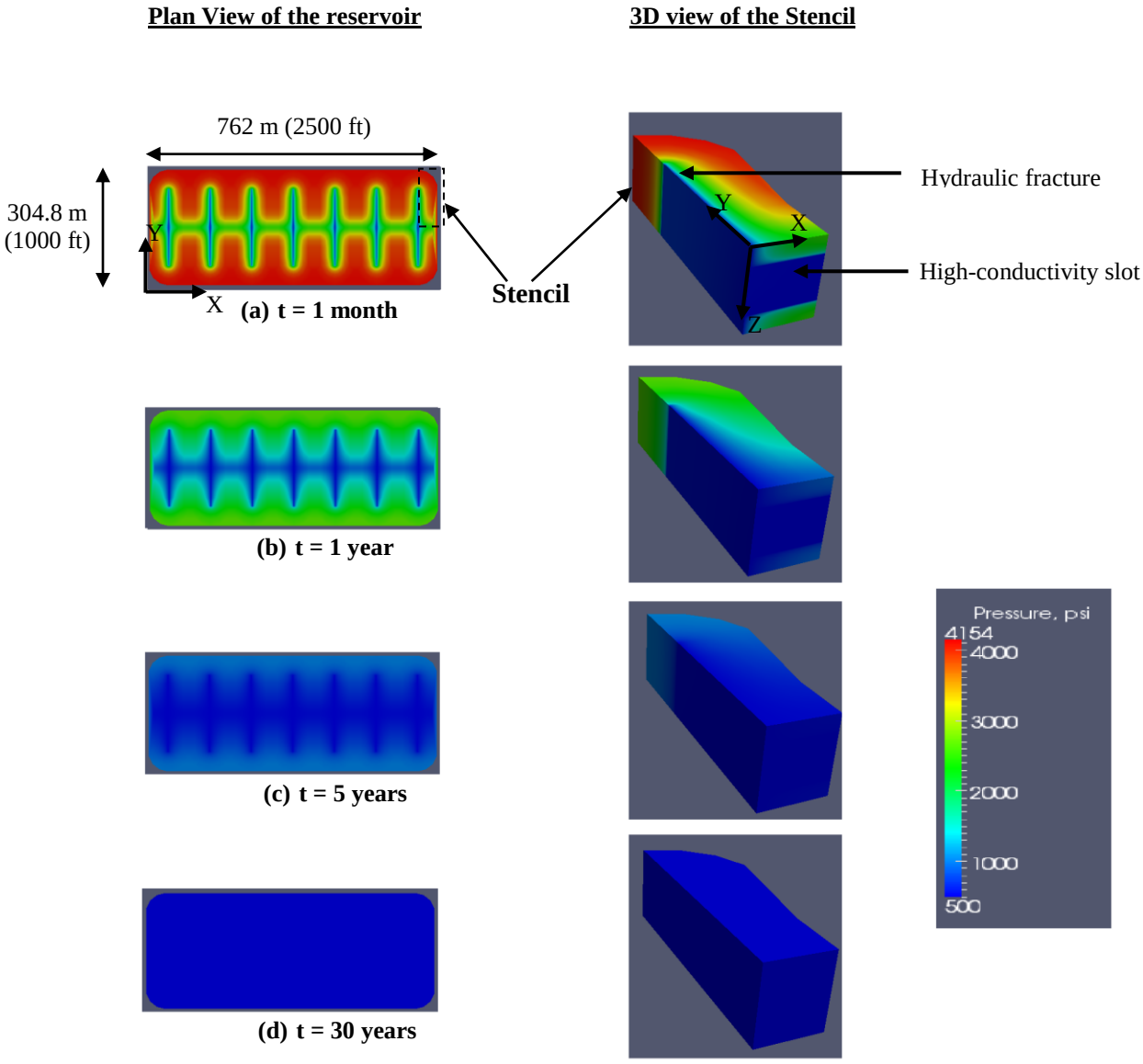

Fig. 4.18—Plan views of the full reservoir and 3D views of the stencil showing the spatial distribution of pressure in a tight-gas reservoir (representative of the Cotton-Valley formation) at various stages of production when completed with a combination of the SD and multistage hydraulic fracturing (Geometry F)

4.2 The shale-gas simulation study

The simulations in this section were conducted using the properties of the Marcellus shale formation listed in **Table 1.2**.

4.2.1 The shale-gas study: Stencil validations

As in the tight-gas study (see section 4.1.1), I conducted simulation runs to confirm the ability of the stencil to accurately predict flow and production in all the reservoir systems of interest (Geometries A through F). The results of these validation runs are shown in Fig. 4.19 through 4.24. With production rates from the stencils (in all the geometries) coinciding with those from their respective full-grid models, I considered the stencil models validated and conducted the rest of my simulation runs using the more efficient stencil models.

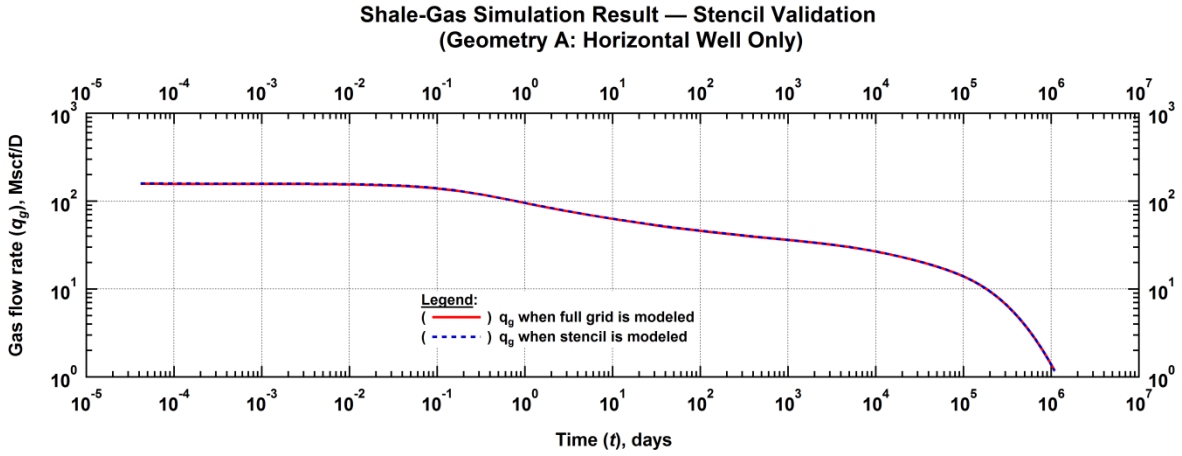

Fig. 4.19— Shale-Gas Simulation: Perfect match between production rates show that the stencil provided an excellent approximation of the full grid model over the reservoir life in the case of Geometry A (the case of the straight horizontal well)

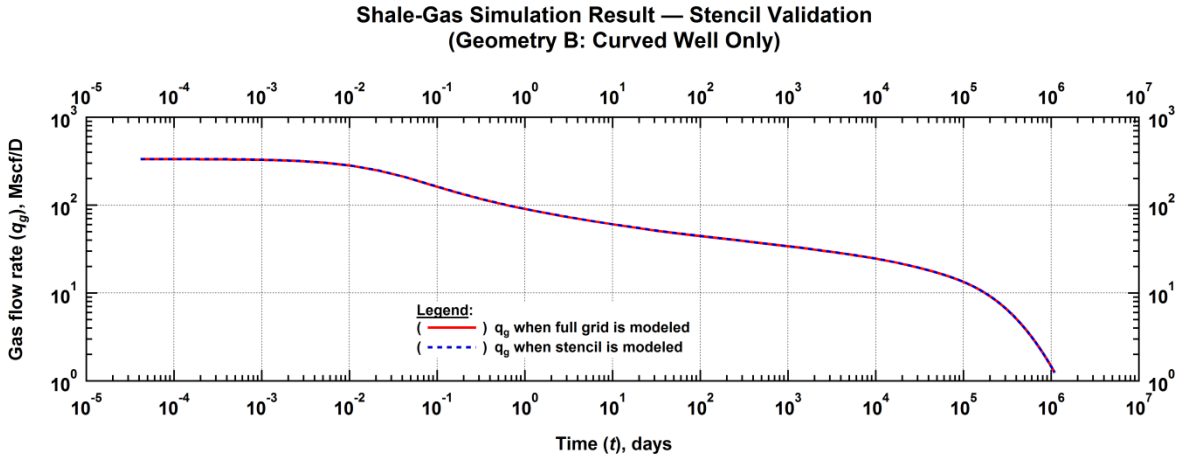

Fig. 4.20— Shale-Gas Simulation: Perfect match between production rates show that the stencil provided an excellent approximation of the full grid model over the reservoir life in the case of Geometry B (the case of the curved well).

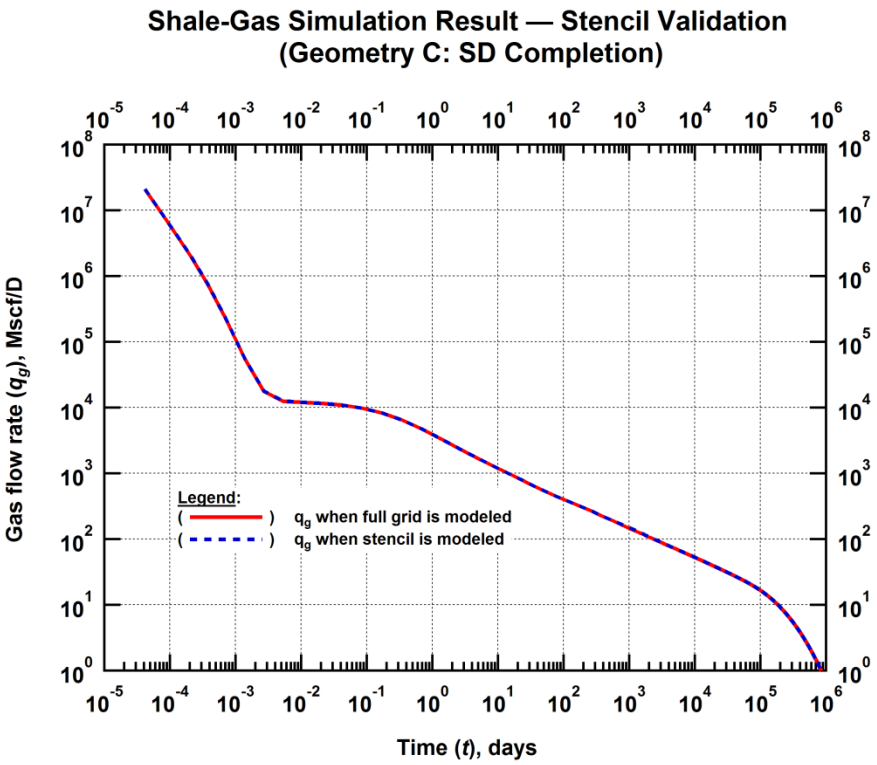

Fig. 4.21— Shale-Gas Simulation: Perfect match between production rates show that the stencil provided an excellent approximation of the full grid model over the reservoir life in the case of Geometry C (the fully described SD Completion).

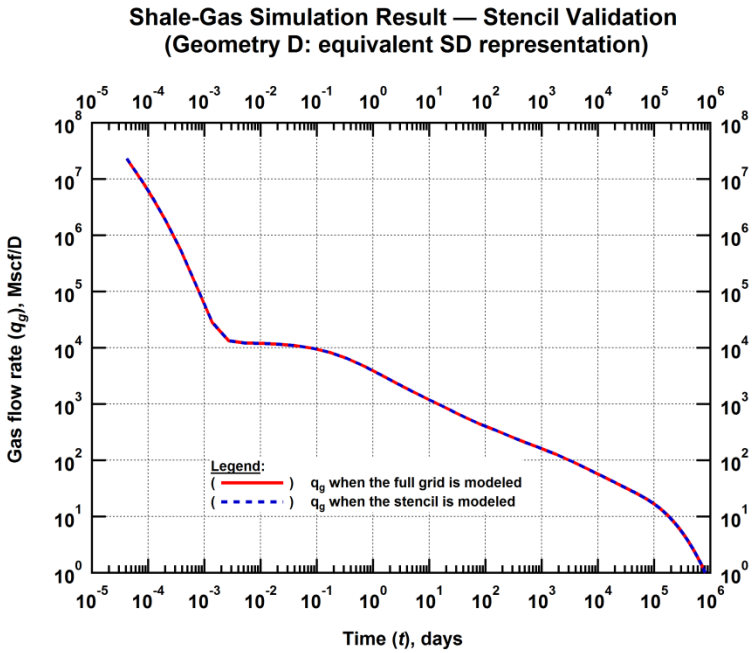

Fig. 4.22— Shale-Gas Simulation: Perfect match between production rates show that the stencil provided an excellent approximation of the full grid model over the reservoir life in the case of Geometry D (equivalent SD representation).

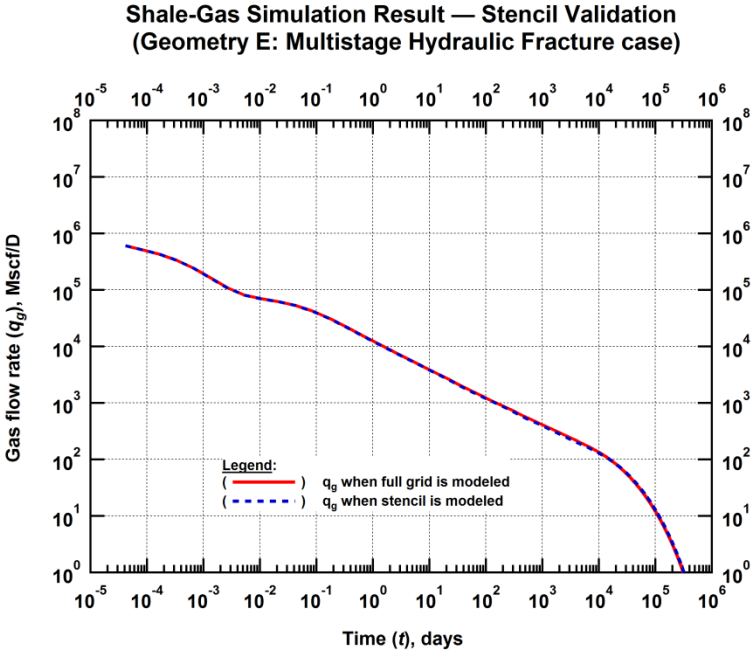

Fig. 4.23— Shale-Gas Simulation: Perfect match between production rates show that the stencil provided an excellent approximation of the full grid model over the reservoir life in the case of Geometry E (Multistage Hydraulic Fracturing).

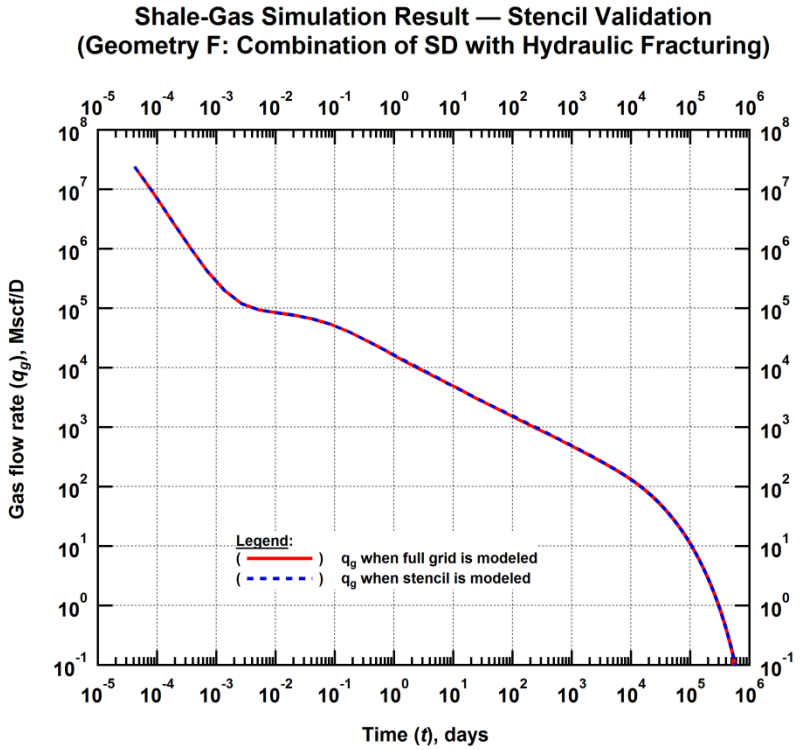

Fig. 4.24— Shale-Gas Simulation: Perfect match between production rates show that the stencil provided an excellent approximation of the full grid model over the reservoir life in the case of Geometry F (Combination of SD with Hydraulic Fracturing).

4.2.2 The shale-gas study: Comparative studies

Here, I also conducted similar comparative studies as I did in the tight-gas study (see section 4.1.2). The findings from these studies are discussed in the sections that follow.

4.2.2.1 The shale-gas study: Straight horizontal well (Geometry A) vs. curved well (Geometry B)

Here also, I investigated if the extra length (and consequently extra surface area available to flow from the formation) of the curved well over the straight horizontal well would provide an advantage to the SD completion in terms of overall gas production. Fig. 4.25 displays the results of this study. Here also, the agreement between the two solutions is excellent after an initial very early stage separation that could be due to numerical discretization errors and can be ignored for practical purposes. Thus we conclude that, under the conditions of the shale gas system we used in this study, the extra length of the curving well appears to offer no advantage over the case of the straight horizontal well (as was the case in production from the tight gas system of Section 4.1.2.1, Fig. 4.7). The evolution of the spatial pressure distribution over time in the reservoir in each of the two cases studied here appear in Fig. 4.26 and 4.27.

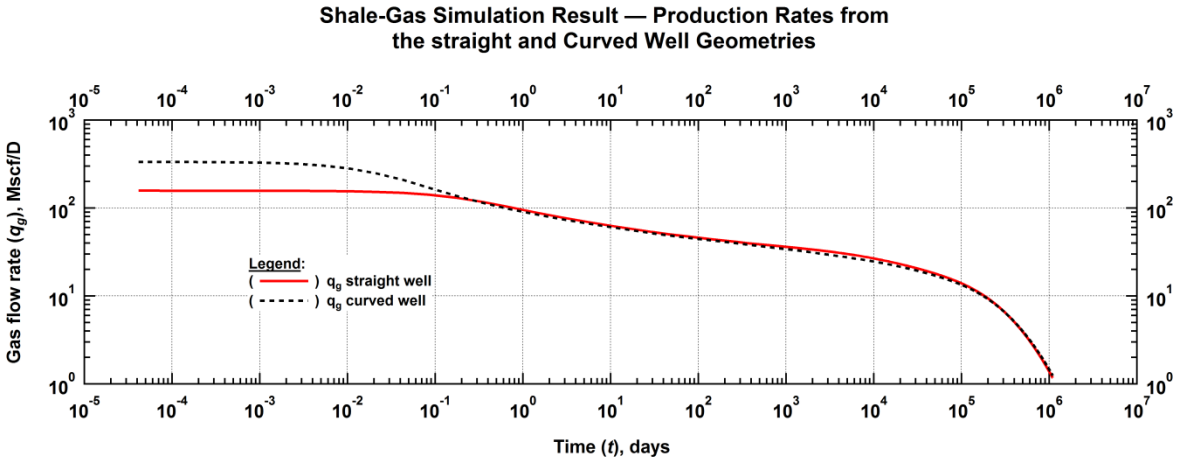

Fig. 4.25— Shale-Gas Simulation: Production rate decline for the curved well matches that of the straight horizontal well after the initial wellbore drainage.

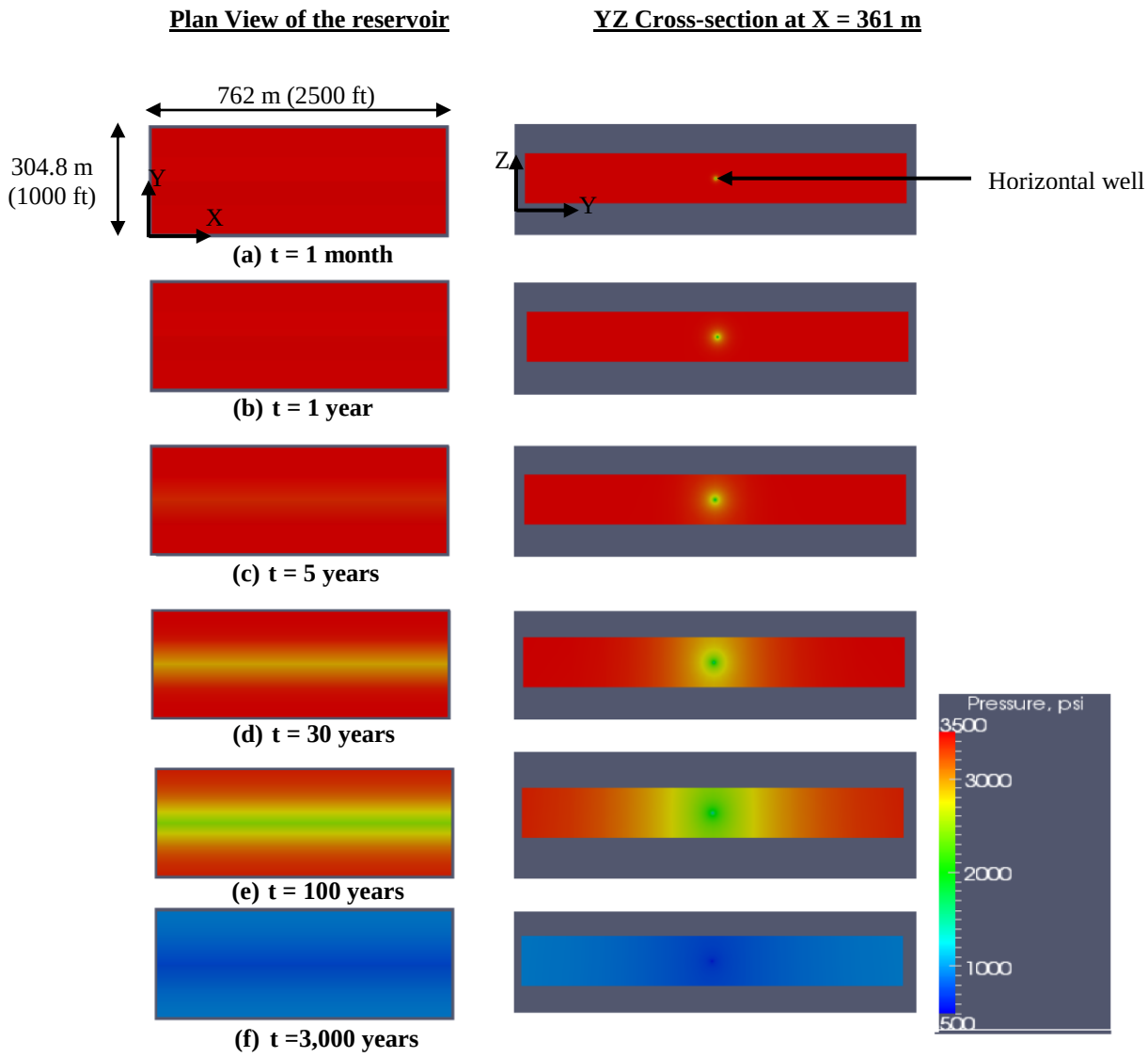

Fig. 4.26— Plan views and cross-sectional views of the pressure distribution over time in the shale-gas reservoir with the properties of the Marcellus formation corresponding to Fig. 4.25 during gas production from a straight horizontal well (Geometry A).

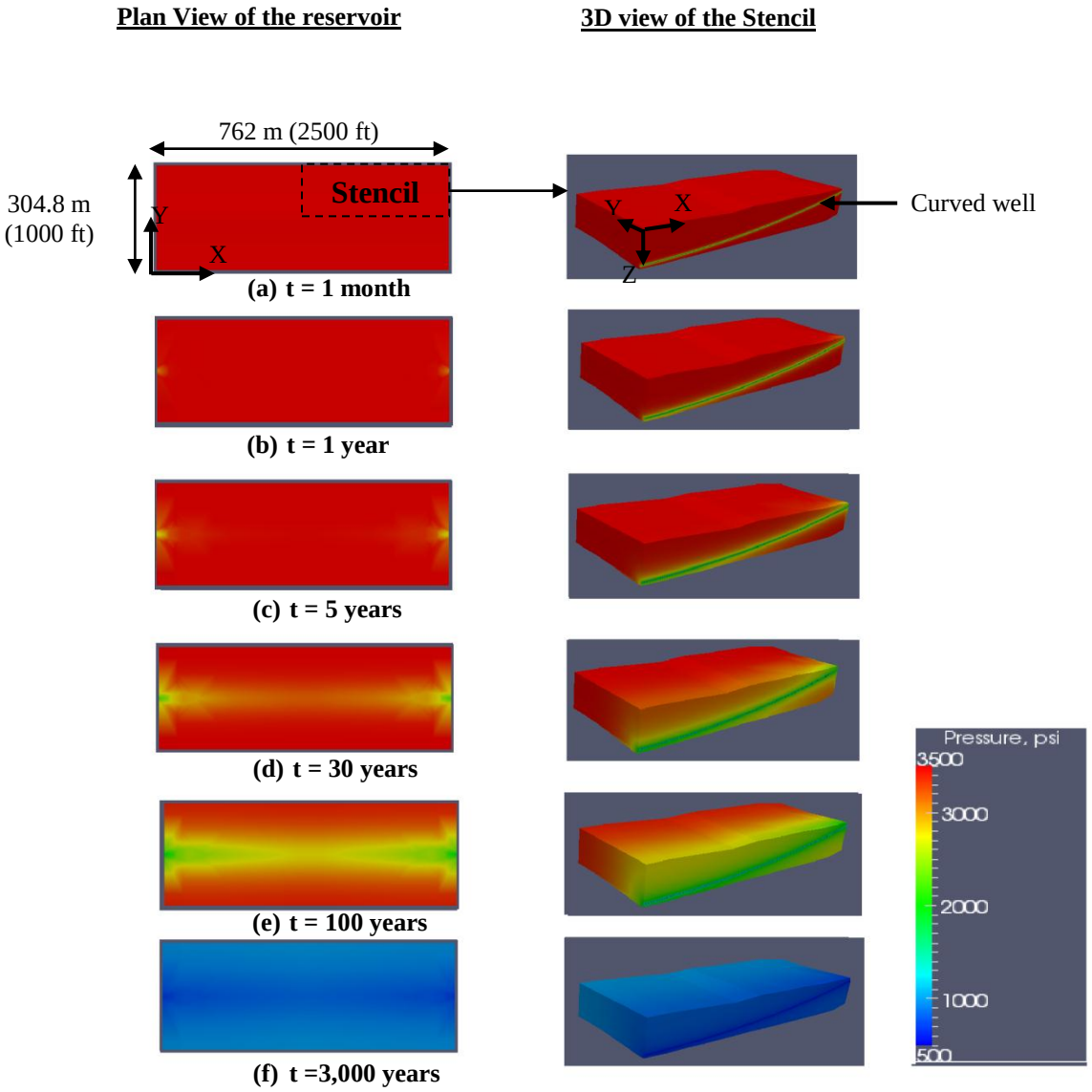

Fig. 4.27—Plan views of the full reservoir and 3D views of the stencil showing the spatial pressure distribution over time in the shale-gas reservoir with properties representative of the Marcellus formation during gas production from a curved well (Geometry B).

4.2.2.2 The shale-gas study: The closely representative discretization of the SD (Geometry C) vs. the "equivalent SD representation" (Geometry D)

I also tested the ability of the equivalent SD representation (see Section 3.4) to accurately model production from the SD completion method. Fig. 4.28 shows the simulated production rates from this representation and those from the fully-described SD representation. Apart from a slight deviation at very early times (less than 0.01 days) a near-perfect match is observed. This deviation was hypothesized to be as a result of early-time differences in the wellbore drainage in the two models caused by their different well trajectories (curved as opposed to straight). The observed match validated the hypothesis that the simpler equivalent SD configuration could accurately represent the full SD completion in the shale-gas reservoir of this study. In Fig. 4.29 and 4.30 I show plots illustrating the change of the spatial distribution of pressure through time in these two systems.

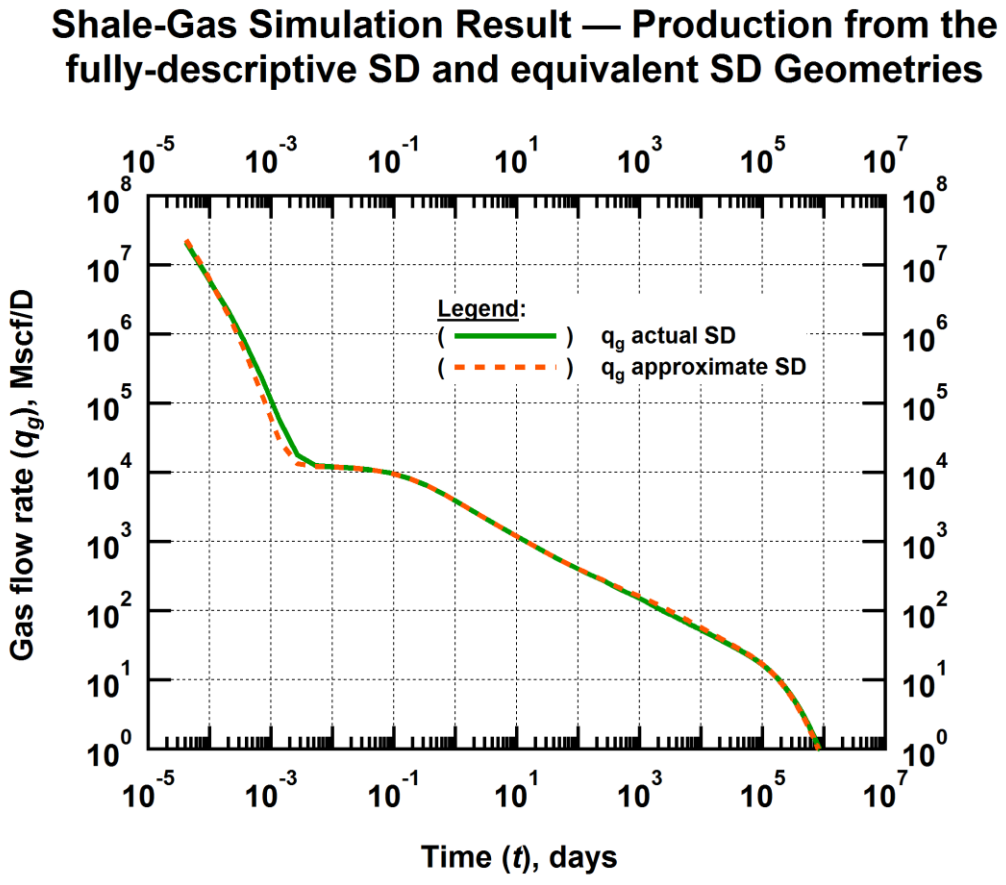

Fig. 4.28—Shale-Gas Simulation: Production rate decline for the equivalent SD representation matches that of the actual.

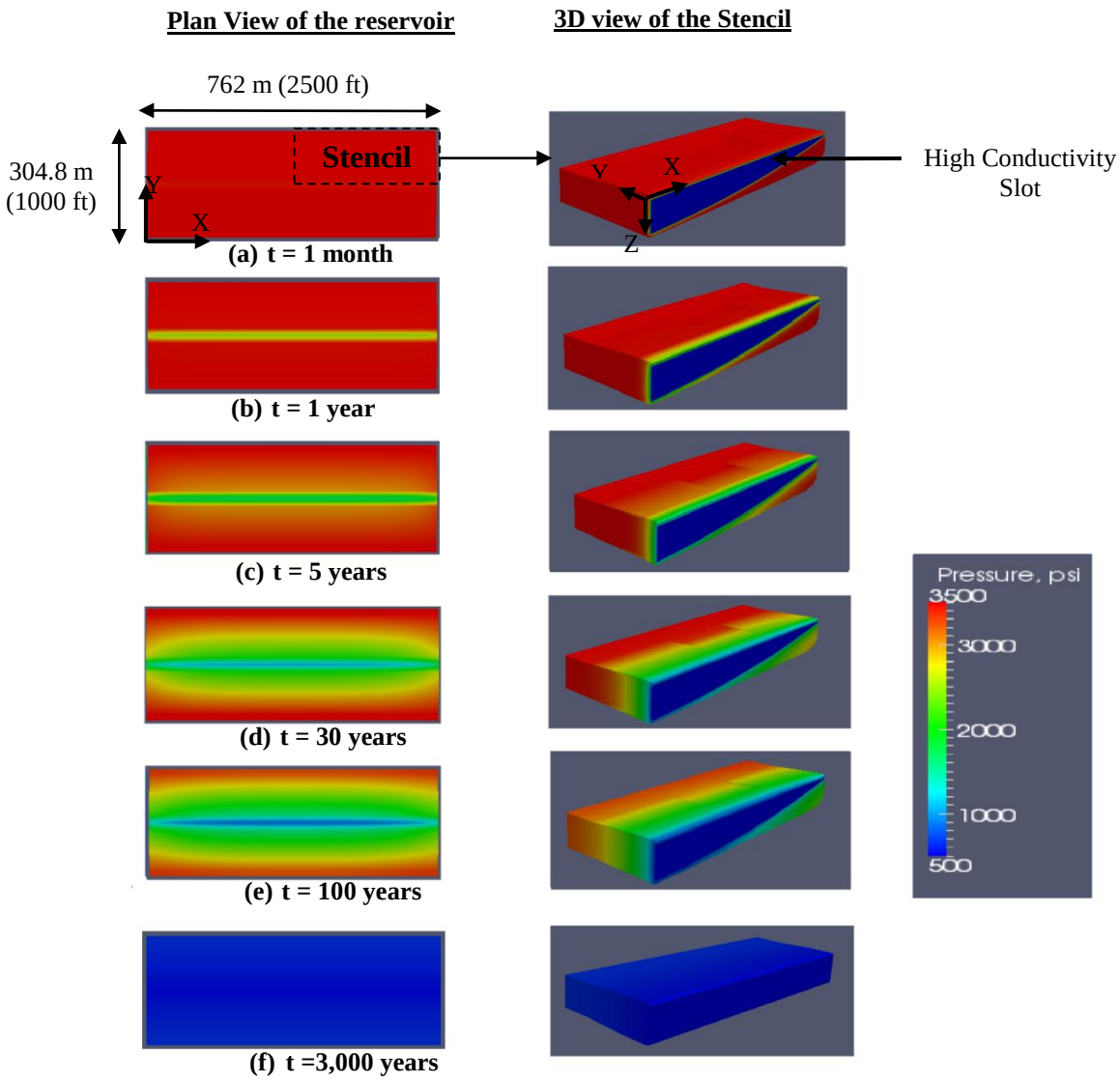

Fig. 4.29—Plan views of the full reservoir and 3D views of the stencil showing the spatial pressure distribution over time in the shale-gas reservoir with properties representative of the Marcellus formation during gas production from the SD completion (Geometry C).

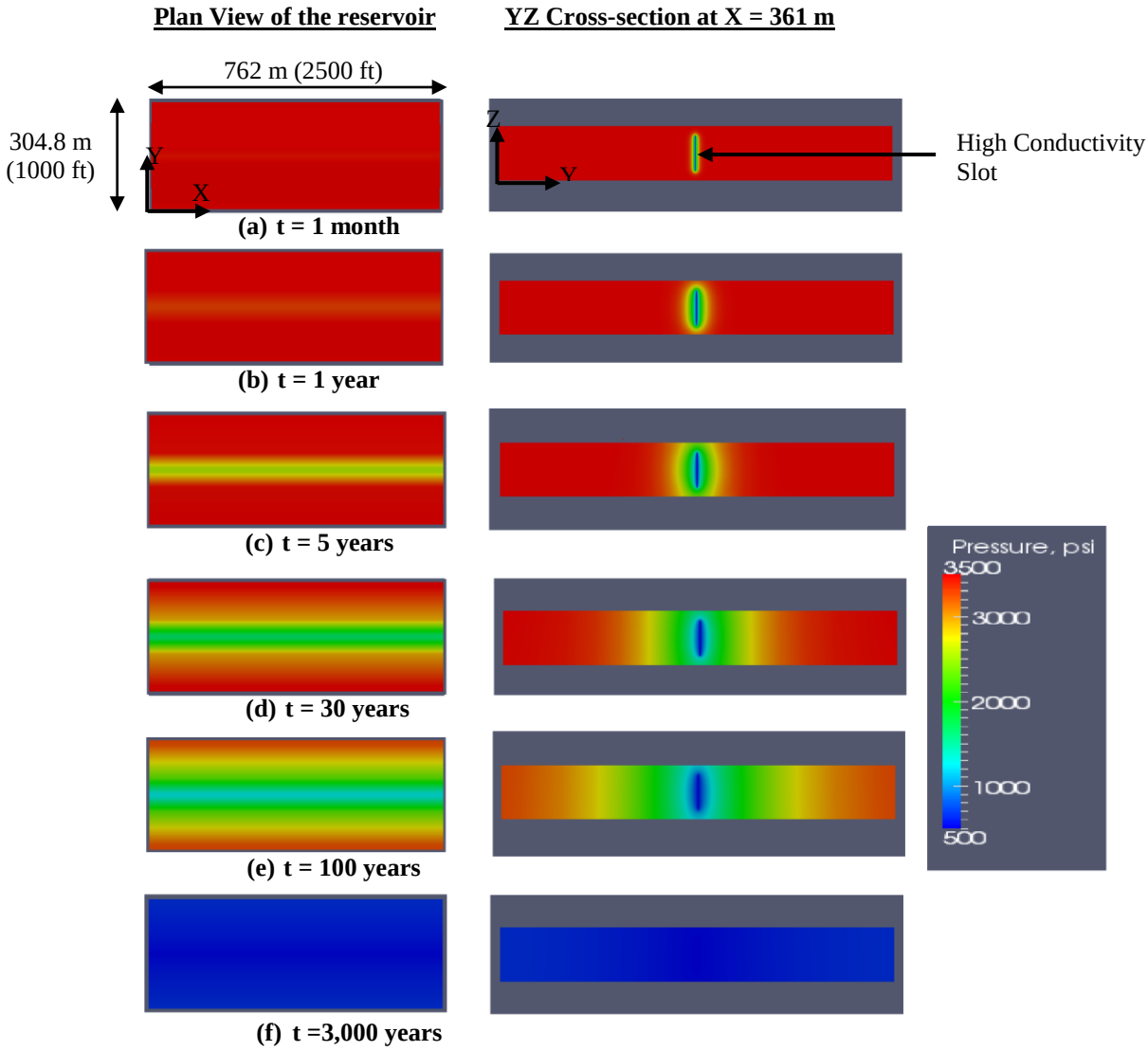

Fig. 4.30—Plan views and cross-sectional views of the pressure distribution over time in the shale-gas reservoir with properties representative of the Marcellus formation during gas production from the equivalent SD representation (Geometry D)

4.2.2.3 The shale-gas study: The SD method (Geometry C) vs. multiple hydraulic fracturing (Geometry E)

I followed the same approach as in the tight-gas case (see Section 4.1.2.3, Fig. 4.13) to compare the production estimate from the SD completion to that from the standard treatment (involving multi-stage hydraulic fracturing). In Fig. 4.31, the production rates from the SD-completed reservoir generally do not compare favorably with the rates from the multistage hydraulically fractured reservoir except at meaninglessly early (from a practical standpoint) times. In fact, when we combine the observation from this plot with what is shown on the cumulative production plot (Fig. 4.32), we see that the standard hydraulically-fractured system far outperforms the SD completion. A longer reservoir life (100 years) was assumed here due to the lower permeability of the shale-gas formation (as compared to the tight-gas formation). This led to the similar conclusion that the larger surface area to flow that multistage hydraulic fracturing provides (1.378×10^6 ft.^{2} for multistage hydraulic fracturing as opposed to 0.401×10^6 ft.^{2} for the SD method) creates a more significant production advantage than the higher conductivity (4208 md-ft. for the SD method as opposed to 499 md-ft. for the hydraulic fractures) achieved using the SD technique. Fig. 4.33 illustrates the decline of the reservoir pressure in the hydraulically fractured reservoir as production progressed through time.

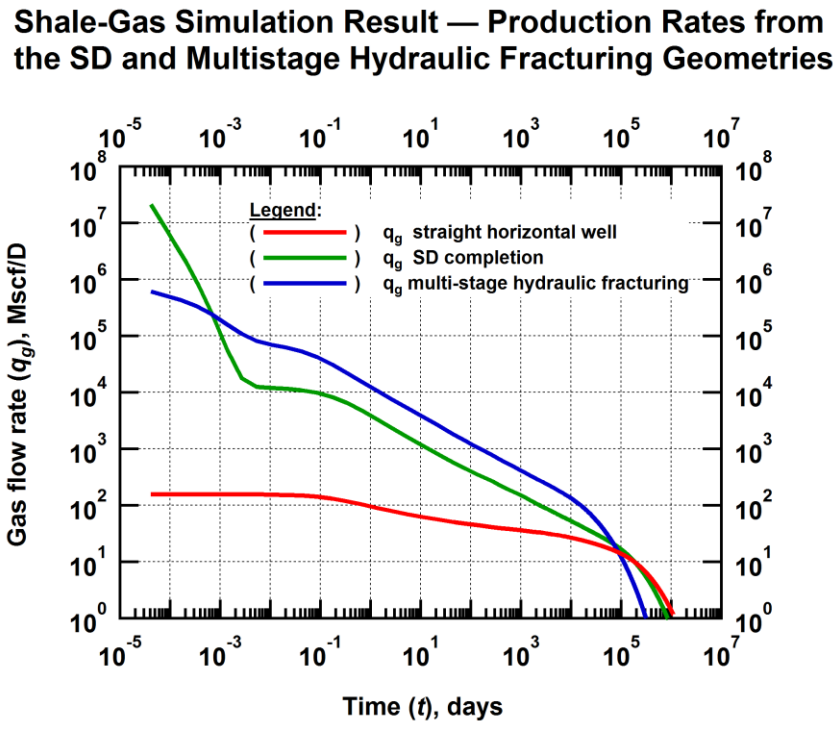

Fig. 4.31—Shale-Gas Simulation: Production rates from the SD completion do not compete favorably with those from multi-stage hydraulic fracturing here also.

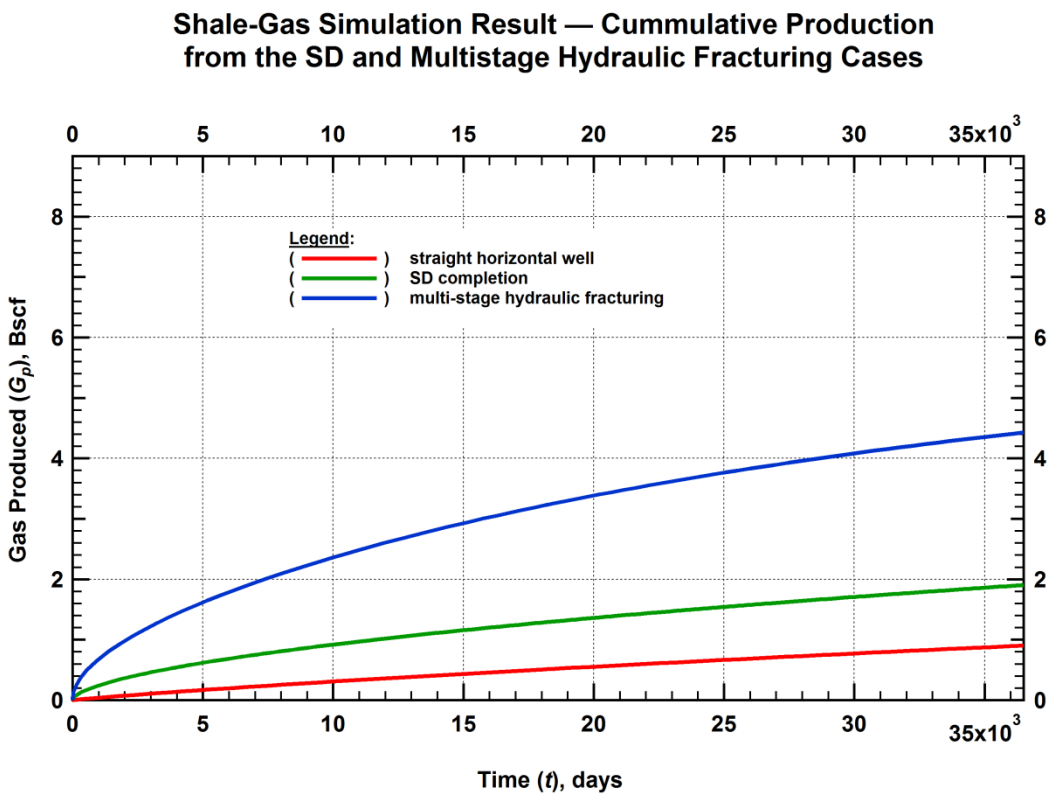

Fig. 4.32—Cumulative Production curves show that the SD completion does not compete favorably in terms of production with multistage hydraulic fracturing for the shale-gas study conducted.

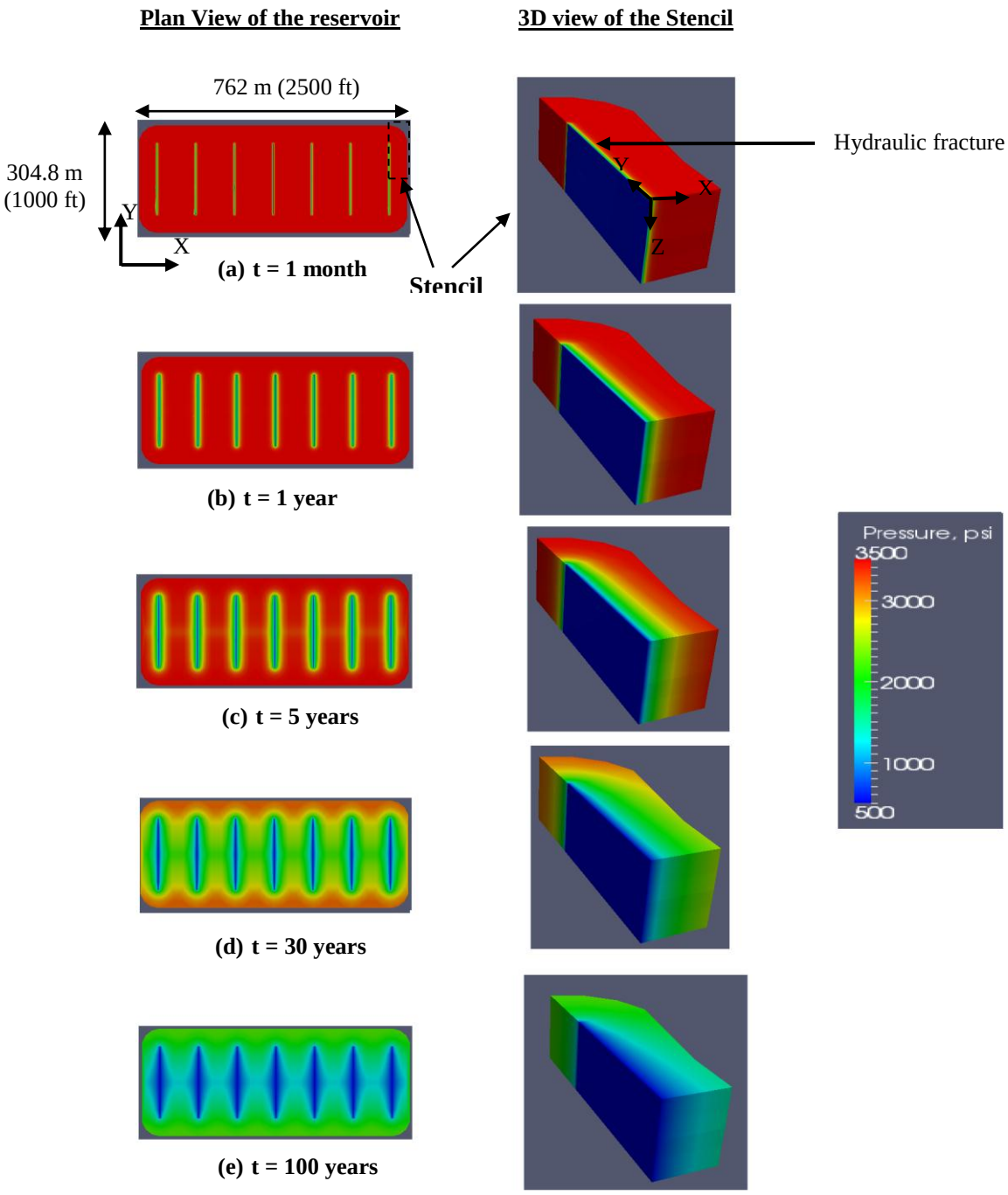

Fig. 4.33—Plan views of the full reservoir and 3D views of the stencil showing the spatial pressure distribution over time in the shale-gas reservoir with properties representative of the Marcellus formation during gas production from the multistage hydraulic fracturing case (Geometry E).

4.2.2.4 The shale-gas study: The standard multistage hydraulic fracturing method (Geometry E) vs. the combination of multiple hydraulic fracturing with the SD method (Geometry F)

For the shale-gas study, when I conducted the simulation of the case of the combination of the SD method with hydraulic fracturing (Geometry F), no significant boost in production over the standard hydraulically fractured system (Geometry E) was achieved. The rate increase (as can be seen in Fig. 4.34) was only marginal, and limited to very early times (too short to make any practical difference). The cumulative production plots presented in Fig. 4.35 however showed a more significant improvement in the production performance of the combination case over the standard treatment case than what was obtained in the tight-gas study. However, here also, a full economic analysis would be required to determine if the production boost is sufficient to justify the extra expense of creating the slot. In Fig. 4.36 I show the evolution of the spatial pressure distribution over time in the shale-gas reservoir system completed with a combination of the SD technique and multistage hydraulic fracturing.

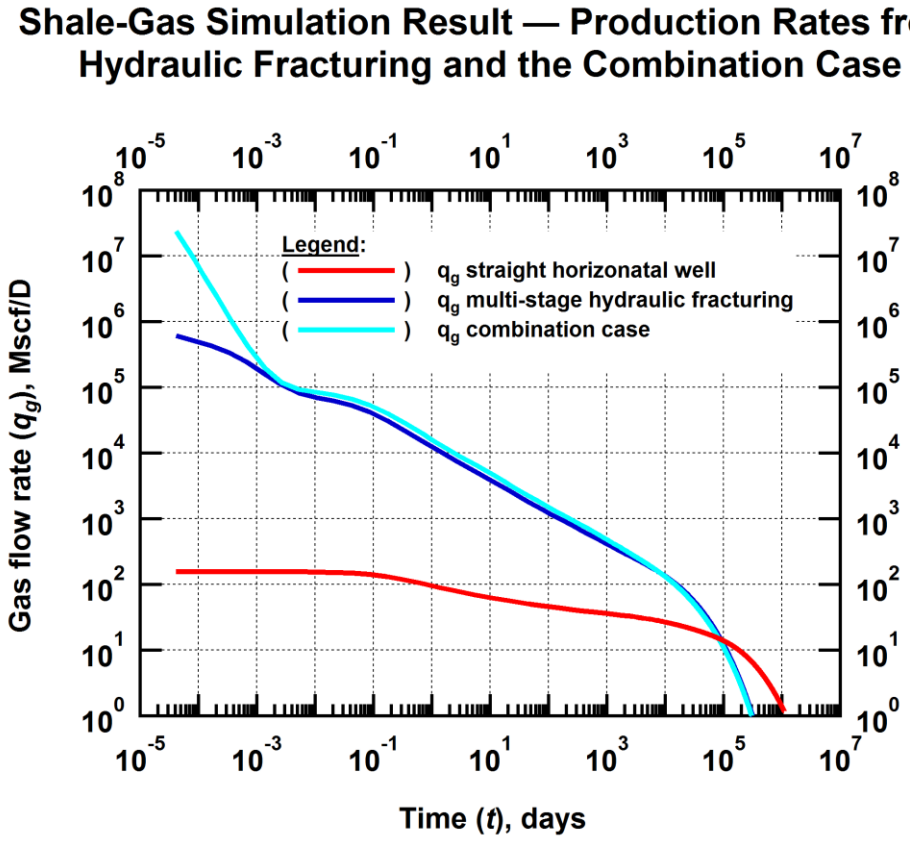

Fig. 4.34—Shale-Gas Simulation: Very marginal increase in production rates observed when SD is combined with multistage hydraulic fracturing.

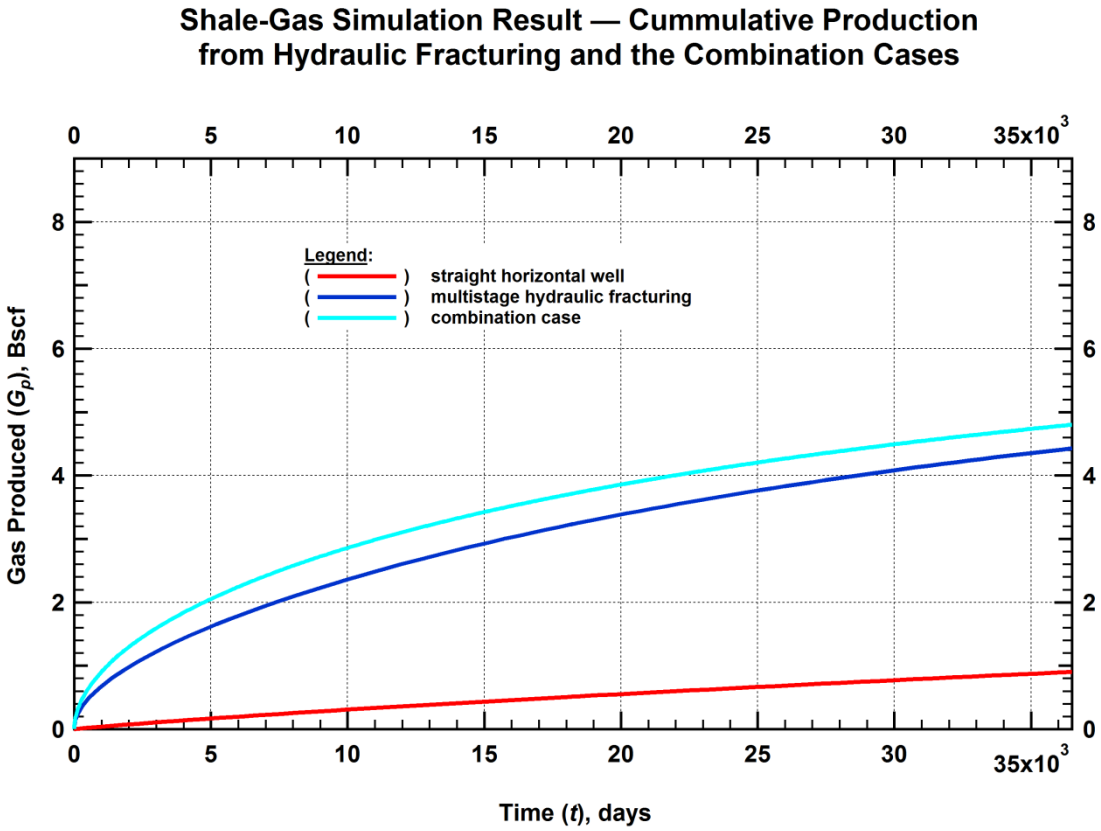

Fig. 4.35—Cumulative Production curves show a bigger production advantage resulting from the combination of the SD with multistage hydraulic fracturing in the shale-gas study than what was observed in the tight-gas study.

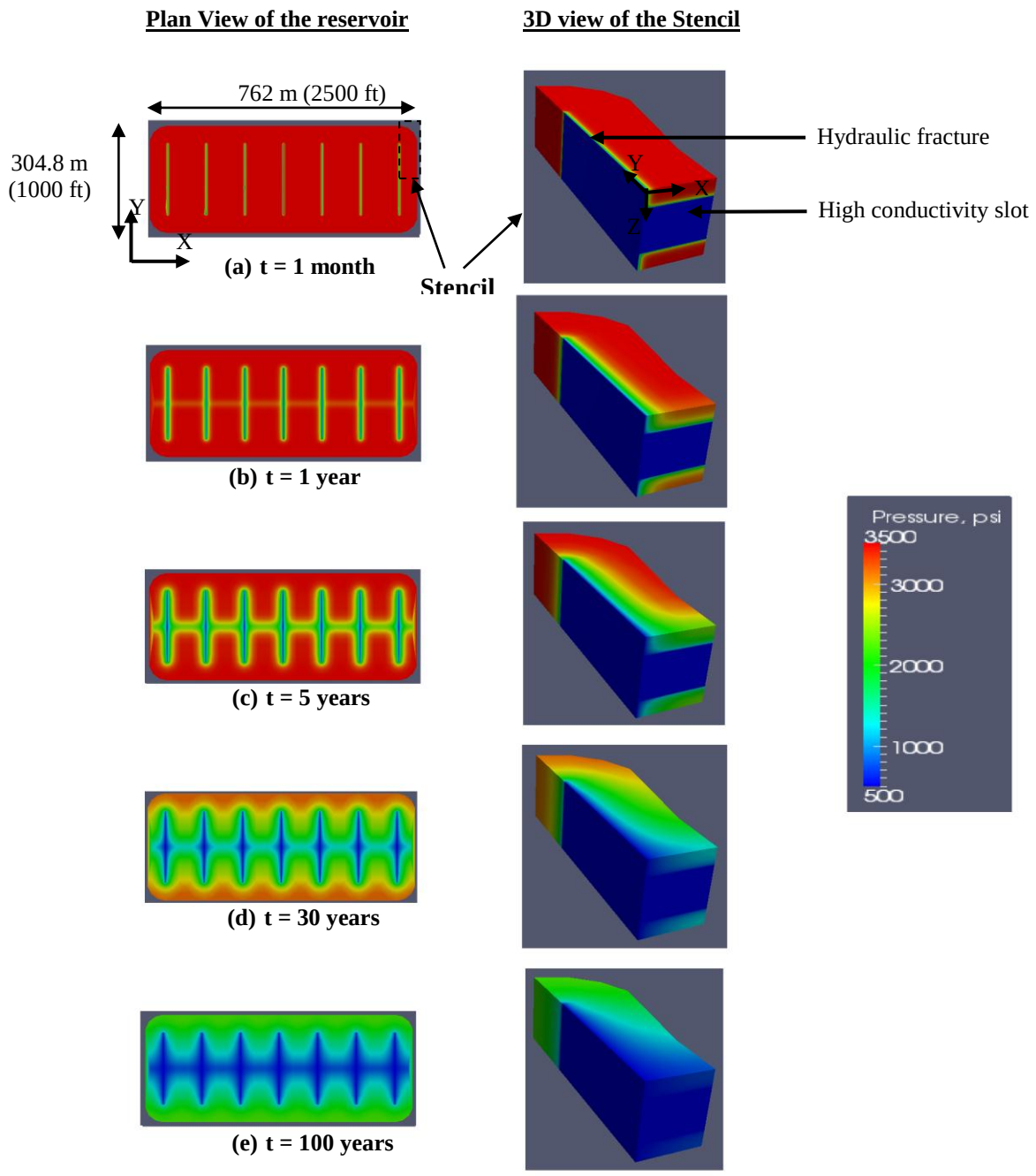

Fig. 4.36— Plan views of the full reservoir and 3D views of the stencil showing the spatial distribution of pressure in a shale-gas reservoir (representative of the Marcellus formation) at various stages of production when completed with a combination of the SD and multistage hydraulic fracturing (Geometry F).

4.3 The tight/shale-oil simulation study

The simulations in this section were conducted using the properties of the Bakken formation in **Table 1.3**.

4.3.1 The tight/shale-oil study: Stencil validations

As in the tight-gas study (see section 4.1.1) and the shale-gas study (see section 4.2.1), I also investigated the ability of the stencil to accurately predict flow and production in all the reservoir systems of interest (Geometries A through F) for the tight/shale-oil study. In Fig. 4.37 through 4.42 I show the simulated production rates obtained from the stencil models in conjunction with those obtained from the full-grid models. Here also, the production rates from the stencils (in all the geometries) matched perfectly with those from their respective full-grid models. The implication of these matches, as in the other two previous studies, meant I could replace the full-grid models with their respective stencils (which are more efficient in terms of time and computational power required) without compromising the accuracy of the solutions in the rest of my simulation runs.

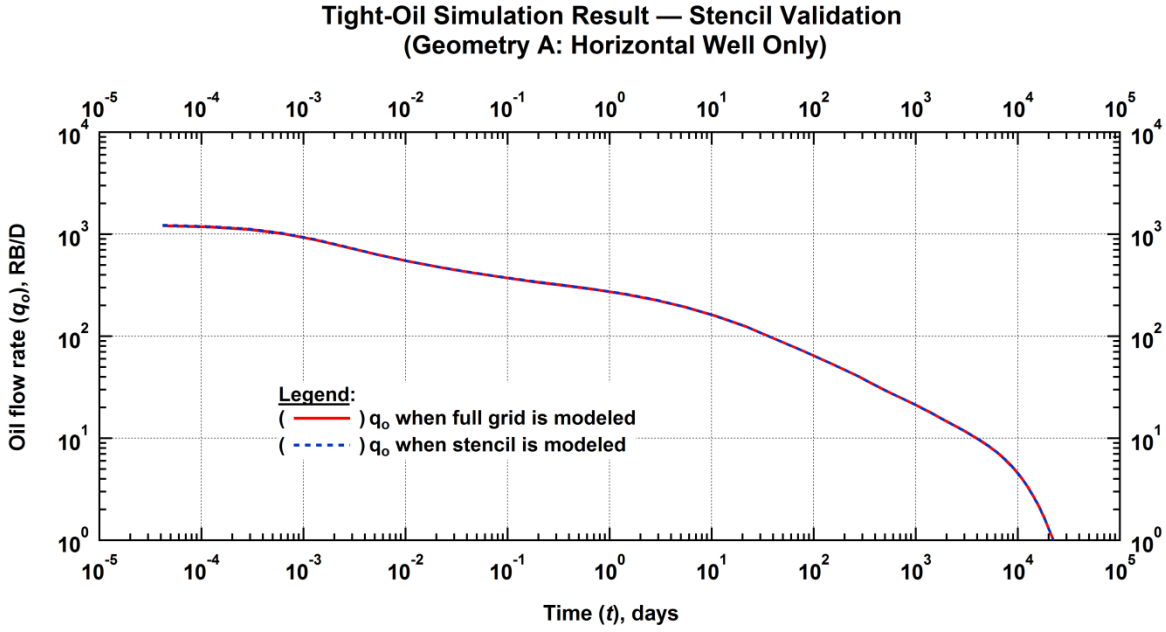

Fig. 4.37—Tight-oil Simulation: Perfect match between production rates show that the stencil provided an excellent approximation of the full grid model over the reservoir life in the case of Geometry A (the case of the straight horizontal well only).

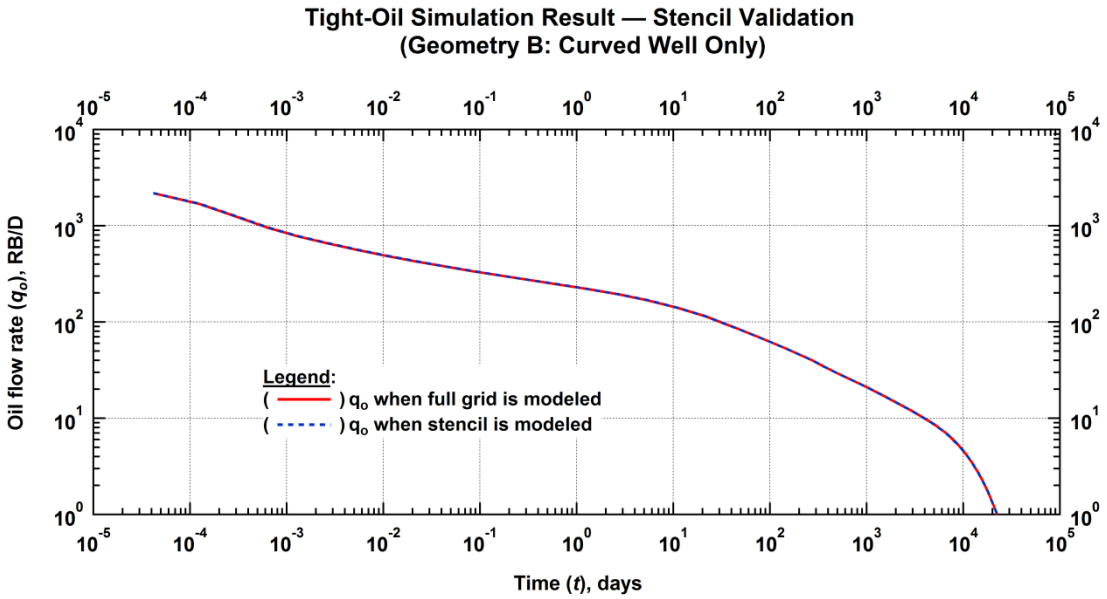

Fig. 4.38— Tight-oil Simulation: Perfect match between production rates show that the stencil provided an excellent approximation of the full grid model over the reservoir life in the case of Geometry B (Curved well only).

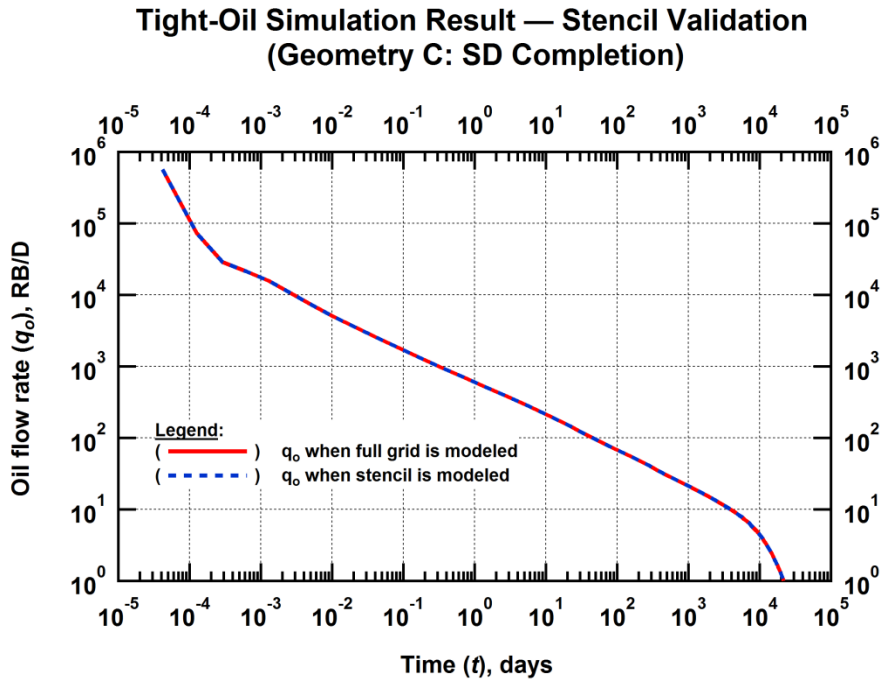

Fig. 4.39— Tight-oil Simulation: Perfect match between production rates show that the stencil provided an excellent approximation of the full grid model over the reservoir life in the case of Geometry C (SD Completion).

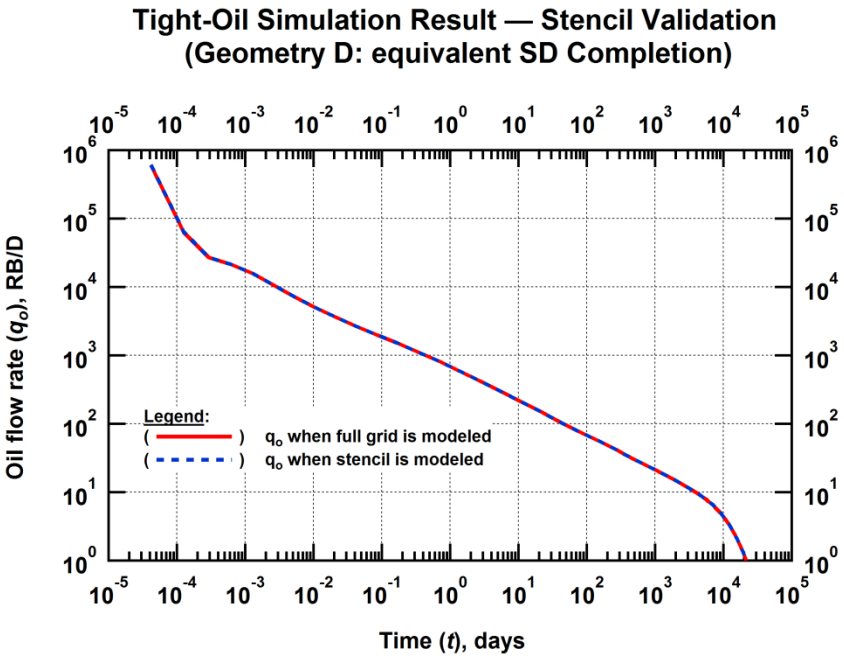

Fig. 4.40— Tight-oil Simulation: Perfect match between production rates show that the stencil provided an excellent approximation of the full grid model over the reservoir life in the case of Geometry D (the equivalent SD representation).

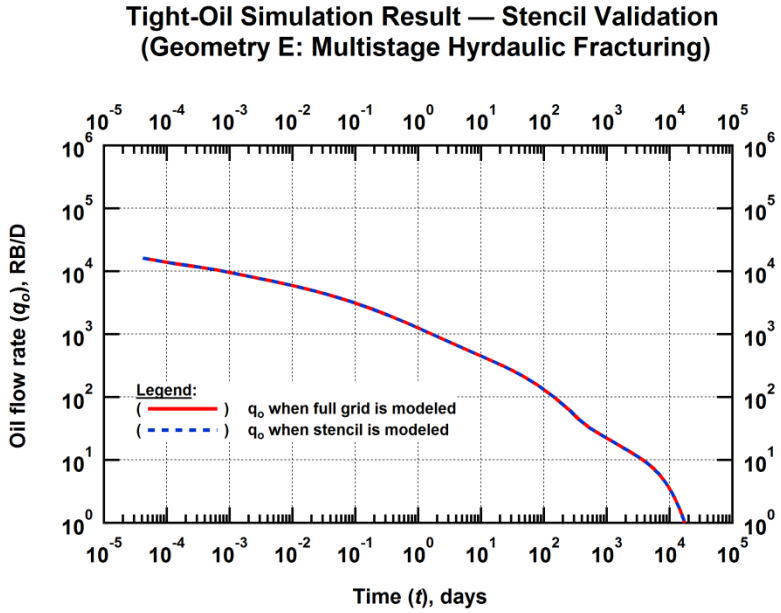

Fig. 4.41— Tight-oil Simulation: Perfect match between production rates show that the stencil provided an excellent approximation of the full grid model over the reservoir life in the case of Geometry E (Multistage Hydraulic Fracturing).

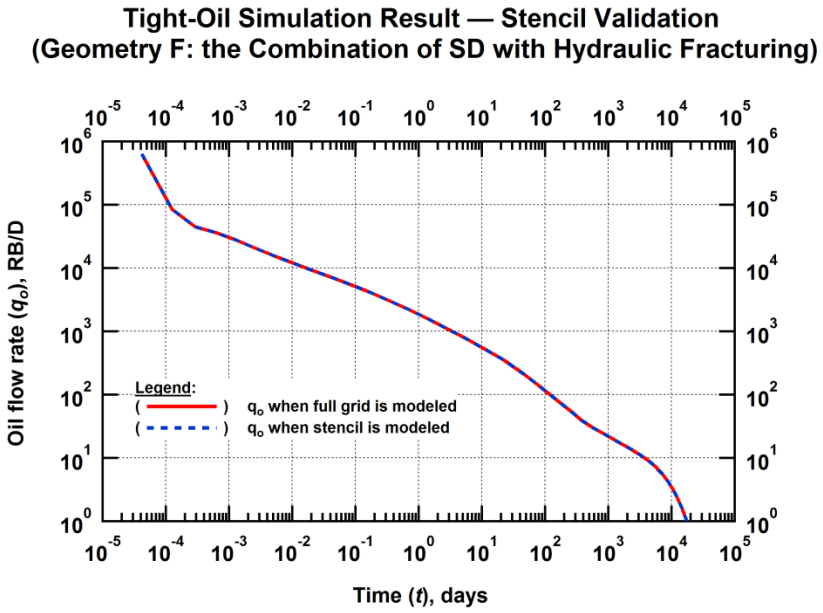

Fig. 4.42—Tight-oil Simulation: Perfect match between production rates show that the stencil provided an excellent approximation of the full grid model over the reservoir life in the case of Geometry F (Combination of SD with Hydraulic Fracturing).

4.3.2 The tight/shale-oil study: Comparative studies

Here, I also conducted similar comparative studies as I did in the tight-gas study (see section 4.1.2). The ensuing sections discuss the result of these studies in detail.

4.3.2.1 The tight/shale-oil study: Straight horizontal well (Geometry A) vs. curved well (Geometry B)

I came to the same conclusion as in the previous studies when I compared production from the straight horizontal well to that from the curved well. Though not as near-perfect as in the previous cases (Sections 4.1.2.1 and 4.2.2.1, Fig. 4.7 and 4.25), a good overall match is observed (see Fig. 4.43), leading to the conclusion that the longer length of the curving well does not provide any production advantage. The less-than-perfect match observed was interpreted to be due to gravity effects that are more significant in this case (oil being denser than gas). The cumulative production curves of these two systems presented in Fig. 4.44 match closely and thus confirm my earlier stated conclusion. The pressure profiles in these reservoir systems corresponding to the curves in Fig. 4.43 and 4.44 are shown in Fig. 4.45 and 4.46. In this case, and in the case of the ensuing studies, I only displayed the plan view of the reservoir. The productive zone of the Bakken formation is thin and extensive (see Table 1.3) – resulting in a sheet-like geometry for the

tight-oil reservoir that was simulated. As a result, presenting 3D views of the formation in this case provided no additional information (to what can be seen in the plan views).

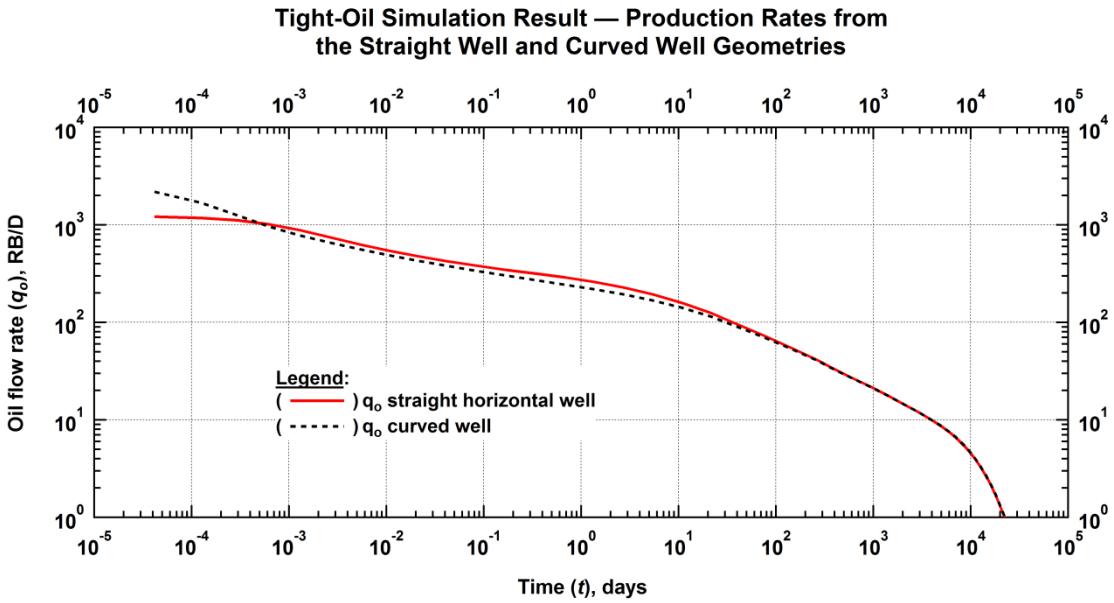

Fig. 4.43—Tight-oil Simulation: Production rate decline for the curved well fairly matches that of the straight horizontal well.

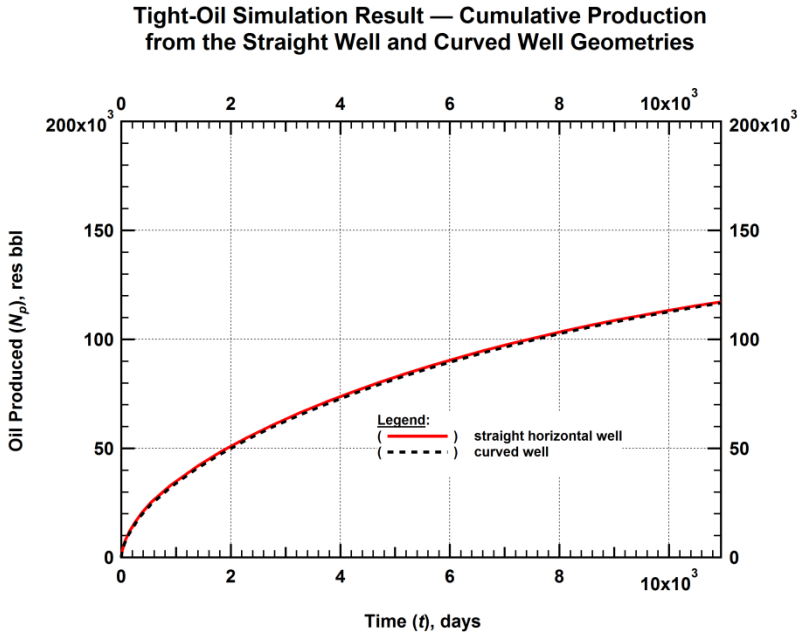

Fig. 4.44—Cumulative production curves show that there is no significant difference in production from the straight and curved well geometries

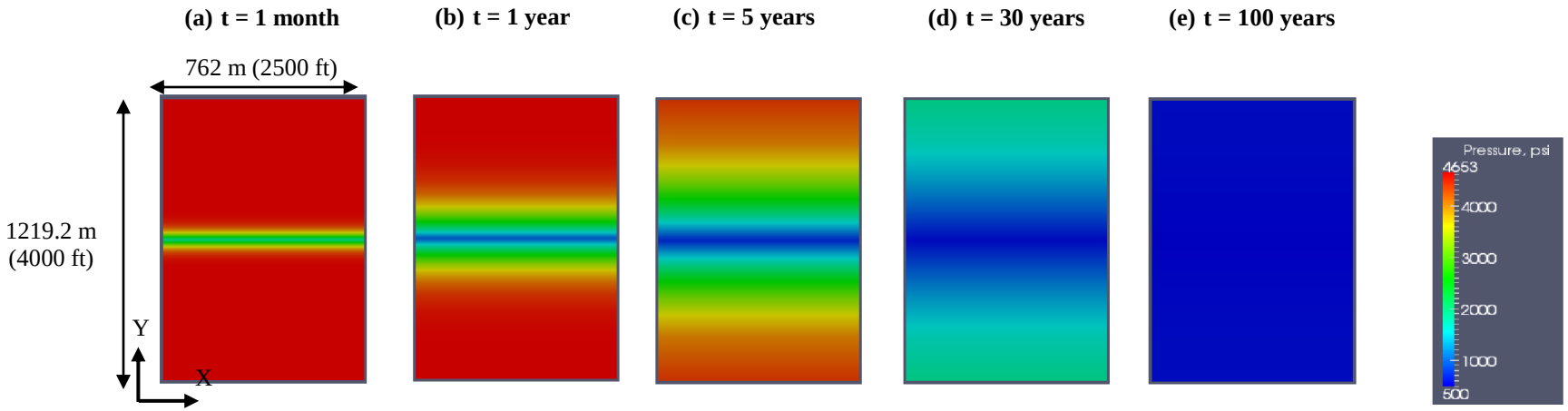

Fig. 4.45—Plan views of the pressure distribution over time in the tight-oil reservoir with properties representative of the Bakken formation during oil production from the horizontal well (Geometry A)

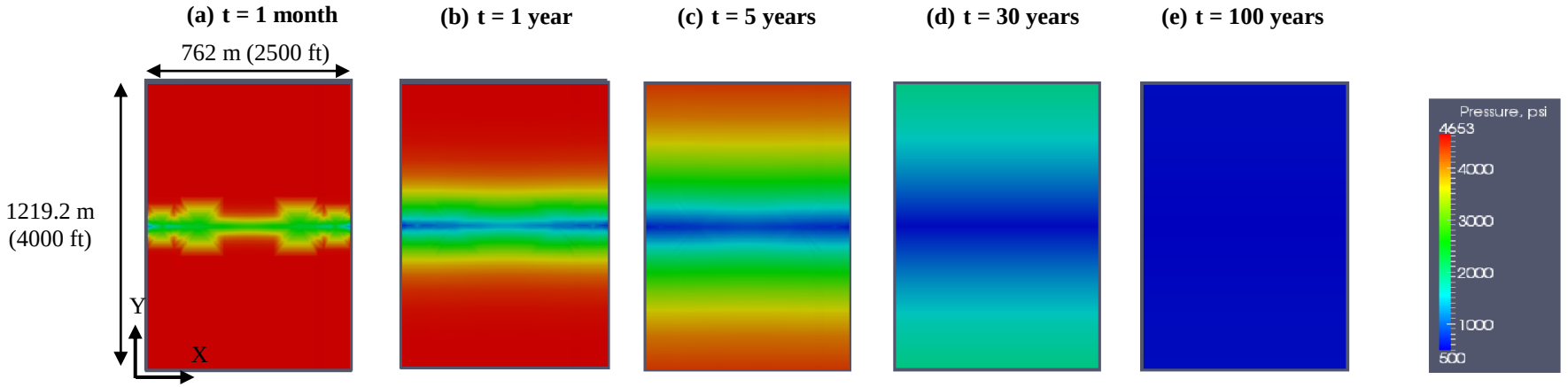

Fig. 4.46—Plan views of the pressure distribution over time in the tight-oil reservoir with properties representative of the Bakken formation during oil production from the curved well (Geometry B)

4.3.2.2 The tight/shale-oil study: The closely representative discretization of the SD (Geometry C) vs. the "equivalent SD representation" (Geometry D)

The ability of the "equivalent SD representation" (see section 3.4) to accurately predict production from the SD configuration was also tested in this study. Fig. 4.47 shows a near perfect match between the simulated production rates from the two cases, thus validating the hypothesis that instigated this study. Pressure profiles illustrating the reservoir depletion with time in both cases are shown in Fig. 4.48 and 4.49.

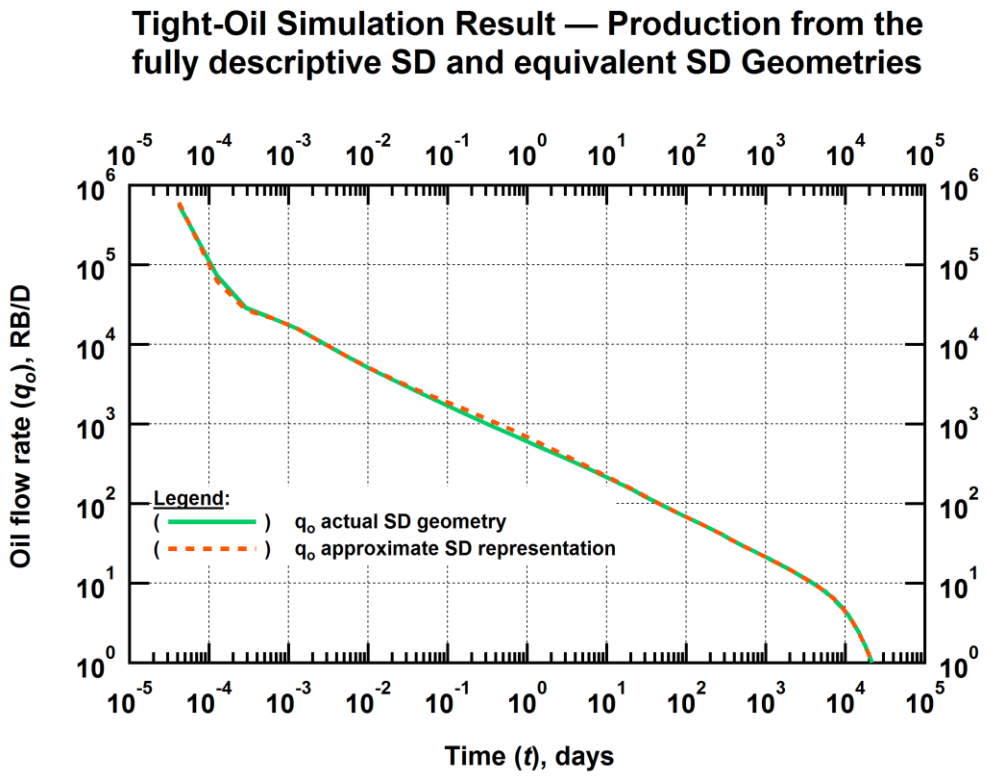

Fig. 4.47—Tight-oil Simulation: Production rate decline for the equivalent SD representation matches that of the actual.

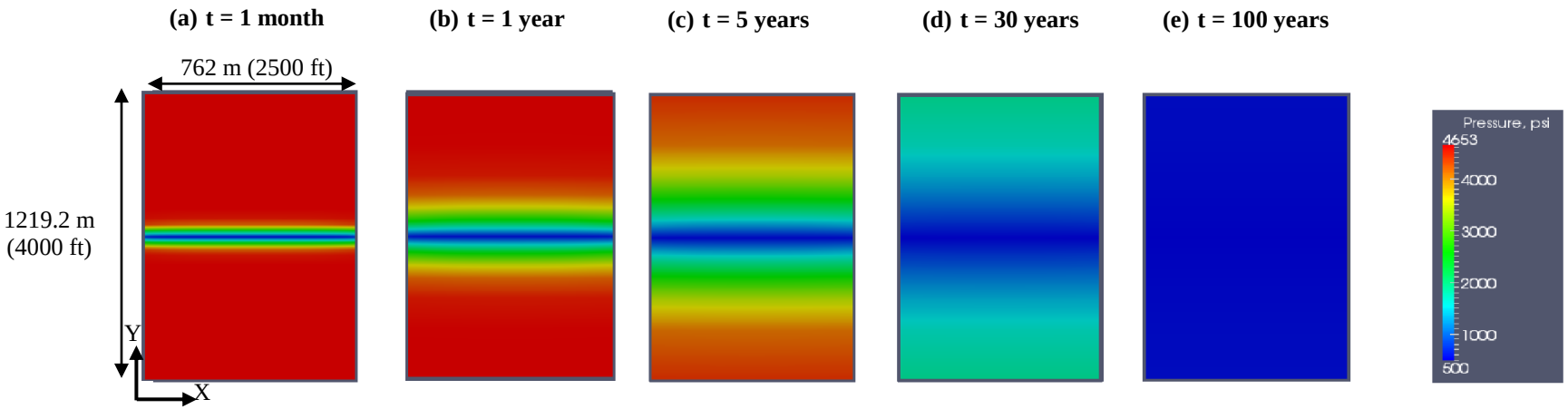

Fig. 4.48—Plan views of the pressure distribution over time in the tight-oil reservoir with properties representative of the Bakken formation during oil production from the SD completion (Geometry C)

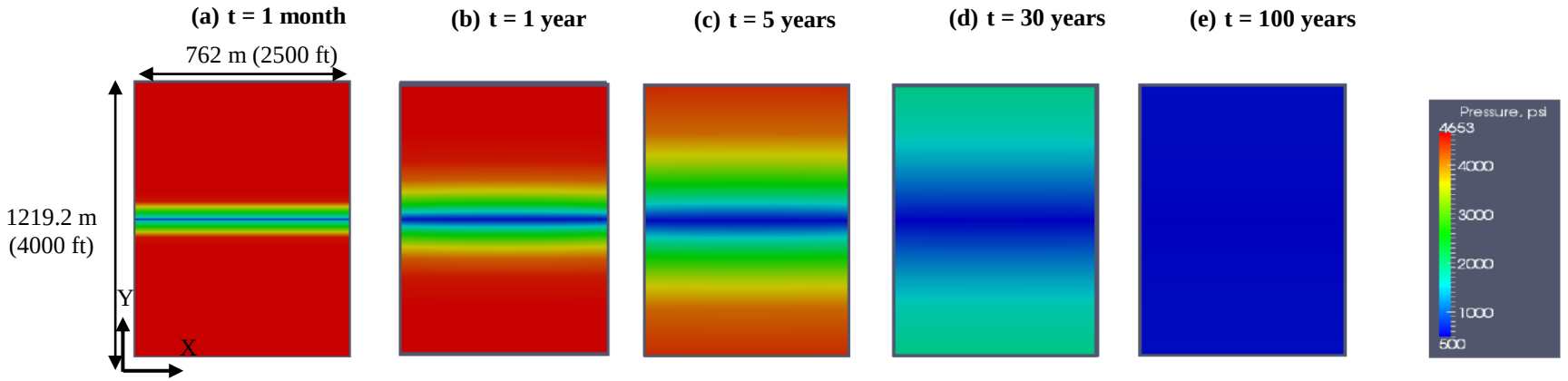

Fig. 4.49—Plan views of the pressure distribution over time in the tight-oil reservoir with properties representative of the Bakken formation during oil production from the equivalent SD representation (Geometry D)

4.3.2.3 The tight/shale-oil study: The SD method (Geometry C) vs. multiple hydraulic fracturing (Geometry E)

The approach to this comparative study here is also the same as was done in the tight-gas (see section 4.1.2.3) and shale-gas (see section 4.2.2.3) studies. In Fig. 4.50, we see that for practically all the important part of the life of the reservoir (with the exception of a very early short period with unimportant impact in the overall behavior), the production rates from the SD-completed reservoir generally do not compare favorably with the rates from the multistage hydraulically fractured. From the cumulative production curves in Fig. 4.51, we see that the standard hydraulically-fractured system outperforms the SD completion. In the case of the tight/shale oil study, multistage hydraulic fracturing resulted in a fracture conductivity of 499 md-ft. and an overall surface area of 0.377×10^6 ft.^{2} while the SD technique resulted in a slot conductivity of 4208 md-ft. but an overall surface area of 0.126×10^6 ft.^{2}. This led me to make the same assertion (as in the previous studies) that the surface area available to flow is a more significant driving factor, in terms of production performance, than the conductivity of the slot or fracture created. Fig. 4.52 illustrates the decline of the reservoir pressure in the hydraulically fractured reservoir as production progressed through time.

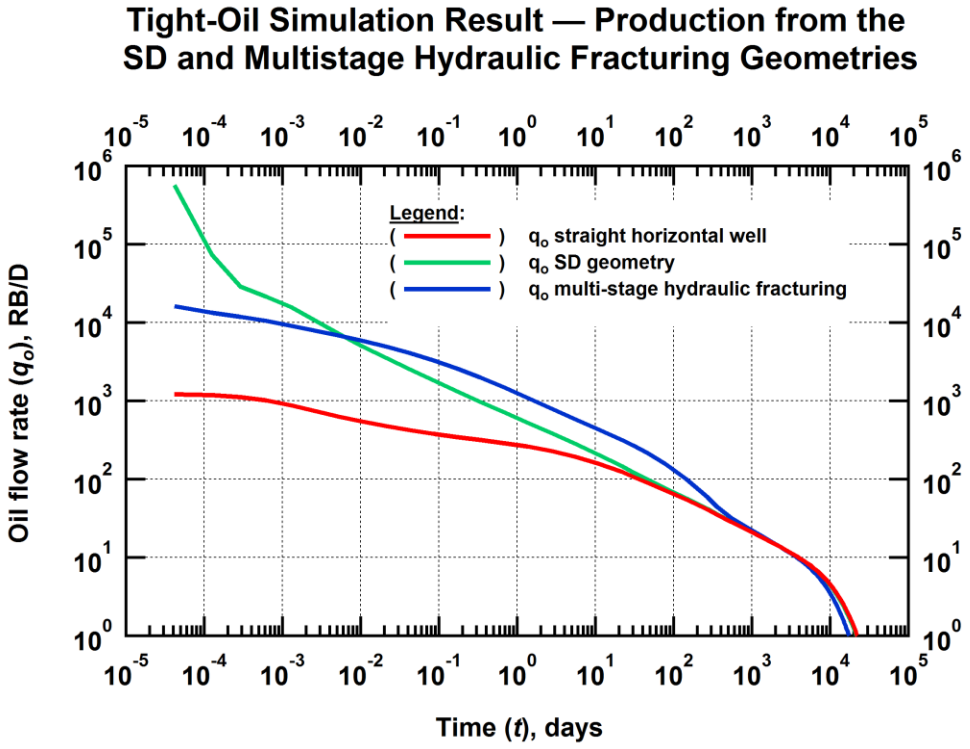

Fig. 4.50—Tight-oil Simulation: Multistage hydraulic fracturing yields higher production rates than those from the SD completion during the fracture/slot linear flow regime of life of the reservoir.

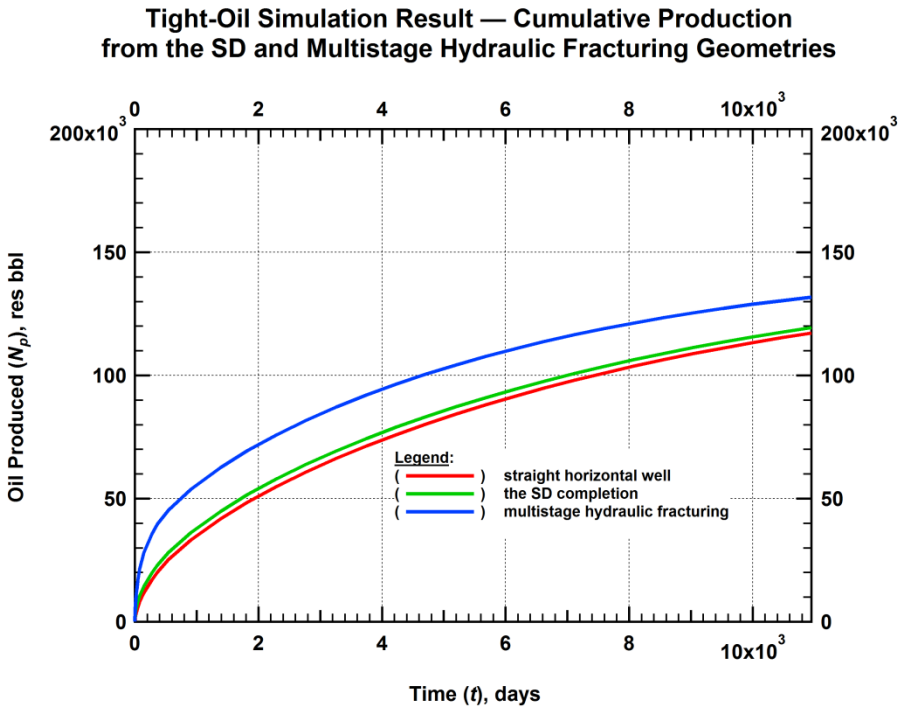

Fig. 4.51—Cumulative Production curves show that the improvement obtained from the implementation of the SD completion over the unstimulated reservoir case is only marginal and does not compare with the improvement achieved when multistage hydraulic fracturing is used in this the tight-oil study.

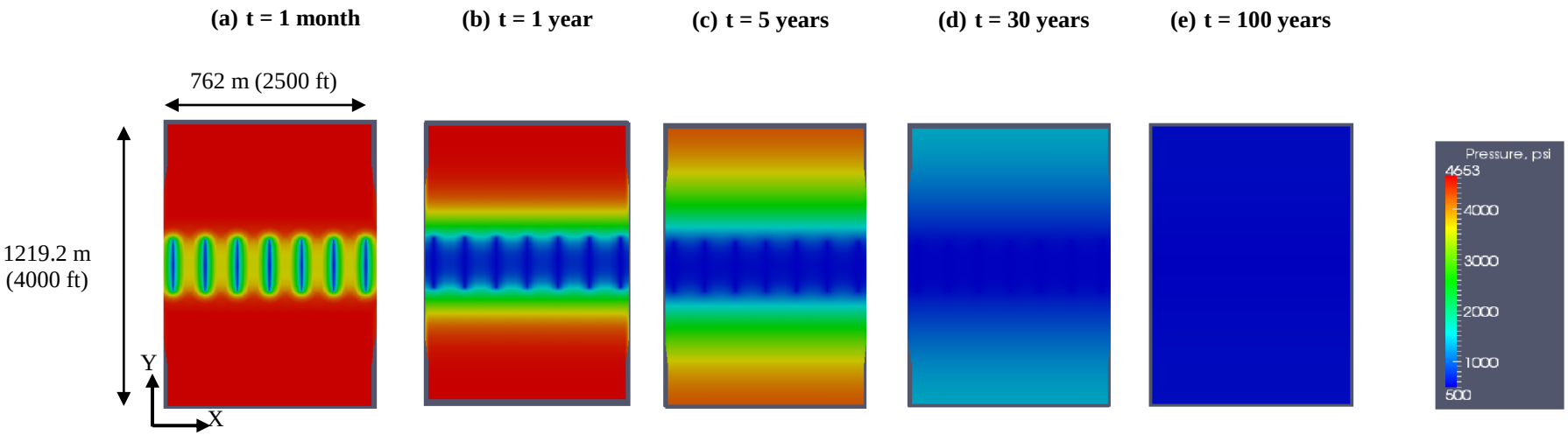

Fig. 4.52—Plan views of the pressure distribution over time in the tight-oil reservoir with properties representative of the Bakken formation during oil production from the multistage hydraulic fracturing case (Geometry E)

4.3.2.4 The tight/shale-oil study: The standard multistage hydraulic fracturing method (Geometry E) vs. the combination of multiple hydraulic fracturing with the SD method (Geometry F)

Fig. 4.53 shows a plot of the obtained simulated production rates from the tight/shale-oil reservoir system completed with the standard treatment (involving multistage hydraulic fracturing only) and those from the case where we have the combination of hydraulic fracturing with the SD completion method. We see that though there is some increase in production rates (from the combination case), the duration over which this advantage is sustained is not very long (about 10 days). The cumulative production curves in Fig. 4.54 show that, as a result of being short-lived, these improved rates at early times were negligible and not even noticeable. Fig. 4.55 shows the evolution of the spatial pressure distribution at different stages of production in the tight/shale-oil system completed with a combination of the SD technique and multistage hydraulic fracturing.

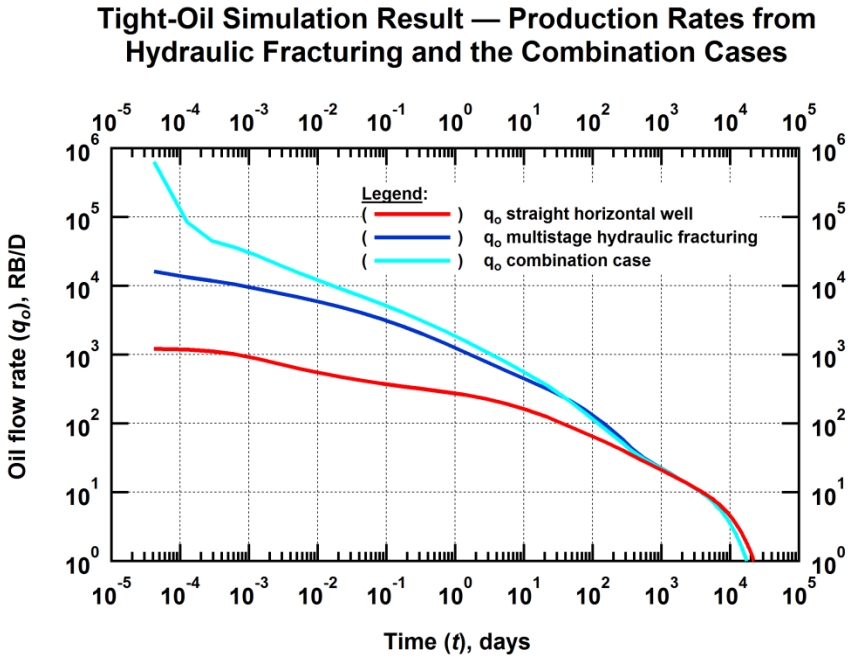

Fig. 4.53— Tight-oil Simulation: Production from the combination case shows only a short-lived (less than 10 days) slight improvement in rates over the multistage hydraulic fracturing case.

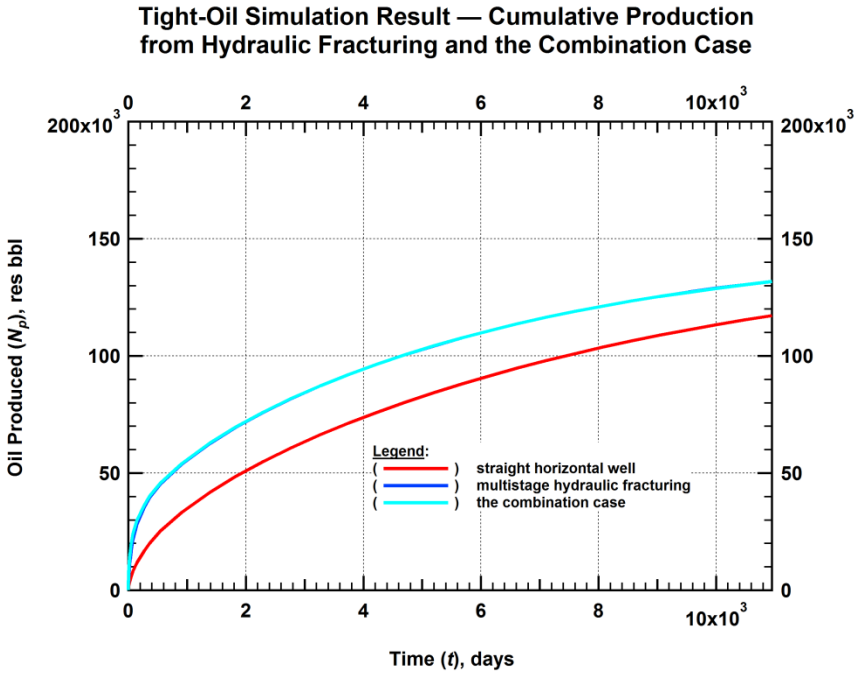

Fig. 4.54—Cumulative Production curves show there is no noticeable production advantage resulting from the combination of the SD with multistage hydraulic fracturing in the tight-oil study

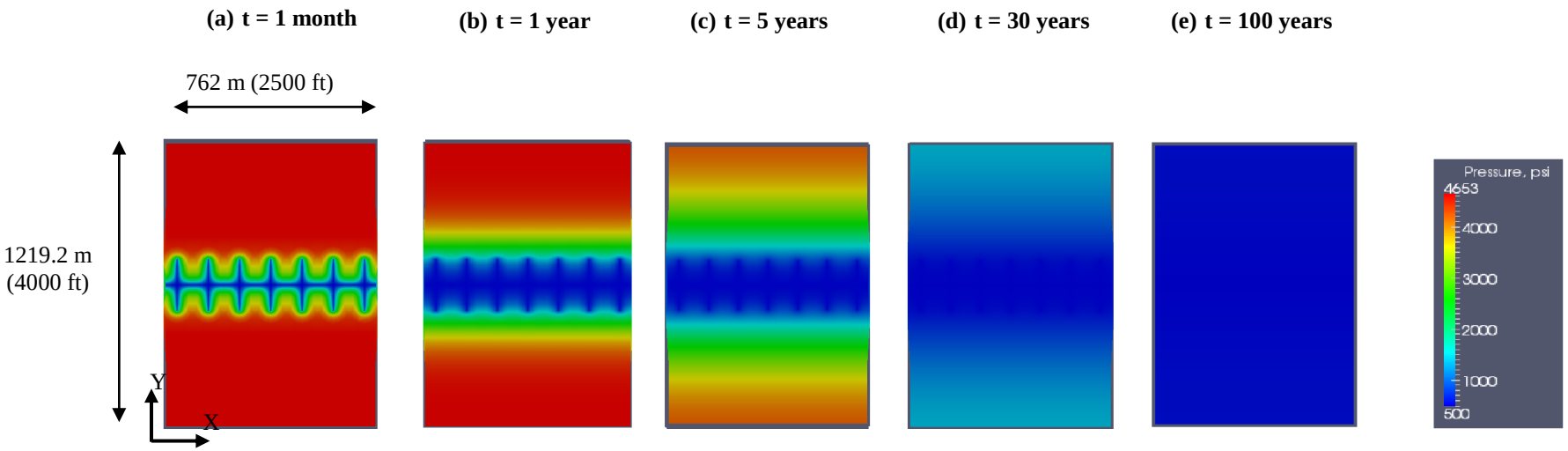

Fig. 4.55—Plan views of the pressure distribution over time in the tight-oil reservoir with properties representative of the Bakken formation during oil production from the combination case (Geometry F)

4.4 Sensitivity studies

This section presents the results of the analysis I conducted to determine the sensitivity of the performance of the SD method to the slot permeability and the formation permeability. The ensuing sections discuss these results in more detail.

4.4.1 Sensitivity of the SD performance to the slot permeability in the shale-gas reservoir system

The purpose of this study was to investigate the sensitivity of the SD's production performance to the permeability of the slot. Simulation runs were conducted using two new higher values of the slot permeability (see Table 4.1). As can be observed from Fig. 4.56, increasing the slot permeability had practically no effect on the production rates for any reasonable time frame because slot permeability at such high levels (in comparison to the formation permeability) resulted in an infinite conductivity conduit in the slot. The observed difference in production rates at very early times was due to the drainage of the artificially created fluid saturation in the slot at very early simulation time. As expected, the drainage was quickest in the case with the highest slot permeability.

Table 4.1—Varied parameters for slot permeability sensitivity studies

Parameters	SI Unit	Field Unit
Slot permeability (higher), k_{slot}	1.0×10^{-9} m^2	1.01×10^{6} md
Slot permeability (highest), k_{slot}	1.0×10^{-8} m^2	1.01×10^{7} md

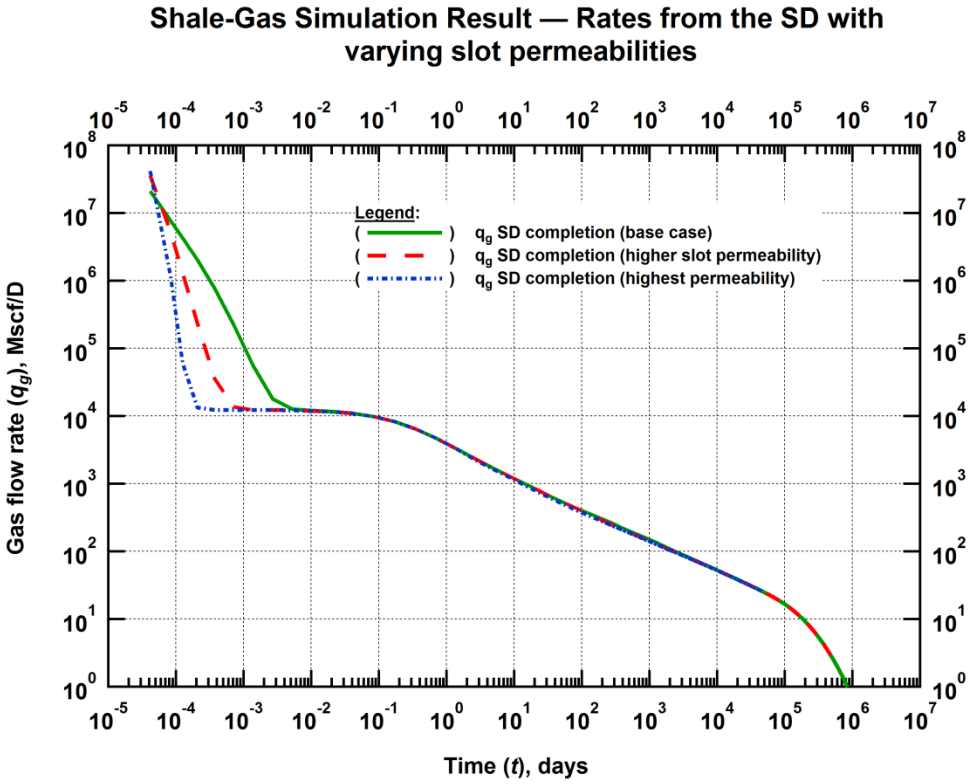

Fig. 4.56—Results showing that simulation rates are insensitive to slot permeability values considered.

4.4.2 Sensitivity of the SD performance to the formation permeability

Sections 4.1, 4.2 and 4.3 contain a thorough analysis of the expected production performance of the SD method in a tight-gas, a shale-gas and a tight/shale-oil reservoir system and insight into how this performance "stacked up" against the performance of multiple hydraulic fracturing (the preferred completion method in these formations). For the most part, the SD method was outperformed by multistage hydraulic fracturing. However, there was the always the question of if a change in the selected formation permeability value would cause a change in this observed trend. It was this question that instigated the studies described in the ensuing sections. The simulation results obtained earlier (see sections 4.1.2.3, 4.1.2.4, 4.2.2.3 and 4.2.2.4) were considered as the base case. This study was conducted for both the tight-gas and shale-gas reservoir systems.

4.4.2.1 Sensitivity of the outcome of the tight-gas comparative studies involving the SD to the formation permeability

The tight-gas comparative studies conducted earlier that involved the SD were (a) the comparison of production from the SD method (Geometry C) with production from multiply hydraulically fractured

system (Geometry E) (see section 4.1.2.3), and (b) the comparison of production from the standard hydraulically fractured system (Geometry E) to production from the system in which the SD technique was combined with multistage hydraulic fracturing (Geometry F) (see section 4.1.2.4). In this study, I considered the sensitivity of the results from these earlier studies to changes in the formation permeability. The values used for the formation permeability are presented in Table 4.2. The base case permeability was increased and decreased by a factor of 5.

First, I reran the cases involved in the first comparative study (between the SD system and the hydraulically fractured system) using the new values of the formation permeability being tested. In Fig. 4.57 and 4.58, I show the production rates obtained when these simulations which were carried out using the lower and higher values of the formation permeability respectively. The cumulative production obtained from these simulations are also shown in Fig. 4.59 and 4.60. From these rate and cumulative production plots, we see that though the magnitude of "by how much" varies, the qualitative deduction stays the same – the multistage-hydraulic fracturing completion always outperforms the SD completion across the range of formation permeability values considered in the tight-gas system studied.

Similarly, to evaluate the sensitivity of results obtained in the second comparative study (between Geometries E and F) to the formation permeability, I conducted the simulations using the new values of this parameter. The production rate and cumulative production curves obtained when the lower formation permeability is used are shown in Fig. 4.61 and 4.63, while those that correspond to the higher formation permeability are shown in Fig. 4.62 and 4.64. In these cases (of the tight-gas systems with the higher and lower permeability), the added production advantage resulting from adding the SD completion to a multiply hydraulically fractured system (the combination case) were observed to be marginal. As a result, a detailed economic analysis would need to be carried out to determine if the additional cost required to combine the SD method with hydraulic fracturing would be justified. This was the conclusion made in the base case (see section 4.1.2.4) and as such, I affirmed that the qualitative inferences I made from the base case study remained unchanged for these tested values of the formation permeability.

Table 4.2—Varied parameters for the tight-gas formation permeability sensitivity studies

Parameters	SI Unit	Field Unit
Formation permeability (base), k_{sand}	5.92×10^{-18} m^2	6.00×10^{-3} md
Formation permeability (higher), k_{sand}	2.96×10^{-17} m^2	3.00×10^{-2} md
Formation permeability (lower), k_{sand}	1.18×10^{-18} m^2	1.20×10^{-3} md

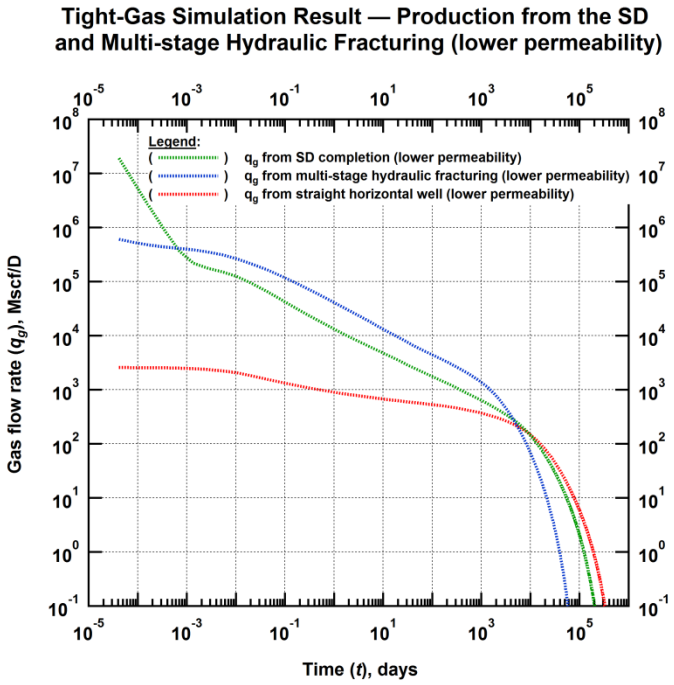

Fig. 4.57—Rates from the SD, multistage hydraulic fracturing and straight well geometries when a lower formation permeability was used to simulate production in the tight-gas system.

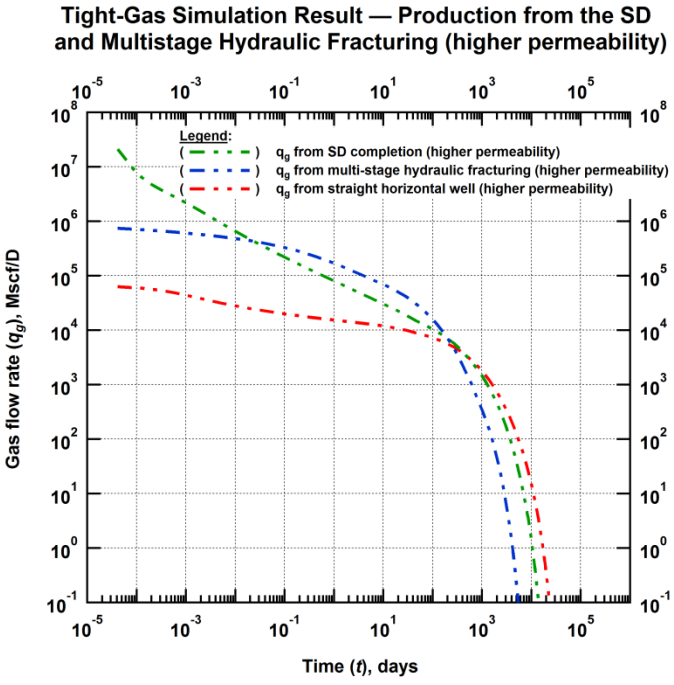

Fig. 4.58— Rates from the SD, multistage hydraulic fracturing and straight well geometries when a higher formation permeability was used to simulate production in the tight-gas system.

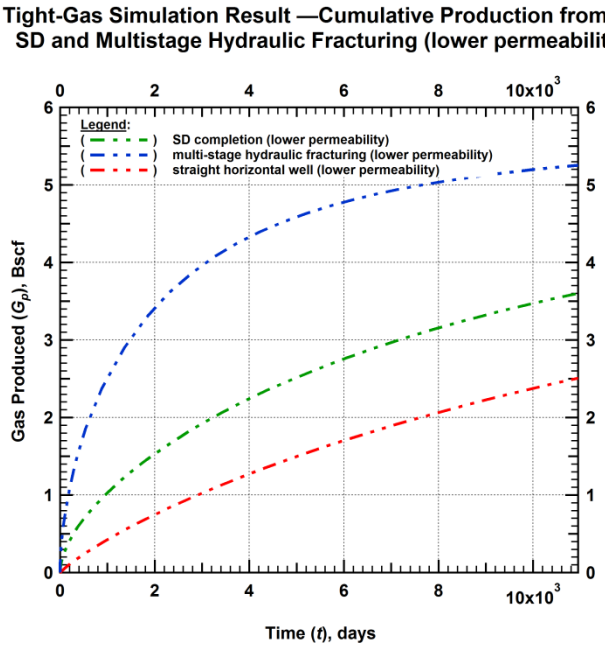

Fig. 4.59—Cumulative production from the SD, multistage hydraulic fracturing and straight well geometries when a lower formation permeability was used to simulate production in the tight-gas system

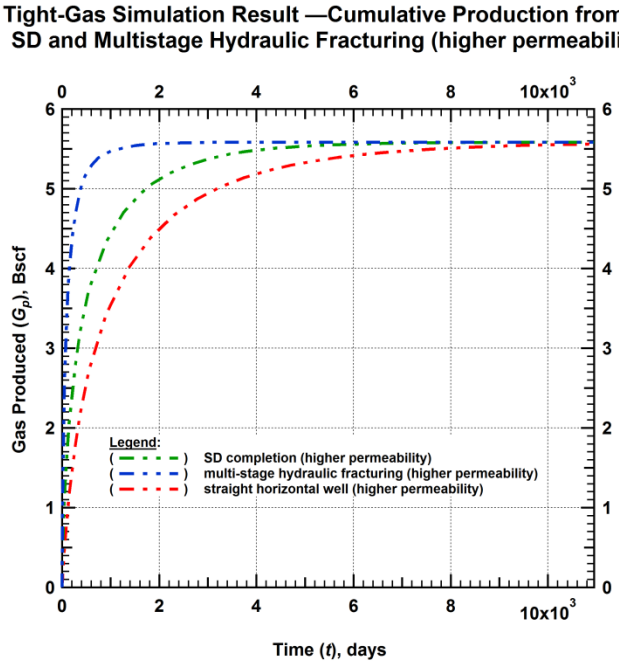

Fig. 4.60—Cumulative production from the SD, multistage hydraulic fracturing and straight well geometries when a higher formation permeability was used to simulate production in the tight-gas system

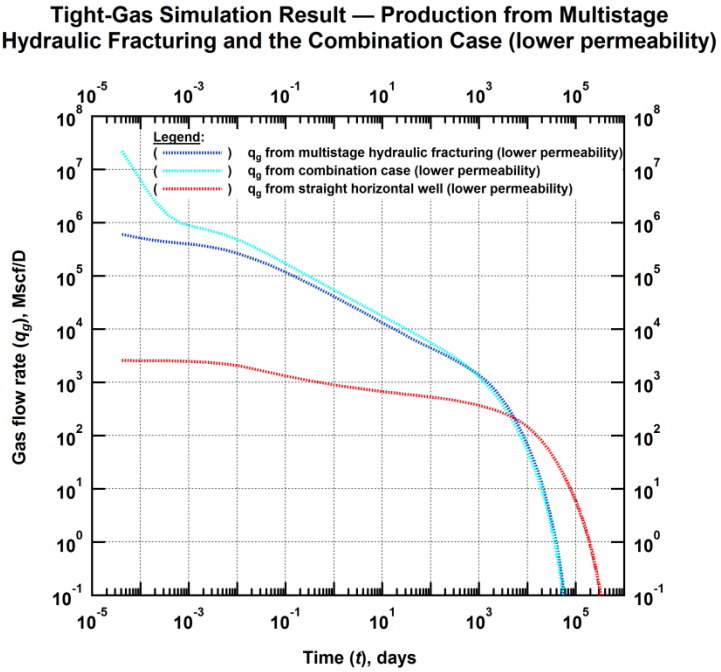

Fig. 4.61—Rates from multistage hydraulic fracturing, the combination case and straight well systems when a lower formation permeability was used to simulate production in the tight-gas study.

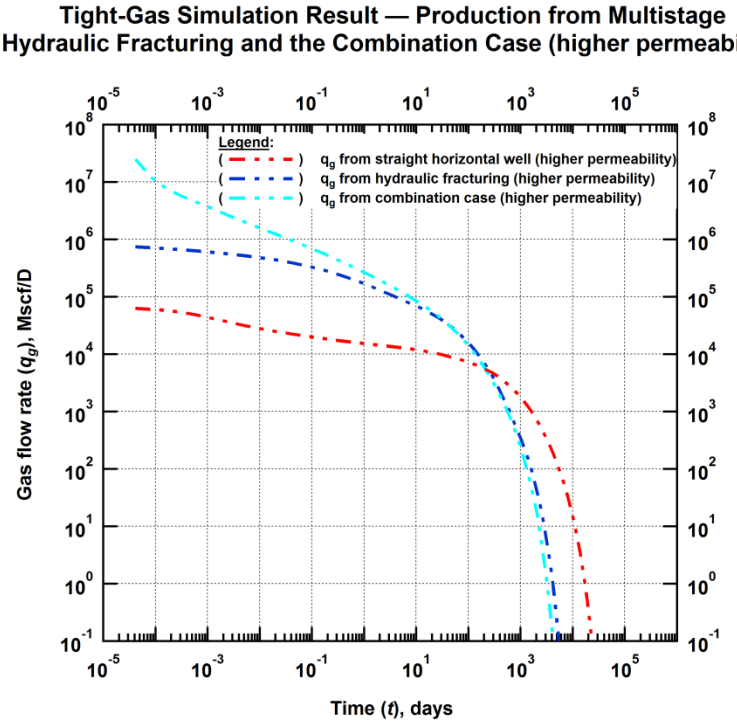

Fig. 4.62—Rates from multistage hydraulic fracturing, the combination case and straight well systems when a higher formation permeability was used to simulate production in the tight-gas study.

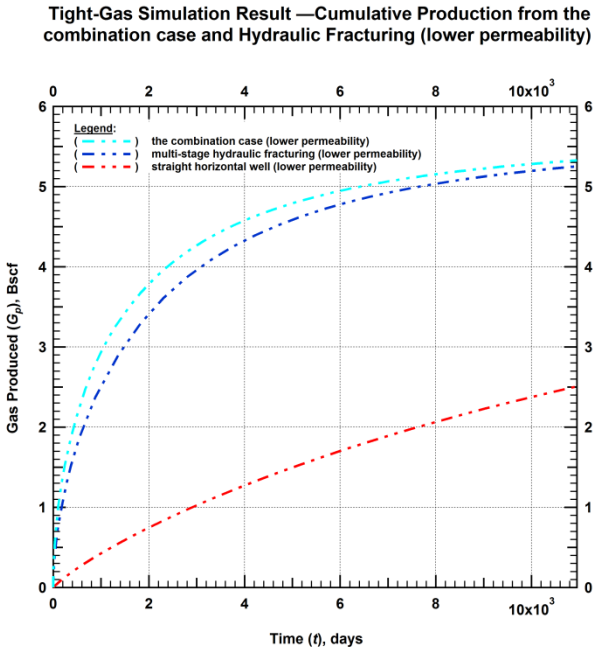

Fig. 4.63— Cumulative production from multistage hydraulic fracturing, the combination case and straight well geometries when a lower formation permeability was used to simulate production in the tight-gas system

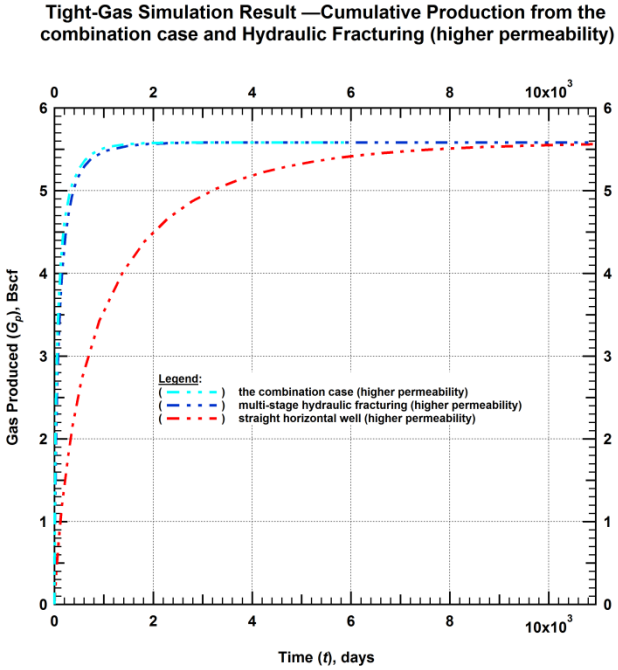

Fig. 4.64— Cumulative production from multistage hydraulic fracturing, the combination case and straight well geometries when a higher formation permeability was used to simulate production in the tight-gas system

4.4.2.2 Sensitivity of the outcome of the shale-gas comparative studies involving the SD to the formation permeability

Here also, as in the tight-gas sensitivity study (see section 4.4.2.1), I investigated the sensitivity of the outcome of the comparative studies between (a) the SD method and multistage hydraulic fracturing, and (b) the standard multistage hydraulic fracturing and a case where the SD is combined with the hydraulic fracturing treatment, to changes in formation permeability. The values used for the formation permeability are presented in Table 4.3. Here, the base case permeability was increased and decreased by a factor of 10.

Fig. 4.65 and 4.66 show the production rates that were obtained when the cases involved in the first comparative study (between the SD system and the hydraulically fractured system) were simulated using the lower and higher values of the formation permeability respectively. The cumulative production obtained from these simulations are also shown in Fig. 4.67 and 4.68. These rate and cumulative production plots show that in this case (as in the tight-gas case; see section 4.4.2.1; Fig. 4.57, 4.58, 4.59 and 4.60), though the magnitude of the difference in production performance varies, the hydraulic fracturing method always performs more favorably than the SD completion across the range of formation permeability values considered in the shale-gas system studied.

For the second comparative study (between Geometries E and F), the production rate and cumulative production curves obtained when the lower formation permeability is used are shown in Fig. 4.69 and 4.71, while those that correspond to the higher formation permeability are shown in Fig. 4.70 and 4.72. We see here that, as in the tight-gas case (see section 4.4.2.1; Fig. 4.61, 4.62, 4.63 and 4.64) the added production advantage resulting from adding the SD completion to a multiply hydraulically fractured system (the combination case) was marginal. Here also, the qualitative deductions made from the results of the high and lower formation permeability studies remain unchanged from those I made earlier when studying the base case (see section 4.2.2.4).

Table 4.3—Varied parameters for the shale-gas formation permeability sensitivity studies

Parameters	SI Unit	Field Unit
Formation permeability (base), k_{shale}	7.402×10^{-20} m^2	7.5×10^{-5} md
Formation permeability (higher), k_{shale}	7.402×10^{-19} m^2	7.5×10^{-4} md
Formation permeability (lower), k_{shale}	7.402×10^{-21} m^2	7.5×10^{-6} md

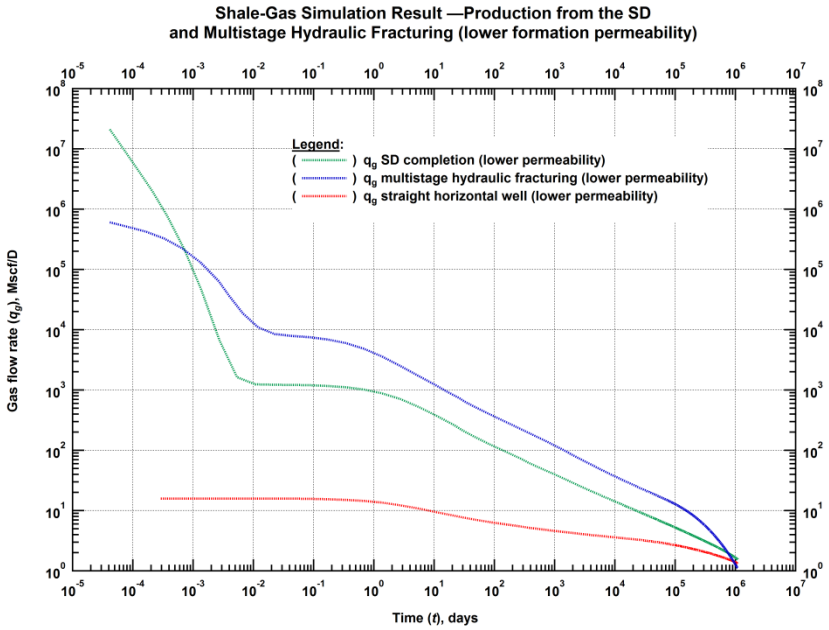

Fig. 4.65—Rates from the SD, multistage hydraulic fracturing and straight well geometries when a lower formation permeability was used to simulate production in the shale-gas system.

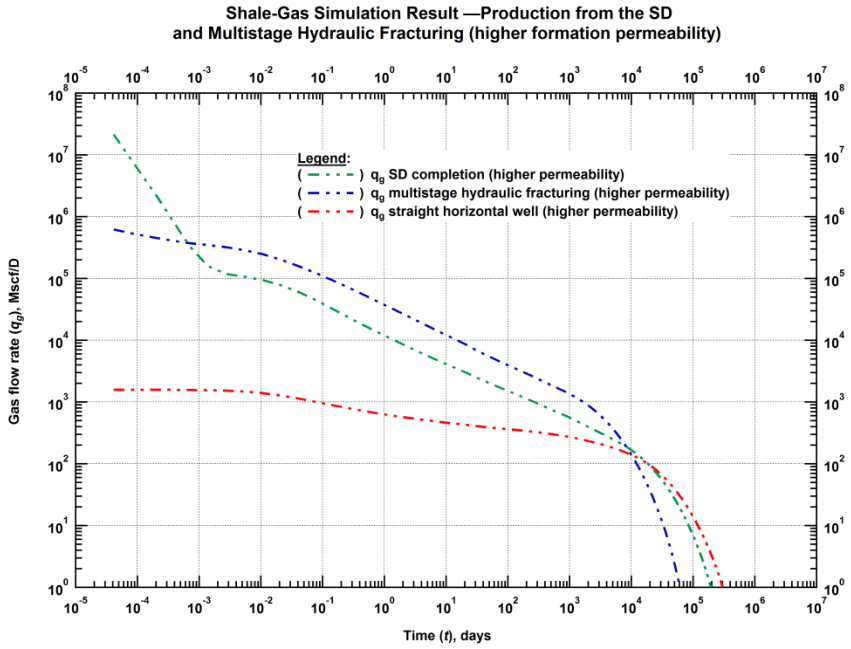

Fig. 4.66— Rates from the SD, multistage hydraulic fracturing and straight well geometries when a higher formation permeability was used to simulate production in the shale-gas system.

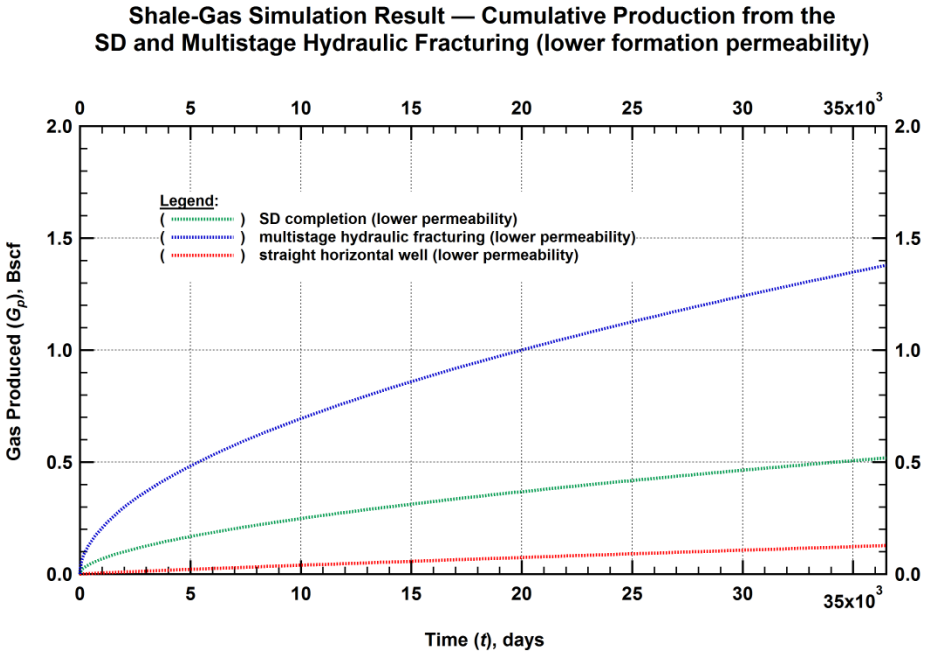

Fig. 4.67—Cumulative production from the SD, multistage hydraulic fracturing and straight well geometries when a lower formation permeability was used to simulate production in the shale-gas system

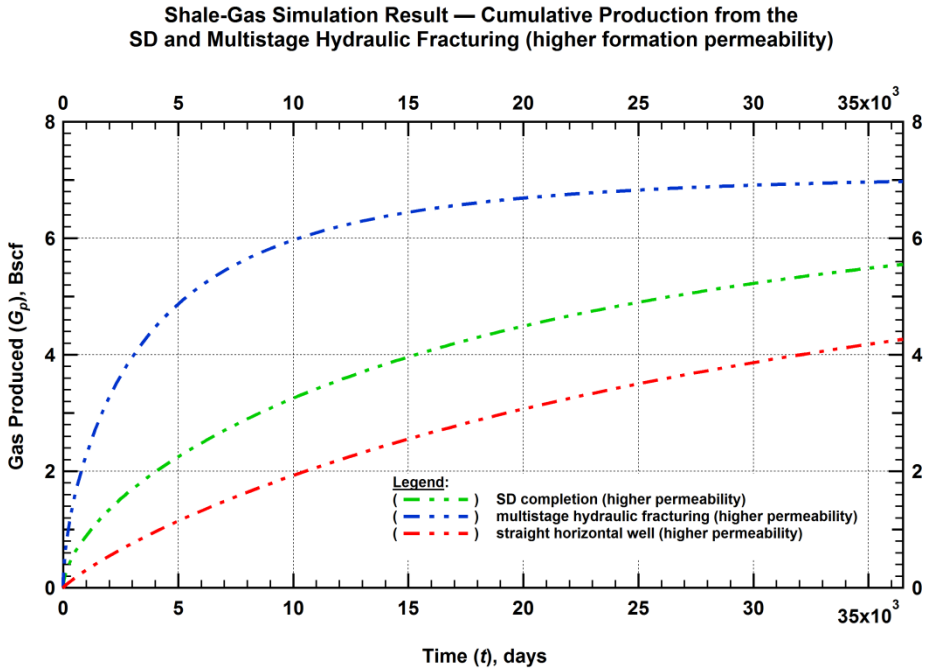

Fig. 4.68—Cumulative production from the SD, multistage hydraulic fracturing and straight well geometries when a higher formation permeability was used to simulate production in the shale-gas system

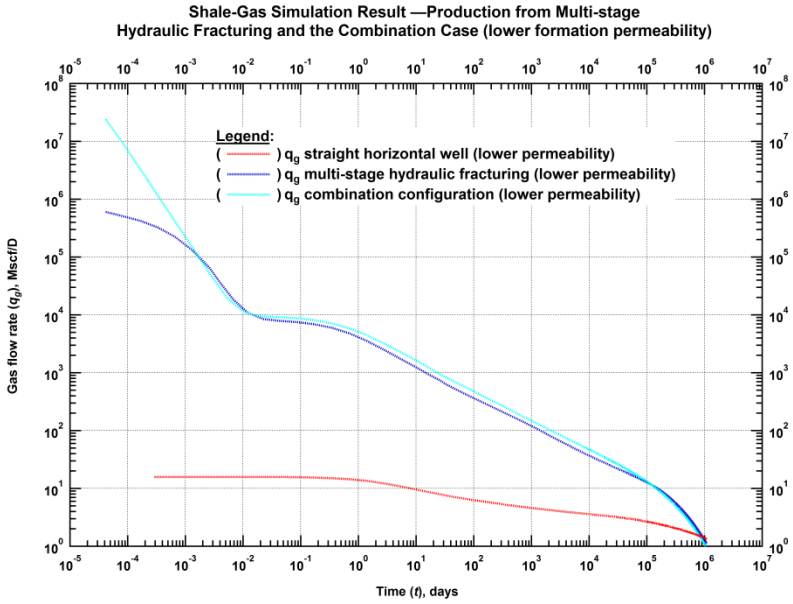

Fig. 4.69— Rates from multistage hydraulic fracturing, the combination case and straight well systems when a lower formation permeability was used to simulate production in the shale-gas study

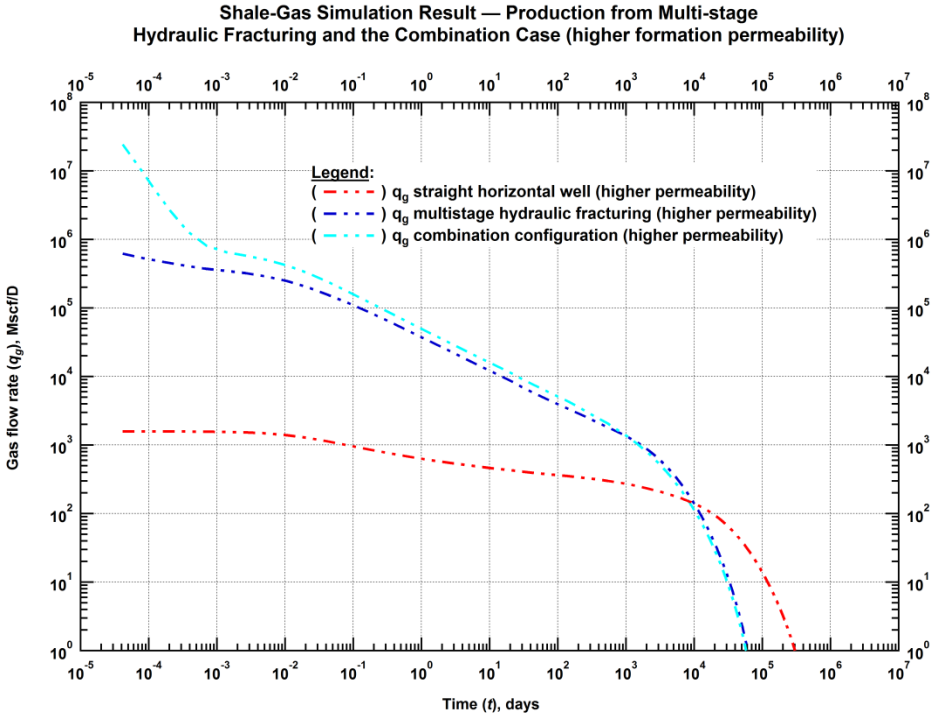

Fig. 4.70— Rates from multistage hydraulic fracturing, the combination case and straight well systems when a higher formation permeability was used to simulate production in the shale-gas study

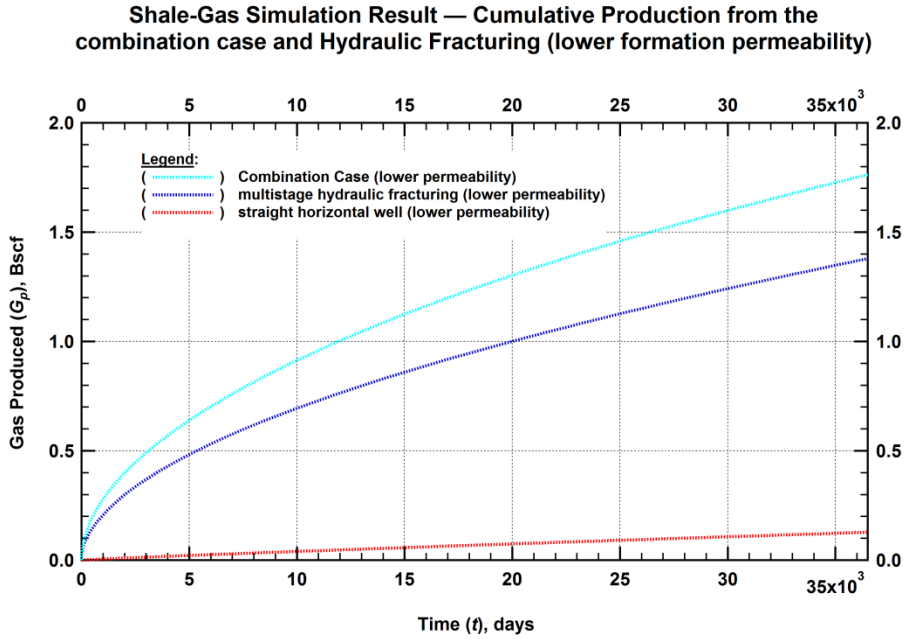

Fig. 4.71— Cumulative production from multistage hydraulic fracturing, the combination case and straight well geometries when a lower formation permeability was used to simulate production in the shale-gas system

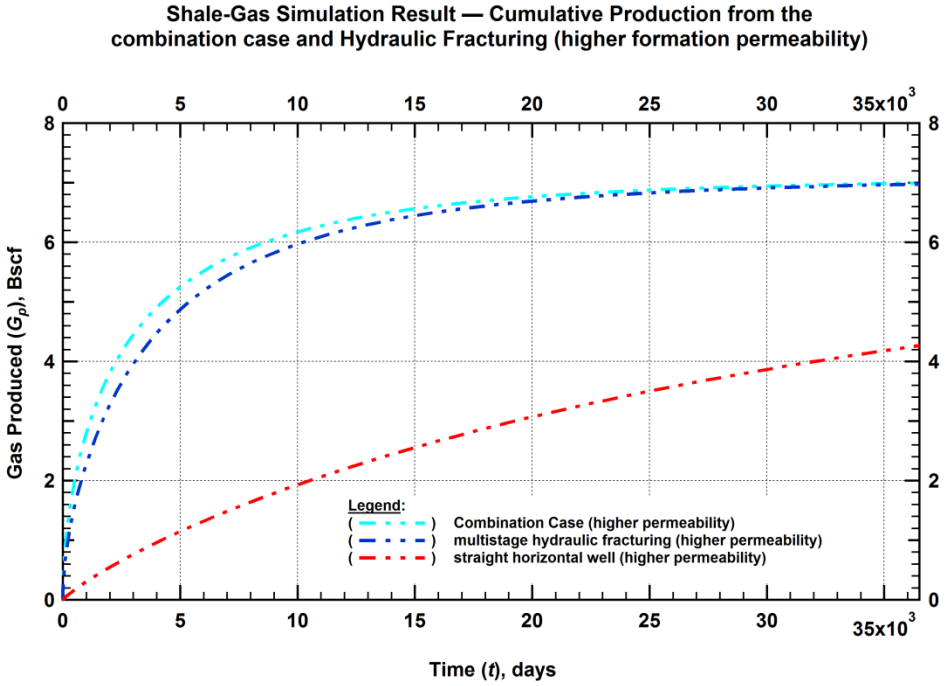

Fig. 4.72— Cumulative production from multistage hydraulic fracturing, the combination case and straight well geometries when a higher formation permeability was used to simulate production in the shale-gas system

4.5 Conclusions

My study involved four comparative studies in three low permeability formations of interest – tight-gas, shale-gas and tight-oil systems. This led to the discretization of six geometries/reservoir systems for the required numerical simulations. I also tested the sensitivity of the results of these studies to the permeability of the slot in the SD completion and the reservoir permeability in the formations of interest.

The implementation of the SD involves drilling a curved well in the target formation. This results in a longer well length and consequently more surface area exposed to flow than in the case of a straight horizontal well. Results from the first comparative study (in all three formations) showed that this extra well length did not in any way provide an extra production advantage for the curved geometries over the other completion methods.

The production rates from the "easier-to-set-up" equivalent SD representation produced excellent matches with rates from the fully-described SD model. This served as validation of this modeling approach for future studies.

The production performance for the SD method was estimated and compared with that of multistage hydraulic fracturing in all three formations I studied. In all the cases, the SD completion was outperformed by the multiple hydraulic fracture completion. This was attributed to be due to the fact that a larger surface area, which in this case appeared to have a more significant effect than the higher slot conductivities achieved with the SD method, was exposed to flow in the multistage hydraulic fracture completion.

Marginal improvements in production performance over the multiply hydraulically fractured were obtained, for the cases of the reservoir systems completed with a combination of both the SD and multistage hydraulic fracturing. Hence, it was concluded that a detailed economic analysis would be required to adjudge the profitability of exploring this option.

The results of the sensitivity analysis indicated the following: (a) over the range of values used (see section 4.4.1) the changes in the value of the slot permeability had no effect on the simulated production rates, and (b) over the range of values used for the formation permeability (see sections 4.4.2.1 and 4.4.2.2), though the magnitude of "by how much" varies, the qualitative deduction made in terms of how the various geometries compared with each other, stayed the same.

CHAPTER V

SUMMARY AND CONCLUSIONS

The purpose of this study was to provide an insight into the expected production performance of the proposed SD completion technique. Using petrophysical and completion parameters representative of the Cotton Valley (tight-gas), Marcellus (shale-gas) and Bakken (tight/shale-oil) formations, I set up simulation models to gain insight on how the SD would perform in these formations

In Chapter I, I presented the objectives and importance of work and also showed validation plots for TAMSIM (the numerical simulator used) from earlier studies (Freeman, 2010b; Olorode, 2011). Tables of representative reservoir and completion parameters for the three target formations chosen for this work are also contained in this chapter.

Chapter II gives a review of relevant literature pertaining to my study. This review provided a detailed background on the SD's concepts and processes involved in its implementation in a formation, a peek into the geology of the selected formations and an overview of modeling and production analysis methods in tight-gas, shale-gas and tight-oil reservoirs.

Chapter III goes over the details and intricacies of the unstructured grid generation algorithms used to set up the simulation meshes for my study. Visualizations of the meshes presented in this section were plotted using "gnuplot", a free UNIX visualization tool. I also discussed how we set up smaller sized stencils from the full grid meshes.

Chapter IV contains all the results obtained from my simulation runs and discussed using appropriate rate, cumulative production and pressure profile plots. The chapter is divided into four main sections - three based on the target formations investigated and the fourth being on the sensitivity studies that were conducted. In each of these formations, four comparative studies were conducted.

Overall, the results showed that the SD completion did not "meet up" in terms of production performance with multistage hydraulic fracturing (which is currently the industry's preferred method of completion in such low permeability formations). Additionally, from the results obtained, I validated the equivalent SD representation for use as an accurate tool for modeling production from the SD method. Finally, varying the formation permeability in the sensitivity studies did not change any of the earlier conclusions that were made.

NOMENCLATURE

Variables:

d_f = Fracture spacing, ft
h = Reservoir thickness, ft
k_{sand} = Matrix permeability, md
k_f = Fracture permeability, md
k_{slot} = Slot permeability, md
L_w = Horizontal well length, ft
p = Pressure, psi
p_i = Initial reservoir pressure, psi
p_r = Pressure at point r in reservoir, psi
p_{wf} = Wellbore flowing pressure, psi
q = Rate, bbl/day or mscf/day
r = Radius, ft
r_D = Dimensionless radius (dimensionless)
r_w = Wellbore radius, ft
t = Time, days, hours or seconds
T = Temperature, K
t_D = Dimensionless time (dimensionless)
w = Fracture width, ft
x = Distance from production source, m
x_f = Fracture half-length, ft

Greek Symbols:

ϕ = Porosity, fraction
ϕ_0 = Initial porosity, fraction
ρ = Density, kg/m^3
ρ_G = Gas phase density, kg/m^3
μ = Viscosity, cP

Subscripts:

G = Gas phase
CH4 = Methane component.

REFERENCES

Anderson, D.M., Nobakht, M., Moghadam, S., and Mattar, L. 2010. Analysis of Production Data from Fractured Shale Gas Wells. Paper presented at the SPE Unconventional Gas Conference, Pittsburgh, Pennsylvania, USA. 131787.

Boleneus, D. 2010. *Estimate of Bakken Oil Resource*. McKenzie County, North Dakota USA: Bakken Resources Inc.

Carter, E.E. 2009. *Novel Concepts for Unconventional Gas Development of Gas Resources in Gas Shales, Tight Sands and Coalbeds*. RPSEA 07122-7.

Cipolla, C.L., Lolon, E., Erdle, J.C., and Rubin, B. 2009. Reservoir Modeling in Shale-Gas Reservoirs. Paper presented at the SPE Eastern Regional Meeting, Charleston, West Virginia, USA. SPE 125530-MS.

Cipolla, C.L., Lolon, E., and Mayerhofer, M.J. 2009. Reservoir Modeling and Production Evaluation in Shale-Gas Reservoirs. Paper presented at the International Petroleum Technology Conference, Doha, Qatar. 2009, International Petroleum Technology Conference 13185-MS.

Civan, F. 2010. Effective Correlation of Apparent Gas Permeability in Tight Porous Media. *Transport in Porous Media* **82** (2): 375-384 Accession Number

Clarkson, C.R., Jensen, J.L., and Blasingame, T. 2011. Reservoir Engineering for Unconventional Reservoirs: What Do We Have to Consider? Paper presented at the North American Unconventional Gas Conference and Exhibition, The Woodlands, Texas, USA. SPE 145080.

Clarkson, C.R. and Pedersen, P.K. 2010. Tight Oil Production Analysis: Adaptation of Existing Rate-Transient Analysis Techniques. Paper presented at the Canadian Unconventional Resources and International Petroleum Conference, Calgary, Alberta, Canada. SPE 137352.

Dyman, T.S. and Condon, S.M. 2006. *Assessment of Undiscovered Conventional Oil and Gas Resources—Upper Jurassic–Lower Cretaceous Cotton Valley Group, Jurassic Smackover Interior Salt Basins Total Petroleum System, in the East Texas Basin and Louisiana-Mississippi Salt Basins Provinces*. U.S. Geological Survey Digital Data Series DDS–69–E.

Flannery, J. and Kraus, J. 2006. Integrated Analysis of the Bakken Petroleum System, U.S. Williston Basin. Paper presented at the AAPG Annual Convention, Houston, Texas, April 10-12, 2006 AAPG

FoxNews. New Drilling Method Opens Vast U.S. Oil Fields. FoxNews.com. http://www.foxnews.com/us/2011/02/10/new-drilling-method-opens-vast-oil-fields/#. Accessed 2011-04-10.

Freeman, C.M. 2010a. A Numerical Study of Microscale Flow Behavior in Tight Gas and Shale Gas. Paper presented at the SPE Annual Technical Conference and Exhibition, Florence, Italy. SPE 141125-STU.

Freeman, C.M. 2010b. Study of Flow Regimes in Multiply-Fractured Horizontal Wells in Tight Gas and Shale Gas Reservoir Systems. MS. Texas A&M University, College Station.

Freeman, C.M., Moridis, G.J., Ilk, D., and Blasingame, T.A. 2009. A Numerical Study of Performance for Tight Gas and Shale Gas Reservoir Systems. Paper presented at the SPE Annual Technical Conference and Exhibition, New Orleans, Louisiana. SPE 124961-MS.

Heck, T.J., LeFever, R.D., Fischer, D.W., and LeFever, J. Overview of the Petroleum Geology of the North Dakota Williston Basin. https://www.dmr.nd.gov/ndgs/Resources/WBPetroleumnew.asp. Accessed 2012-03-06.

Mattar, L. 2008. Production Analysis and Forecasting of Shale Gas Reservoirs: Case History-Based Approach. Paper presented at the SPE Shale Gas Production Conference, Fort Worth, Texas, USA. SPE 119897-MS.

Moridis, G.J., Blasingame, T.A., and Freeman, C.M. 2010. Analysis of Mechanisms of Flow in Fractured Tight-Gas and Shale-Gas Reservoirs. Paper presented at the SPE Latin American and Caribbean Petroleum Engineering Conference, Lima, Peru. SPE 139250.

Olorode, O.M. 2011. Numerical Modeling of Fractured Shale-Gas and Tight-Gas Reservoirs Using Unstructured Grids. MS. Texas A&M Univerisity, College Station.

Palagi, C.L. and Aziz, K. 1994. Use of Voronoi Grid in Reservoir Simulation. *SPE Advanced Technology Series* **2** (2). 22889 Accession Number

Rycroft, C.H. 2007. Multiscale Modeling in Granular Flow. Ph.D. Dissertation. Massachusetts Institute of Technology.

Stright Jr., D.H. and Gordon, J.I. 1983. Decline Curve Analysis in Fractured Low Permeability Gas Wells in the Piceance Basin. Paper presented at the SPE/DOE Low Permeability Gas Reservoirs Symposium, Denver, Colorado. 1983 Copyright 1983 Society of Petroleum Engineers of AIME 11640.

Valko, P.P. and Amini, S. 2007. The Method of Distributed Volumetric Sources for Calculating the Transient and Pseudosteady-State Productivity of Complex Well-Fracture Configurations. Paper presented at the SPE Hydraulic Fracturing Technology Conference, College Station, Texas USA. SPE 106279.

Vestergaard, H., Olsen, H., Sikandar, A.S., Abdulla, I.A., and Noman, R. 2007. The Application of Unstructured Gridding Techniques for Full Field Simulation of a Giant Carbonate Reservoir Developed with Long Horizontal Wells. Paper presented at the International Petroleum Technology Conference, Dubai, U.A.E. IPTC 11512.

Wattenbarger, R.A., El-Banbi, A.H., Villegas, M.E., and Maggard, J.B. 1998. Production Analysis of Linear Flow into Fractured Tight Gas Wells. Paper presented at the SPE Rocky Mountain Regional/Low-Permeability Reservoirs Symposium, Denver, Colorado. SPE 39931.

Zagorski, W.A., Douglas C. Bowman, Martin Emery, and Wrightstone, G.R. 2011. An Overview of Some Key Factors Controlling Well Productivity in Core Areas of the Appalachian Basin Marcellus Shale Play. Paper presented at the AAPG Annual Convention and Exhibition, Houston, Texas, USA, April 10-13, 2011. AAPG Search and Discovery Article #110147.

VITA

Name:	Tioluwanimi Oluwagbemiga Odunowo
Address:	Harold Vance Department of Petroleum Engineering Dwight Look College of Engineering Texas A&M University 3116 TAMU College Station TX 77843-3116
E-mail Address:	toluene_odu@yahoo.com
Education:	Texas A&M University, College Station, Texas, USA M.S., Petroleum Engineering May 2012 University of Ibadan, Oyo, Nigeria B.S., Petroleum Engineering June 2007
Affiliations:	Society of Petroleum Engineers